MICROCOPY RESOLUTION TEST CHART

NATIONAL BUREAU OF STANDARDS-1963-A

(3)

AD A122551

Technical Report No. 3
to
Air Force Office of Scientific Research
under
Grant No. AFOSR-80-0015
by
K.A. Dannemann, N.S. Stoloff & D.J. Duquette
Materials Engineering Department
Rensselaer Polytechnic Institute
Troy, NY 12181
November 30, 1982

DTIC
SELECTE
MAR 1 4 1983
S

DTIC FILE COPY

83 03 14 008

③

REPORT DOCUMENTATION PAGE	READ INSTRUCTIONS BEFORE COMPLETING FORM

1. REPORT NUMBER	2. GOVT ACCESSION NO.	3. RECIPIENT'S CATALOG NUMBER
AFOSR-TR- 83-0059	AD-A125 571	

4. TITLE *(and Subtitle)*	5. TYPE OF REPORT & PERIOD COVERED
MICROSTRUCTURE AND FATIGUE BEHAVIOR OF THREE NICKEL BASE EUTECTIC COMPOSITES	Technical 12/1/81 - 11/30/82
	6. PERFORMING ORG. REPORT NUMBER

7. AUTHOR(s)	8. CONTRACT OR GRANT NUMBER(s)
K. A. Dannemann and N. S. Stoloff and D. J. Duquette	AFOSR-80-0015

9. PERFORMING ORGANIZATION NAME AND ADDRESS	10. PROGRAM ELEMENT, PROJECT, TASK AREA & WORK UNIT NUMBERS
Rensselaer Polytechnic Institute Troy, NY 12181	6 1102 F 2306/AL

11. CONTROLLING OFFICE NAME AND ADDRESS	12. REPORT DATE
Air Force Office of Scientific Research Building 410 Bolling AFB DC 20332	11/30/82
	13. NUMBER OF PAGES
	166

14. MONITORING AGENCY NAME & ADDRESS*(if different from Controlling Office)*	15. SECURITY CLASS. *(of this report)*
	Unclassified
	15a. DECLASSIFICATION/DOWNGRADING SCHEDULE

16. DISTRIBUTION STATEMENT *(of this Report)*

Approved for public release; distribution unlimited.

DTIC

MAR 14 1983

17. DISTRIBUTION STATEMENT *(of the abstract entered in Block 20, if different from Report)*

18. SUPPLEMENTARY NOTES

19. KEY WORDS *(Continue on reverse side if necessary and identify by block number)*

aluminum	fatigue
carbide	fracture
composite	molybdenum
eutectic	nickel

20. ABSTRACT *(Continue on reverse side if necessary and identify by block number)*

The high cycle fatigue behavior of three advanced unidirectionally solidified nickel-base eutectic alloys has been studied. AG-170, strengthened by α-Mo fibers, and brittle carbide reinforced Nitac 14B and Cotac 744 were tested in vacuum under axial tension-tension, sinusoidal loading at 20 Hz. Fatigue properties of the as D.S. and heat treated conditions were examined at both 25°C and 825°C. In addition, the effects of reduced frequency on the high temperqaure fatigue life of aged Nitac 14B have been determined. (Cont'd)

DD FORM 1 JAN 73 **1473** EDITION OF 1 NOV 68 IS OBSOLETE
S/N 0102-014-6601

Fatigue resistance of the as D.S. material decreased between $25°C$ and $825°C$. This has been related to a variation in the mode of cracking. Room temperature failures were surface initiated and propagation proceeded along crystallographic planes, whereas Stage II crack propagation was observed at $825°C$. Nitac 14B was shown to be superior at both temperatures owing to its high matrix strength and large γ' volume fraction.

Post solidification heat treatments were the principal means of varying microstructure by causing alterations in the γ' size and distribution. These were most effective in improving the fatigue resistance at $825°C$, although aged AG-170 has been found to display a marked increase in fatigue life over the as D.S. material at room temperature. The most outstanding fatigue properties were revealed by aged Nitac 14B and AG-170 at $825°C$ where the endurance limits reached 0.89 and 0.81, respectively. Microstructural variations are believed to have caused the beneficial increase in fatigue strength.

The elevated temperature fatigue life of aged Nitac 14B was substantially reduced at low test frequencies in vacuum. The decrease in frequency caused a shift from surface initiated failure to an almost featureless fracture surface where the initiation, fatigue, and overload zones were not easily identified. Reduced specimen life was postulated to be the result of enhanced creep.

Accession For

NTIS CRA&I
DTIC TAB
Unannounced
Justification

By
Distribution/
Availability Codes
Dist | Avail and/or Special

DTIC
COPY
INSPECTED

CONTENTS

LIST OF TABLES

LIST OF FIGURES

v

vii

PART 1

INTRODUCTION

A substantial increase in the operating temperature of gas turbines has been the impetus behind the demand for high temperature materials possessing adequate properties for use in the hot stage. In this section the turbine blades are subjected to temperature excursions in a very hostile environment. Several directionally solidified eutectic alloys based on nickel have been identified as candidate blade materials. Creep, fatigue and other mechanical properties which are suitable for turbine operating conditions must be demonstrated by these aligned eutectics if they are to compete with single crystal and oxide dispersion strengthened superalloys.

Much work has already been done on the high cycle fatigue of eutectic composites, although few studies have dealt with microstructural effects on fatigue life. To date, the only research incorporating such effects has been conducted in our own laboratory on model eutectic systems.[1-5] Significant effects of frequency and post solidification heat treatments on the elevated temperature fatigue properties were revealed.

In view of these results, the present program was undertaken to study microstructural effects on the high temperature, high cycle fatigue behavior of three candidate turbine blade alloys. These included Nitac 14B, AG-170 and Cotac 744, reinforced respectively by TaC, Mo and NbC fibers. All three rely on ordered γ' (Ni_3Al) particles for

1

strengthening. Once again, frequency and post solidification heat treatment were the variables introduced into the test program. Varying the frequency should also aid in determining the importance of a creep effect on the high temperature fatigue lives.

PART 2

HISTORICAL REVIEW

Over the last decade, considerable advances have been made in
the area of directionally solidified eutectic composites. Both the
physical and mechanical properties, as well as the solidification pro-
cess, have been extensively characterized for various aligned eutectic
systems. This review will focus on the alloy systems under present in-
vestigation, namely Nitac, Cotac and Ni-Al-Mo. General reviews of eu-
tectic composites[6-8] should be consulted for more detailed information
on this topic.

2.1 Alloy Development

The early D.S. eutectics were found to have limited usefulness
due to numerous inadequacies, including low thermal fatigue resistance,
low creep shear strength and poor transverse properties. Extensive al-
loying additions have been employed as a means for overcoming these
problems and improving mechanical properties. This has led to the de-
velopment of a second and third generation of in-situ composites.

2.1.1 Nitac 14B

The Nitac system appears to offer the best potential for tur-
bine blade application because of its good balance of strength, ductil-
ity and toughness. Nitac alloy development has been fruitful and signi-
ficant strength improvements have been achieved. The high strength
Nitac 14B[9] alloy is the most advanced alloy in the series, differing

3

from its most recent predecessor, Nitac 13, primarily in the elimination of vanadium and the addition of boron. The boron addition was found to increase transverse ductility. Nitac 14B also has demonstrated slightly improved creep resistance for temperatures exceeding 870°C and considerably better oxidation and corrosion resistance. These improvements over the base alloy, Nitac 13, should prove beneficial.

The Nitac 14B structure consists of a strong, ductile fcc γ matrix containing 60 vol % of γ' precipitates and brittle carbide reinforcing fibers which comprise of 3-5 vol % of the structure. Previous work at G.E.[10,11] has confirmed the growth direction of both the TaC fibers and the γ' strengthened γ matrix as <100>.

2.1.2 Cotac 744

Early Cotac alloys were originally composed of TaC fibers in a Co-base matrix. The small volume fraction of carbide fibers accounted for a major portion of the strength of these systems in the absence of γ' precipitates. The forerunners in this family, Cotac 3* and Cotac 33*, were both found to have insufficient thermal cycling resistance at elevated temperatures.[12] Cotac 74* and Cotac 741* were developed to overcome this problem. However, their creep strengths were subsequently proved deficient at low and intermediate temperatures.[13] These alloys also exhibited lower strength at these temperatures than the IN 100 superalloy for lives of 1000 hours and less.

---

* Cotac 3:   Co-10Ni-20Cr-13.2Ta-0.78C (weight percent)
  Cotac 33:   heat treated version of Cotac 3
  Cotac 74:   Ni-20Co-10Cr-10W-4Al-4.9Nb-0.6C
  Cotac 741:   Ni-10Co-10Cr-10W-5Al-4.7Nb-0.5C

Cotac 744,[14] a 4% Cr modification of Cotac 74, is the latest alloy in the series. It was developed at ONERA in France and consists of NbC fibers, directionally solidified in a Ni-base matrix. Like Nitac 14B, Cotac 744 is based on the simple pseudo-binary Ni-MC eutectic. NbC fibers, rather than TaC, were chosen as the reinforcing phase because of their higher acceptable volume fraction and lower density.

The new Cotac alloy shows optimized mechanical properties, including superior tensile and creep properties, excellent structural stability, and satisfactory oxidation and corrosion resistance. This advanced alloy in the γ/γ'-NbC system exhibits a very unique phenomenon, the "Length memory effect". It can be explained as a recovery of initial specimen length, upon heat treatments after creep, and a restoration of the creep strength.

Maroni et al.[15] found the γ/γ'-NbC composites to have a columnar morphology with both the fibers and the matrix solidifying in the <100> growth direction. The fibers possess a square cross-section having {110} facet planes and {100} truncated planes. The two phases are semi-coherent.

2.1.3 AG-170

The Ni-Al-Mo system proves especially interesting because of the ductile nature of its reinforcement. Its high temperature strength and ease of processing could prove beneficial for turbine applications. The first generation of alloys in this series was developed and tested as early as 1975. Jackson et al.[16] reported on the AG-8 and AG-15 alloys. Reasonable strengths and ductilities were observed. AG-34[5,17]

and AG-60[18] proved superior to these. AG-170 offers an even further improvement beyond AG-60, displaying the best balance of properties in the series. Its most significant advantage is improved longitudinal and off-axis ductility which contribute to its high transverse strength. It is also noted for its strong response to heat treatments.

AG-170 like the earlier alloys in the series, directionally solidifies with a <100> growth axis for both ductile phases. The $(100)_\gamma$ is parallel to $(110)_\alpha$ at the fiber/matrix interface. Fiber volume fraction varies from 15 to 20 percent depending on the composition location on the liquidus in the ternary phase diagram.[19]

Tartaglia[20] has written a review of the physical metallurgy of the Ni-Al-Mo system. Similar work performed by Henry[19] and Tartaglia[20] has proved the existence of a eutectic between γ and α, where γ is an fcc Ni-base matrix containing α bcc Mo-base fibers. The alloys solidify as $\gamma-\alpha$ with subsequent precipitation of γ' from the γ matrix. The γ can be completely consumed by γ' precipitation for sufficiently high Al contents. This refutes the earlier work of Lemkey[21] who reported the system to have a $\gamma'-\alpha$ eutectic from 8 w/o Al down to 5 w/o Al and a $\gamma-\alpha$ eutectic at lower Al contents.

2.2 Tensile Strength

Directionally solidified eutectics are noted for their high strengths at elevated temperatures. Their strengths remain rather high with increasing test temperature until the melting point is reached. Above 1000°C most eutectic alloys are stronger than conventional super-alloys. Appreciable ductilities also have been demonstrated by the

aligned eutectics even when reinforced by brittle fibers (e.g. Nitac and Cotac alloys[8,23]).

A comparison of the effect of temperature on tensile strengths of several advanced aligned eutectics is shown in Fig. 1.[24] Cotac 74 is seen to be the strongest at room temperature, while Nitac 13 proves superior at temperatures exceeding 1000°C. Tensile results of the alloys under investigation have since been published.

Cotac 744 has been found to have much better high temperature strength and ductility than the earlier Cotac alloys.[13,14] Its ultimate tensile strength decreases monotonically with increasing temperature. The elongation reaches a maximum at 950°C.

The γ/γ'-Mo alloy, AG-170, is weaker in longitudinal strength than Nitac 14B and Cotac 744 over most of the temperature range of interest.[22] It does have an advantage in tensile elongation for the transverse orientation. Like Cotac 744, this alloy undergoes a decrease in tensile strength with increasing temperature. However, the yield strength experiences an increase until it reaches its maximum at 850°C. This unusual increase in the yield strength of γ' with temperature is characteristic of alloys containing γ' as one of the phases. It is responsible for the good strength retention of in-situ composites at elevated temperatures.

2.3 Creep

The microstructural stability of aligned eutectics contributes to their excellent creep and stress rupture properties. Generally, this class of materials exhibits creep and stress rupture properties which are
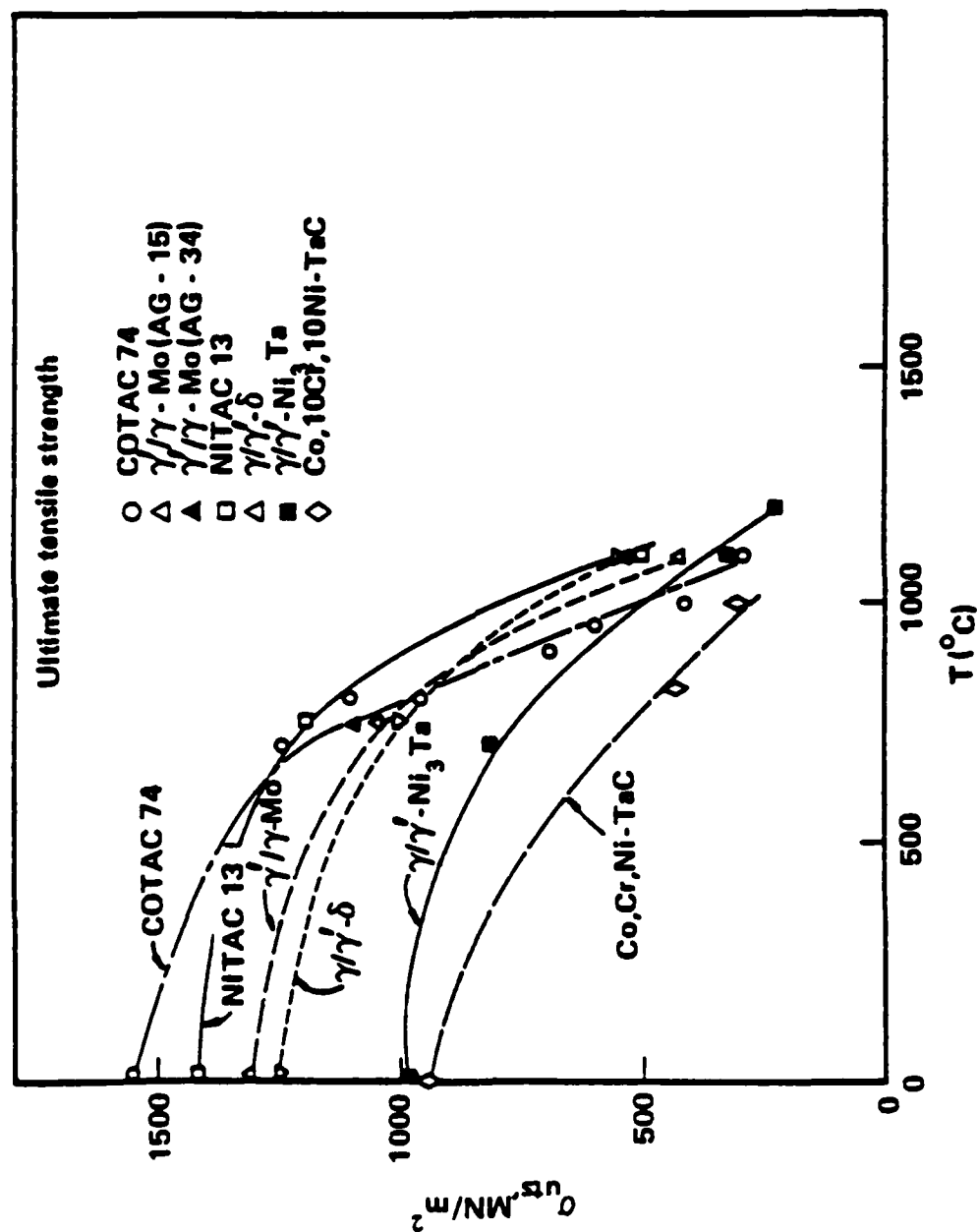
Fig. 1 Effect of temperature on tensile strength of aligned eutectics [24].

superior to conventionally cast superalloys.

If the steady-state creep rate is expressed by an Arrhenius equation:

$$\dot{\varepsilon}_s = A\,\sigma^n\,\exp\left(^{-Q}/_{RT}\right)$$

directionally solidified eutectics are found to have high stress sensitivities, n, and high activation energies, Q, when compared to conventional alloys.[8,24,25] The high activation energy for creep of eutectics has been attributed to slowed diffusion in the ordered intermetallic compounds or reinforcing carbides.[26] The stress sensitivities have been measured for several eutectic alloys. $(Co,Cr)-(Co,Cr)_7C_3$[27] and $Ni-Ni_3Nb$[28] have stress components of 7 and 22, respectively. Nitac[29] has a stress exponent in the 15-22 range. Most conventional metals and alloys have n's varying between 3 and 5. The stress sensitivities of some in-situ composites appear to be temperature or stress dependent.[28,30,31] Therefore, the above equation may not be the most suitable formulation for creep of eutectics.

Creep strength, like tensile strength, can be improved by decreasing the interphase spacing. Several investigators have carried out studies in this area.[30,32] Cellular microstructures obtained at high growth rates lead to inferior stress rupture properties, as shown by Jackson et al. for AG-15.[33] A large fiber volume fraction and increased phase alignment also lead to increased creep resistance.[8]

Aside from these microstructural factors, post solidification heat treatments may be utilized to reduce creep damage. For example, heat treatment of Cotac 3 precipitates fine TaC particles between the fibers. The heat treated version, termed Cotac 33, results in a major improvement in stress rupture resistance of CoTaC alloys.[34]

Cotac 74 and 741, hardened by γ' precipitates and reinforced by NbC fibers, showed creep strengths which are superior to the best current superalloys only at high temperatures.[34] However, it is difficult to compare these Cotac-type composites with superalloys since a small drop in stress increases the rupture life almost tenfold. Their real potential is only evidenced through long duration tests (i.e. at least 1000h). Cotac 744 was developed because of the inferior creep lives of Cotac 74 and Cotac 741 at low and intermediate temperatures. It was successfully shown to have creep lives an order of magnitude longer than Cotac 74.[13] In terms of 1000h density corrected strength, Cotac 744 has a much higher creep strength than IN 100 at all temperatures. It has also been reported to have comparable or superior creep strengths to Mar M200 at $850^\circ C$ - $990^\circ C$.[13]

One of the most unusual aspects of this alloy is the improvement of its creep rupture life by a few simple re-heat treatments.[14] The re-heat treatment of creep-tested, heat-treated Cotac 744 specimens resulted in the restoration of creep strength in addition to the recovery of the initial length. This phenomenon, the "length memory effect", is attributed to the removal of stress concentrations against the fibers upon re-heat treatment.

Cotac 744 has similar rupture lives to Nitac 13 at stresses under 200 MPa. Although Nitac 13 exhibits good rupture properties, Woodford[35] has shown that extensive oxidation of this alloy occurs in air, especially for long time tests. An advanced Nitac alloy, Nitac 14B, has revealed a slight improvement in stress rupture properties above 870°C. Coating of this alloy results in an increase in creep resistance.[36]

Two γ/γ'-Mo alloys, AG-15 and AG-34, have been found to have equivalent stress rupture properties to Nitac 13 at high temperatures and low stresses.[33] At high stresses Nitac 13 remains superior. AG-170, the newest alloy in this series, exhibits improved longitudinal stress rupture strength at low stresses and high temperatures. Its low temperature properties are also improved by utilization of a proper coating.[22] In the transverse orientation, AG-170 offers a significant strength advantage over other eutectics at high stresses.

The γ/γ'-Mo system behaves quite differently from conventional superalloys and other directionally solidified eutectics in resistance to creep deformation.[22] Nitac 13 and other conventional superalloys creep to 1% elongation in approximately half of their rupture lifetime. The same elongation for AG-170 occurs in as little as 10% of its lifetime. At 1000°C, Cotac 744 elongates 4-10% before rupture.

2.4 Fatigue

High cycle fatigue response in most materials can be roughly correlated with tensile strength. Thus, in parallel with tensile

strength, the fatigue strength of D.S. eutectics is generally out-
standing both at ambient and elevated temperatures. The aligned eutec-
tics exhibit superior fatigue properties when compared with convention-
al superalloys. The ratio of endurance limit to ultimate tensile
strength has been used as a measure of relative fatigue resistance. A
plot of fatigue ratio versus number of cycles to failure at 25°C is
shown in Fig. 2 for several eutectic systems.[24] All the alloys have
ratios in excess of 0.4. Grossman and Stoloff[4] have reported an out-
standing value of 0.84 for $\gamma/\gamma'-\delta$. These values are considerably
greater than 0.25 for many conventional superalloys.[37]

The excellent fatigue properties of in-situ composites have
been attributed to several factors. One advantage is the elimination
of grain boundaries perpendicular to the stress axis.[7] This requires
fracture to occur by a transgranular path which is slower than inter-
granular cracking. Obviously the reinforcing phase plays an important
role in resisting fatigue. The reinforcement often has a high load-
carrying capacity.[38] Thus, the overall load on the matrix is reduced,
matrix fatigue cracks are diverted out of preferred paths, and crack
propagation is retarded. Fatigue resistance is governed by the matrix
as well, whereby strong, ductile matrix materials are able to accommo-
date plastic strain.[39] Finally, the interface contributes. The in-
terface in eutectic alloys is not a source of weakness.[7] The presence
of debondable interfaces causes crack branching which also reduces the
crack propagation rate.
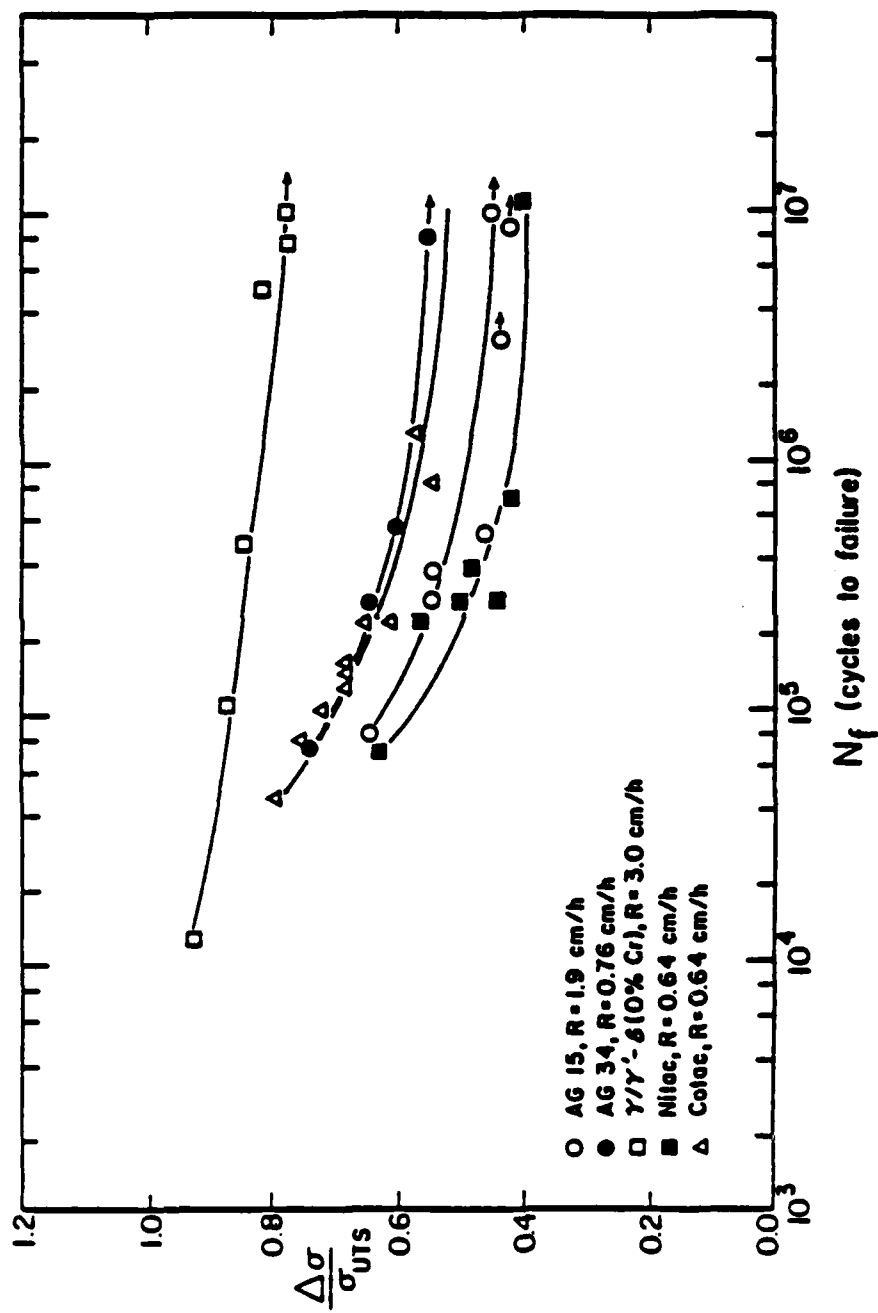
Fig. 2 Normalized high cycle fatigue properties of eutectics, 25°C[24].

2.4.1 Microstructure and Composition

Several studies have been conducted on the effects of inter-phase spacing on fatigue resistance. Generally, a decrease in inter-phase spacing results in an improvement in mechanical properties. This is also true for fatigue properties although it is not observed at all temperatures or stress levels.

Maurer's study of $Al-Al_3Ni$ is the most extensive.[1] He found no effect of growth rate on room temperature fatigue within the normal range of growth rates (3.5-11 cm/hr). However, at very high growth speeds (∿30 cm/hr), there was an improvement in fatigue resistance. At elevated temperatures a growth speed effect occurred even at low solidification rates.

Reduction of the inter-fiber spacing in $\gamma/\gamma'-\delta$ revealed a significant increase in the room temperature fatigue life at high stresses with no effect on the fatigue limit.[4] Work by Koburger[40] showed a similar improvement for Cotac at all stress levels. Decreased inter-fiber spacing resulted in a reduced slip distance between fibers and fewer dislocation pileups. The increased fatigue resistance was attributed to the shorter crack growth distances which require a greater number of crack re-nucleation events as the crack passes through broken fibers.

Kim et al.[41] have also shown high solidification rates to improve the room temperature fatigue life of $Ag_3Mg-AgMg$, particularly at low stress levels. In addition, they demonstrated that the ordered condition of Ag_3Mg experienced a longer fatigue life than the disordered

condition for specimens solidified at the same growth speed. Patarini

and Kattamis[42] reported an increase in the elevated temperature fa-

tigue properties of a Co-NbC eutectic with an increase in growth speed.

However, their reasoning was different from the others. They explained

this effect as a change in carbide morphology from rodlike at high R

to trimellar at low growth speeds.

Fatigue resistance can be altered by compositional as well as

microstructural factors. Investigations of some Cotac alloys have shown

the addition of varying amounts of Ni and Cr to increase fatigue re-

sistance.[43-45] This effect may be partly due to the stabilizing ef-

fect of nickel on the fcc crystal structure of cobalt-base alloys. Ad-

dition of aluminum to a Co-Cr-Ni matrix, as well as substitution of NbC

for TaC fibers, did not seem to have any effect on fatigue results.[43]

2.4.2 Temperature

An abundance of research has been conducted on the tempera-

ture dependence of fatigue of aligned eutectics. Initial work was begun

as far back as 1970. At that time, deSilva and Chadwick[46] reported

on $Fe-Fe_2B$ at room temperature and $500^{\circ}C$. The fatigue resistance at

$500^{\circ}C$ was found to be superior to that at room temperature. They at-

tributed the longer lives to the greater ductility of the matrix, plus

the reasonable ductility of the fibers at $500^{\circ}C$. There also was a de-

creased occurrence of fiber cracking in front of the crack owing to the

enhanced fiber ductility.

Since 1970, extensive high temperature fatigue studies have

been conducted on Nitac,[2,8] Cotac,[3,8] γ/γ'-Cr_3C_2,[47] Co-Cr_7C_3,[48] and γ/γ'-Mo.[49] The early work of Bibring[8] on monocarbide eutectics set the precedent. The matrix was shown to play the major role in high cycle fatigue. More recent work on these alloys[2,3] has pointed out the differences in fracture mode at ambient and elevated temperatures. At room temperature Stage I (crystallographic) crack propagation was revealed in Nitac and Cotac. However, no evidence of faceted fracture in these alloys has yet been observed at high temperatures. The deformation substructure of Cotac changed from planar at room temperature to wavy at high temperature.

Work by May on γ/γ'-Cr_3C_2[47] showed the 800°C fatigue resistance at some stress levels to be greater than at room temperature. This increase was attributed to the unbroken fibers which bridged the cracks in the matrix. Likewise, Tartaglia[49] found a Ni-Al-Mo eutectic, AG-15, to exhibit superior fatigue properties at elevated temperatures. The S-N properties of this alloy were inferior at 825°C when compared to those at room temperature. However, the fatigue properties experienced a peak at 725°C. The tensile properties of this alloy also exhibited a peak at 725°C[50] which correlates with the unique temperature dependence of the flow stress of the γ' matrix. A shift from surface to internal fatigue crack initiation was observed upon increasing the test temperature from 725°C to 825°C. Stage II crack propagation was shown to be the mode of crack propagation at both elevated temperatures.[49]

2.4.3 Post Solidification Heat Treatments

Significant improvements in the fatigue resistance of several eutectics have been achieved through post solidification heat treatments. Once again Bibring[8] pioneered work on the effects of heat treatment on the fatigue life of Nitac. The heat treatment consisted of a 1h solution treatment at 1150°C and a double age (1150°C/1h + 760°C/24hr). Heat treatment was found to have no effect on the room temperature fatigue life.

However, Koburger[40] observed a 25% increase in the 10^7 cycle, room temperature fatigue limit of a Cotac alloy upon heat treatment. The Co, Ni, Cr-TaC aligned eutectic was solution treated, water quenched and aged. A fine dispersion of TaC particles which precipitated in the matrix were responsible for the increase. They were related to the inhibition of tensile fiber fracture and dislocation pile-ups. At 825°C in vacuum the effect proved even stronger. A 50% increase in the fatigue limit was noted.[51]

Johnson and Stoloff[2] collected data for Nitac in three conditions: as directionally solidified, solution treated, and aged to precipitate γ'. Room temperature results revealed no substantial increase in fatigue life due to heat treatment. However, later results showed aged specimens to have longer lives at 825°C.[29]

The $\gamma/\gamma' - \alpha$ alloys have been found to be most responsive to heat treatments. Solution and aging treatments on this system results in the formation of a fine γ/γ' mixture.[20,22,52] Tartaglia and Stoloff[5] reported on the improvement in room temperature high cycle

fatigue properties after solution treatment. An even more outstanding increase was observed after aging for 1hr at 850°C. Ishii[17] and others[22,53] have found an elliptical precipitate which was formed upon aging. It has been identified as molybdenum rejected from γ'.[17] The improved high cycle fatigue resistance was attributed to it.

2.4.4 Frequency

At sufficiently high temperatures (>0.5 Tm), frequency becomes an important variable in fatigue behavior. Most of the research on frequency effects on the fatigue life of D.S. eutectics has been conducted in our own laboratory. Still further investigations are needed to confirm the mechanism of damage accumulation at low frequencies.

Maurer et al.[1] studied the effect of frequency on fatigue of an aligned Al-Al$_3$Ni eutectic in air at 185°C (0.5 Tm). The number of cycles to failure was found to decrease with decreasing frequency. They explained this phenomenon as enhanced creep at low cycling rates. If the process was solely due to fatigue, the number of cycles to failure at a given stress level would have remained constant with varying frequency.

A similar frequency effect has also been observed in both Nitac[2] and Cotac[45] tested in vacuum at 825°C (~0.68 Tm). The number of cycles to failure, as well as failure times, decreased as the frequency was lowered. Comparison of TEM dislocation substructures produced in creep and in fatigue was sufficient evidence to suggest the action of a strong creep component at low frequencies. Fractographs of

the 825°C specimens were also indicative of creep failures.

Most recently, Tartaglia and Stoloff[49] have reported on the time-dependent deformation of a γ/γ'- α eutectic, AG-15, tested at 725°C in vacuum. Creep appeared to play an important role in the decreased number of cycles to failure at lower frequencies. However, the evidence did not clearly establish a creep-fatigue interaction mechanism in low stress fatigue. An environmental effect may have been responsible.

2.5 Time Dependent Fatigue

At elevated temperatures, time dependency becomes of utmost importance. "Pure fatigue" is no longer the only operative process. Environmental and other time dependent phenomenon strongly influence the failure process as well. These time dependent effects can be studied through careful consideration of frequency, hold times and waveform.

Studies on the effects of frequency on elevated temperature fatigue of aligned eutectics have shown fatigue life to decrease with decreasing frequency.[1,2,45,49] This decrease in life was attributed to the increased importance of the creep component in the fatigue cycle, appropriately designated creep-fatigue interaction. Investigations have been carried out on other materials also. Several nickel-base superalloys have been found to exhibit a decrease in fatigue life in air as the frequency is lowered, including: Nimonic 90,[54] Hastelloy X,[55] Haynes alloy 188,[55] and Multimet.[55] This experimental evidence supports elevated temperature fatigue as a cyclic creep process (i.e. involving the interaction of both creep and fatigue). Several review

papers on creep-fatigue interactions provide further information on this topic.[56-58]

Emphasis on creep-fatigue suggested that creep and rupture mechanisms play an important part in high temperature fatigue. However, evidence can be cited to support the position that the time-dependency of high temperature fatigue may be the result of environmental attack. White,[59] Achter et al.[60] and Nachtigall et al.[61] reported an increase in fatigue life in vacuum. Moreover, Coffin and coworkers[62,63] have conducted tests on A286 and Udimet 500 at elevated temperatures in high vacuum, with no apparent frequency effect. The frequency effect found in air disappeared when the experiments were conducted in a vacuum of 10^{-8} torr. Wareing[64,65] has suggested that these two viewpoints may not be totally incompatible. The environment could be an important factor in crack growth which takes place at or near the specimen surface; however, creep damage occurring by internal cavitation would be unaffected by the surface conditions.

For tests conducted with long hold times in tension, chemical processes lead to accelerated crack propagation. The imposition of a tensile hold period reduces fatigue life since there is an extensive period where creep and environmental interaction can take place. Hold time effects should disappear in vacuum if the material is only sensitive to environmental effects. Yet, these same effects will be present in vacuum if the material is creep sensitive.

Krempl and Walker[66] performed hold time tests on a 1 Cr-1 Mo-0.25 V steel at 1400°F in air. The cycles to failure decreased

significantly as hold times were lengthened. An increasing degree of intergranular fracture accompanied the decreased life. A creep rupture type of damage was thought to occur during the dwell periods. Berling and Conway[67] obtained similar results with an AISI 304 stainless steel at 650°C.

Coles and Skinner[68] examined the combined effects of frequency and hold period. A simultaneous decrease in frequency and an increased hold time lowered the number of cycles for failure.

Several instances of hold time effects on the fatigue behavior of eutectic composites have been reported.[69,70] However, these single instances are not sufficient evidence from which a theory can be deduced. Tests on $\gamma/\gamma'-\delta$[69] at 1000°C in air revealed a sharp increase in the crack growth rate with the application of a one minute hold time. This can be explained by either a creep component superimposed on fatigue or an environmental effect. Austin[70] has obtained limited data on hold-time effects in Cotac. He concluded that a maximum load dwell period causes faster cracking than a minimum load dwell period.

Tensile hold periods generally have been found to be more damaging than equal hold periods in tension and compression, or compression hold periods only. However, cast nickel-base superalloys have shown damaging effects of compressive hold periods. An investigation of René 80[71] showed the adverse effect to occur as a result of the development of tensile mean stresses with time.

Changes in the waveform employed in elevated temperature

fatigue tests are useful in evaluating time dependent effects. Fatigue crack growth rates have been observed to be susceptible to change as the waveform is changed. Unequal ramp rates lead to some form of bulk damage process.

Coffin[72] conducted unequal ramp rate tests at a constant frequency on AISI 304 stainless steel both in air and in vacuum. The fatigue life was lengthened relative to balanced cycle tests when the tensile strain rate exceeded the strain rate in compression. Upon reversal of the loading sequence to a "slow-fast" waveform, lives were reduced. He attributed this decrease in fatigue life to the nucleation and growth of creep cavities at grain boundaries during cycling. The "fast-slow" wave shape was thought to cause the collapse of cavities.

Some other waveform experiments have been performed on Cotac at 825°C in vacuum.[70] The Cotac alloy also exhibited faster crack growth with slow loading and fast unloading. This was explained by a creep process. The fast unload allowed little time for relaxation. Much slower crack growth was noted for "fast-slow" cycling where there was insufficient time for creep to occur.

PART 3

EXPERIMENTAL PROCEDURE

3.1 Materials and Microstructure

Directionally solidified ingots of the three nickel-base test alloys were purchased from General Electric Company. These ingots, which had been directionally solidified in a Bridgeman furnace, were received in the form of right cylinders approximately 2.2 cm in diameter and 28.9 cm long. Alloy compositions are listed in Table I. AG-170, the α-Mo reinforced alloy, was solidified at 1 cm/hr while Nitac 14B and Cotac 744 were grown at 0.635 cm/hr.

Prior to testing, flat sections were polished along the length of several of the ingots to reveal the quality and length of the aligned fibrous region. The longitudinal flat was ground wet using 240, 320, 400 and 600 silicon carbide papers, followed by polishing with 9μ and 3μ diamond paste and 0.3μ alumina powder. Optical examination of the flats along the length of the ingot generally revealed approximately 20 cm of acceptable fibrous structure. However, some microstructural faults were discernible even in the supposed aligned regions. These included eutectic cells and cellular growth fronts, dendrites, and blocky carbides.

The transverse microstructure was observed by mounting a cross sectional slice from the center of the ingot in bakelite. These mounts were mechanically polished as described above. Marbles reagent was employed as an etchant to reveal the fibers in Nitac and Cotac; Kallings

23

Table I

Chemical composition (wt%)

Alloy	AG170	Cotac744	Nitac14-B
Ni	61.53	63.7	62.56
Co		10	3.93
Cr		4	4.20
Mo	29.74	2	3.16
W		10	4.52
Re	1.2		6.84
Al	5.88	6	5.5
C		0.5	0.27
others	1.65 V	3.8 Nb	9.01 Ta,0.01B

reagent was used for AG-170. Preferential etching of the γ and γ' phases was achieved with a solution of 50 ml HCl, 10 ml HNO_3 and 10 ml H_2SO_4.

3.2 Specimen Preparation

Most ingots contained enough acceptable fibrous structure such that five sections, each 3.8 cm to 4 cm long, could be cut for production of specimens. Insufficient aligned structure in other ingots allowed for the cutting of only three or four sections, these being from the center of the ingot. Four right cylinders were electro-discharge machined from each section with the growth direction aligned lengthwise. Specimens were then machined from these cylinders.

Two specimen geometries were employed for fatigue testing. Specimens of the as D.S. material were obtained from 3.8 cm long cylinders having a 0.76 cm diameter. Fig. 3 shows the final specimen configuration.

This design proved to be unsatisfactory for all of the fatigue testing. Many specimens having this geometry were tested and found to fail prematurely in the shoulder due to a sizable stress concentration there. The design was subsequently modified and extensive changes were made to the shoulders. To allow for a more uniform concentration of stress, an angle was incorporated which would support a greater amount of the load over a larger area. Also, the diameter of the gage section was reduced to 0.254 cm to ensure a proper fatigue failure and fracture in the center. The overall design of this specimen is shown in Fig. 4.
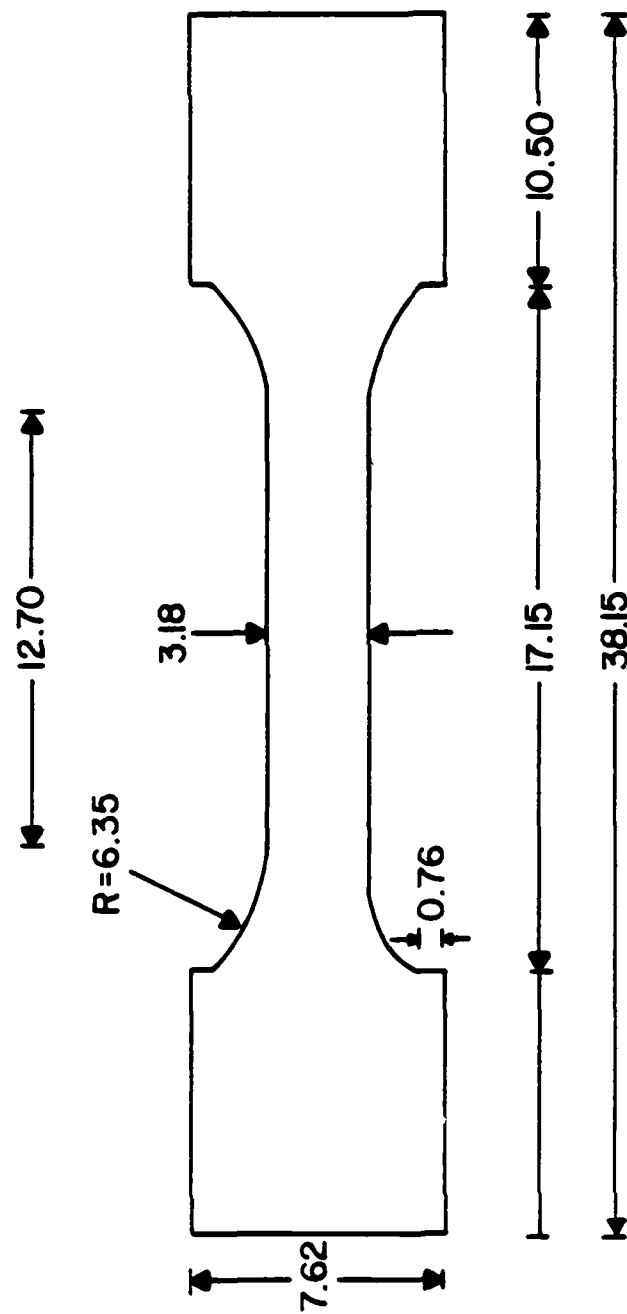
All dimensions in mm.

Fig. 3   Fatigue specimen configuration for as D.S. material.
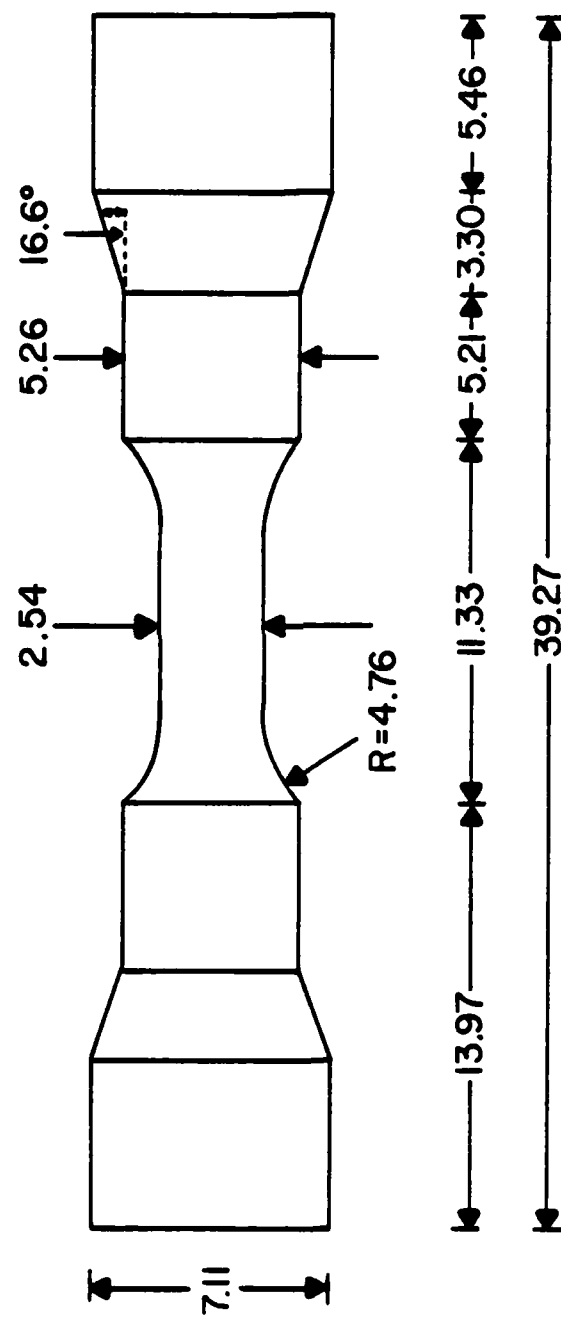
All dimensions in mm.

Fig. 4   Fatigue specimen configuration for heat treated material.

All specimens were then mechanically polished through 600 grit SiC paper using a high speed tensile lathe. Specimens were examined for non-uniformities, such as deep undercuts, on a stereomicroscope at 70X. This was followed by electropolishing to provide a uniform deformation-free surface. The best electropolish results were obtained using an electrolyte composed of 140 ml methanol, 35 ml H_2SO_4 and 50 ml glycerin cooled with an ice water bath to $-10^\circ C$. A voltage of 32-35 V was applied for 15-30 seconds depending on the alloy. Heat treated specimens were polished differently. The solution was equilibrated at room temperature and a potential of 20 V was applied for 20 seconds. Just prior to testing the gage diameter of each specimen was measured with a Unitron microscope.

3.3 Heat Treatments

To determine the optimum heat treatments, well-aligned scrap material from each of the three alloys were given various experimental heat treatments. Hardness tests, optical and transmission electron microscopy were critical factors in choosing a specific treatment for each alloy. From these experiments, similar heat treatments were specified for Nitac 14B and Cotac 744. AG-170, having a slightly different structure, was given a different treatment.

After machining, specimens to be heat treated were sealed in quartz ampules (1 specimen/ampule). These were evacuated to a pressure of 0.13 Pa to prevent excessive oxidation during heating. All heat treatments were performed in a high temperature box furnace heated with

super Kanthal elements.

Solution treatments for Nitac 14B and Cotac 744 consisted of 1 hour exposure at 1200°C. AG-170 was held at 1250°C for 4 hours to partially solutionize*. Solutionized specimens were then quenched in an ice-brine solution. After sufficient cooling ampules were broken and specimens retrieved.

Several specimens required further heat treatments. Solutionized specimens requiring an aging treatment were again encapsulated in another quartz ampule, also evacuated to 0.13 Pa. All three alloys were given the same aging treatment which consisted of a 4 hour exposure at 850°C, followed by an ice-brine quench.

Heat treated specimens were then mechanically polished as described in the previous section.

3.4 Fatigue Testing

High cycle fatigue tests were conducted on an Instron closed loop, servohydraulic dynamic test machine, equipped with a 10 kip load cell. Load-controlled, tension-tension tests were performed with the stress axis oriented parallel to the fibers. The machine was programmed with a sinusoidal stress waveform. Cycling was between a constant minimum stress of 34.5 MPa and varying maximum stresses.

The gripping mechanism used consisted of a threaded split-grip system. The split grips screwed into the pull rod assembly. The materials used for the gripping system were various Ni-base superalloys suitable for elevated temperature exposure. For the as D.S. design, the

---

* Complete solution of the precipitates was not possible in any experimental heat treatments.

specimen was restrained at the flats present at the specimen shoulder. However, the grips for the heat treated specimens were machined to the exact specimen dimensions. These two sets of split grips are illustrated in Fig. 5 a and b.

Tests at 25°C and 825°C were performed on the three alloys in both the as D.S. and heat treated onditions at a frequency of 20 Hz. In addition, aged Nitac 14B was tested at 825°C at frequencies of 2 Hz, 0.2 Hz and 0.02 Hz. An oscilloscope was used to monitor the waveform at low frequencies. All tests were conducted under vacuum in a stainless steel, water-cooled vacuum chamber manufactured by Centorr Associates Inc. The chamber housed a high temperature furnace capable of reaching temperatures in the 900°C range. Specimen heating was accomplished by radiation from Kanthal heating elements and the temperature was monitored by a chromel-alumel thermocouple placed in contact with the specimen gage section. Figure 6 shows the entire setup.

3.5 Specimen Examination

3.5.1 Optical Microscopy

To acquire information on the effects of microstructure on fatigue life, optical microscopy was used. Standard metallographic techniques were employed for most optical microscopic investigations.

Transverse slices were cut from selected specimens with a diamond blade, mounted in bakelite, and polished through 0.3 μm alumina. Marbles reagent was chosen as the etchant for Nitac 14B and Cotac 744 since it produced excellent contrast between the matrix and the fibers
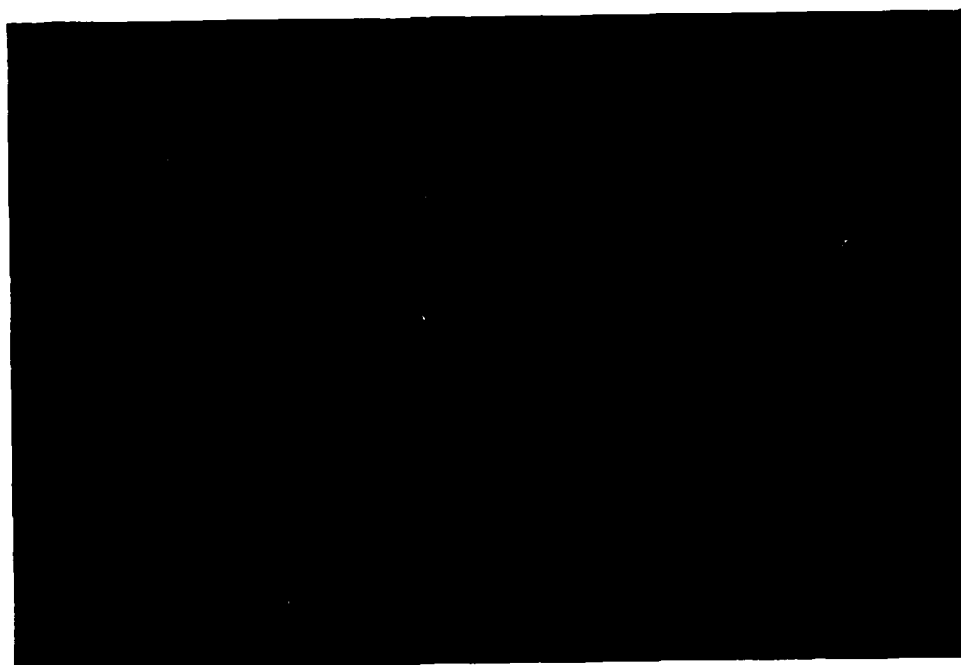
(a)
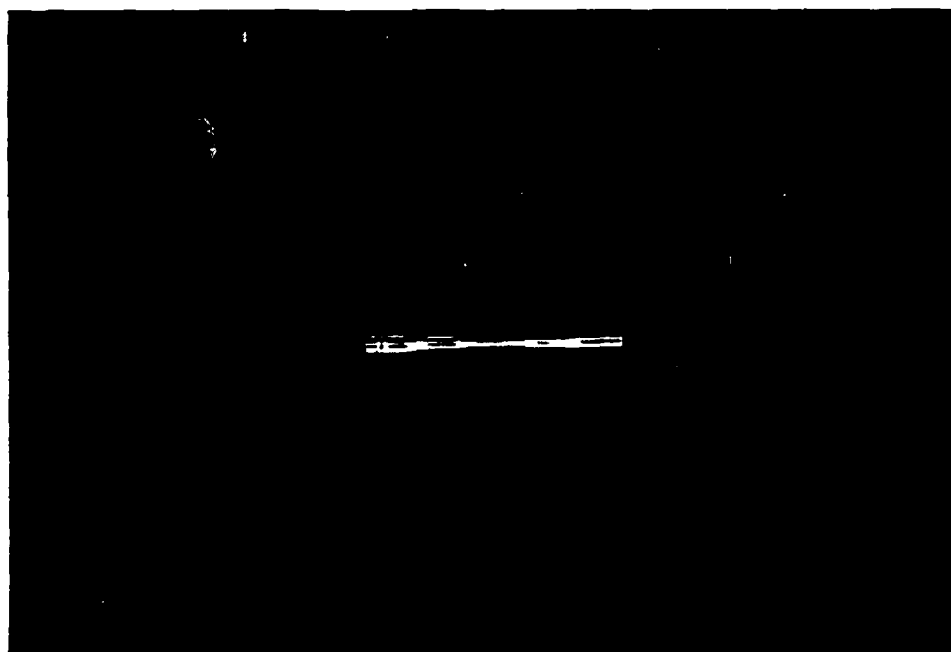
(b)

Fig. 5 Threaded and split fatigue inserts for (a) as D.S. fatigue
specimens, and (b) heat treated fatigue specimens.
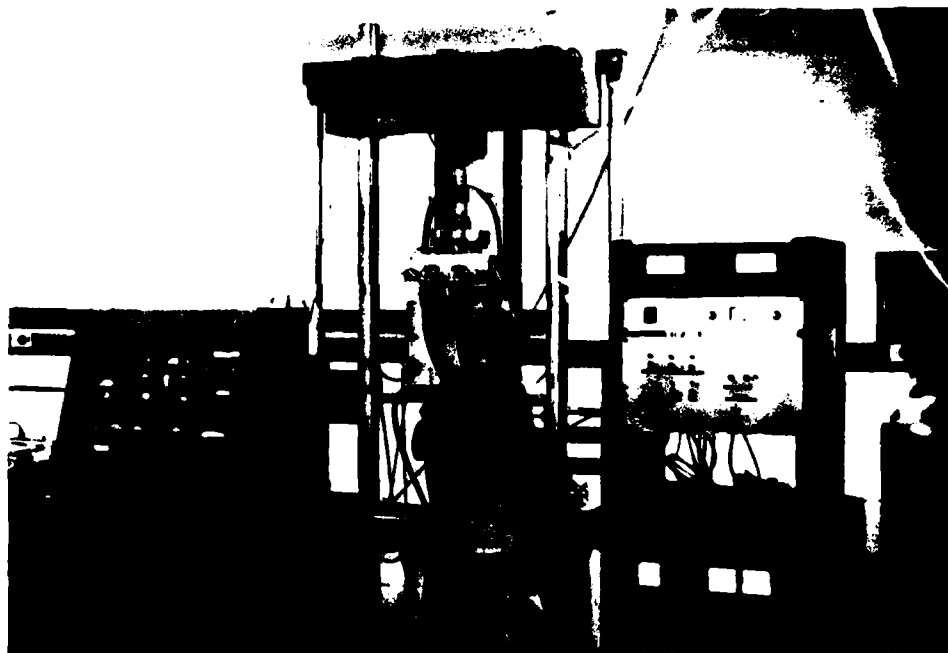
Fig. 6   Elevated temperature fatigue testing setup, equipped with vacuum system.

after etching for only several seconds. Kallings reagent produced a similar contrast for AG-170. Photography and analysis were performed on a Bausch and Lomb Research Metallograph at magnifications up to 1000X.

3.5.2 Scanning Electron Microscopy

The scanning electron microscope (SEM) was used extensively for fractographic examination. An AMR model 1000, operating at an accelerating voltage of 20 kV, was used to study crack initiation and propagation and surface slip.

Minimal specimen preparation was required. Fractured specimen halves were mounted without modification in the microscope stage. For keener observation of surface fibers, specimens were gold coated prior to mounting.

3.5.3 Transmission Electron Microscopy

The transmission electron microscope (TEM) was utilized in this investigation for the observation of microstructures and heat treated morphologies, as well as the study of dislocation substructures generated by fatigue.

Foils were obtained from the tested specimens by slicing wafers perpendicular to the stress axis with a water-cooled diamond saw. These wafers were then mechanically polished through 600 grit SiC paper until a thickness of 0.15 mm was obtained. Next, the disks were ultrasonically cleaned in acetone to remove any adhesives.

An E.A. Fischione twin jet electropolishing apparatus was used to perforate and thin the foils electrochemically. The thinning solution was similar to the electrolyte used for electropolishing. A solution of 20% H_2SO_4 in methanol at $0^{\circ}C$ proved acceptable for all three alloys. However, polishing conditions varied depending on the specific material. Speeds of 5 with a potential of 80 V were generally the conditions used.

The thin foils were examined on two microscopes, a JEOL-100C and a JEOL-100S. Both operated at an accelerating voltage of 100 kV.

PART 4

RESULTS

4.1 Microstructure

Initial examination of the longitudinal structure of the directionally solidified ingots generally revealed several distinct regions. A few of these regions may be seen in Fig. 7 for the Nitac 14B alloy. A blocky carbide region exists at the base, as shown in Fig. 7a. Dense, hypereutectic carbides which have a high melting point, precipitate out and settle to the bottom of the ingot. This carbide region corresponds to the molybdenum sort-out zone in the directionally solidified Ni-Al-Mo ingots where the lack of carbon precludes the precipitation of carbides.

A transition zone consisting of TaC carbide dendrites (see Fig. 7b) occurs before a well-aligned structure is achieved. Fig. 7c shows the start of the aligned region. The test ingots usually contained approximately 19 cm of well-aligned fibrous structure. The degree of alignment decreases as the uppermost portion of the ingot is approached. Another dendritic zone is observed at the top. This is due to the decrease in thermal gradient in front of the solid-liquid interface, which also causes a drop in the $\frac{G}{R}$ ratio.

Fig. 8 shows well-aligned, transverse microstructures of Nitac 14B, Cotac 744 and AG-170. Nitac 14B and Cotac 744 (see Fig. 8 a and b) have very similar structures consisting of carbide fibers, which

35
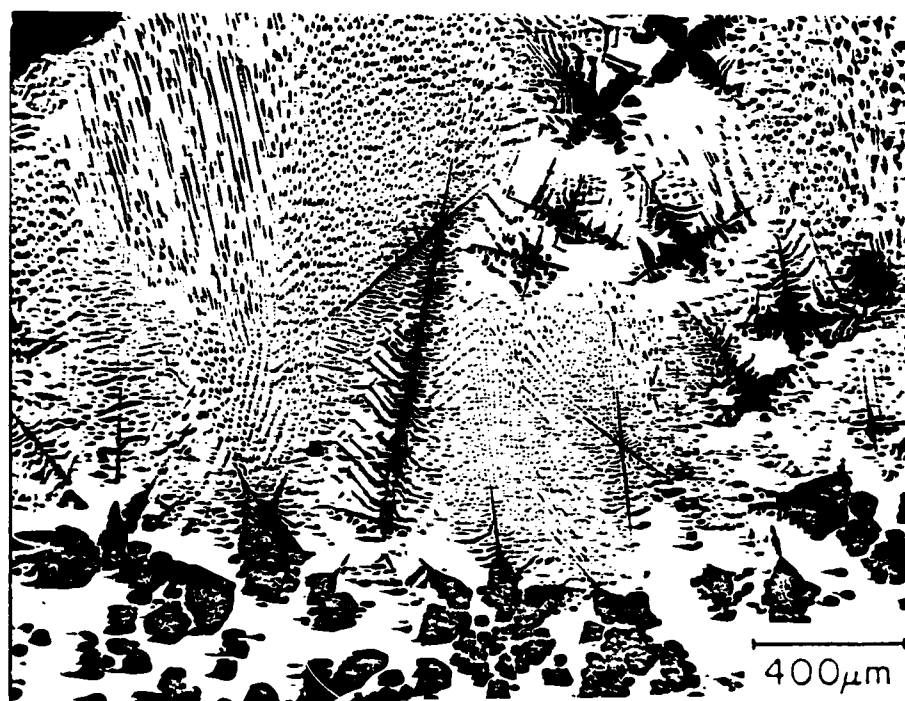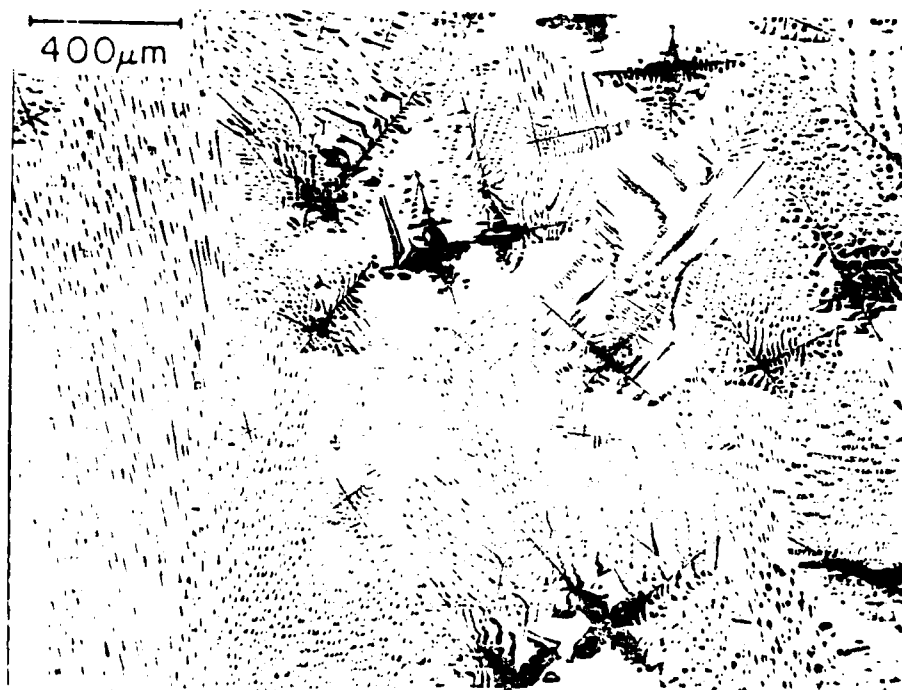
Fig. 7   Longitudinal section of a directionally solidified Nitac
          14B ingot. (a) Blocky carbides. (b) Transition zone.

400μm
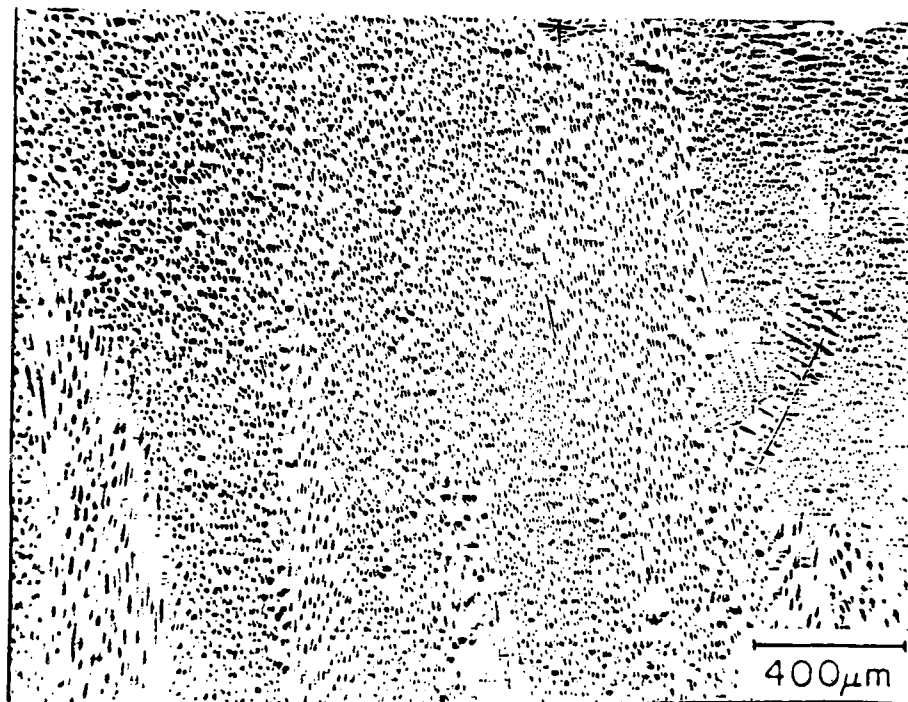
(c)

Fig. 7   Longitudinal section of a directionally solidified Nitac
           14B ingot. (c) Aligned section.
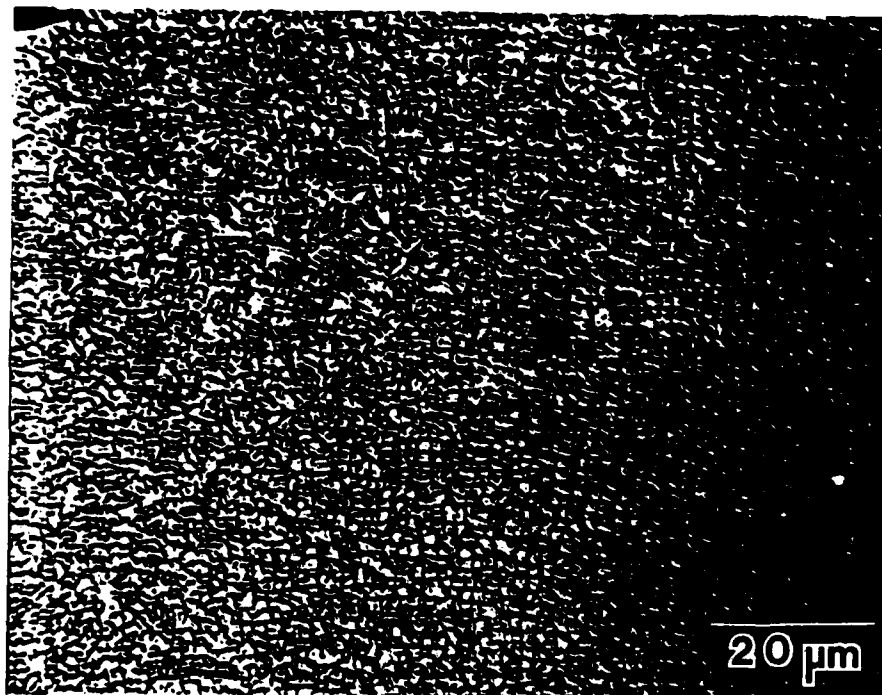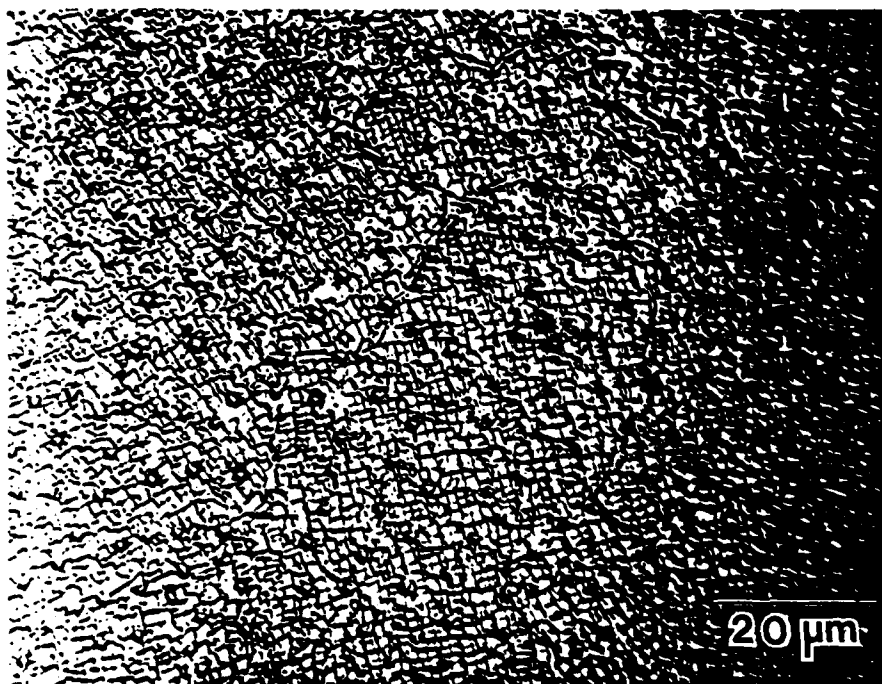
Fig. 8   Well-aligned, transverse microstructures.   (a)   Nitac 14B.
          (b)   Cotac 744.
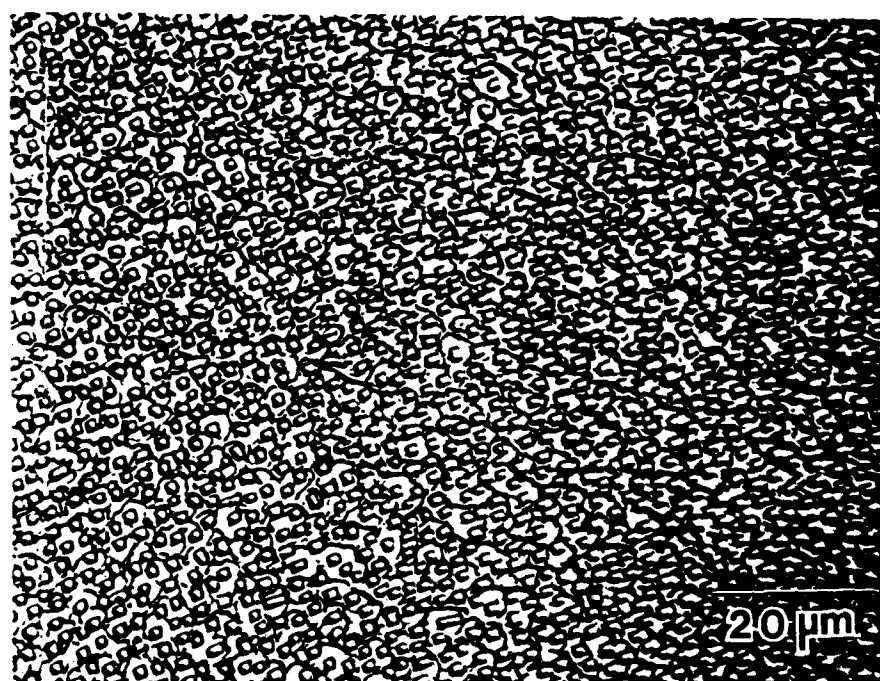
(c)

Fig. 8 Well-aligned, transverse microstructures. (c) AG-170.

are practically square in cross section, in a γ/γ' matrix. Fine γ' is distributed between the reinforcing fibers. The NbC-reinforced alloy has a slightly greater fiber volume fraction than Nitac.

The microstructure of AG-170 (Fig. 8c) consists of 3 phases. The α-Mo is the square fibrous phase. The fibers are surrounded by γ' (the light grey phase) which is interspersed in the γ matrix (the black phase). AG-170 clearly shows a much larger volume fraction of fibers than either Nitac 14B or Cotac 744. The α-Mo volume fraction is between 25 and 30 percent, whereas the carbide phase only occupies 3 to 5 percent of the volume in the carbide-reinforced eutectics. This difference in fiber volume fraction is also evident upon examination of the well-aligned longitudinal microstructures. These are shown in Fig. 9.

The Mo-fibers shown in Fig. 8c are approximately square in cross section. However, the fiber shape varied as different areas of the transverse slice were examined. Some regions showed elongated fibers almost lamellar in nature. This is not unexpected since a fibrous-lamellar transformation is known to occur near a fiber volume fraction of 20.

AG-170 also exhibited the most irregularity in structure. Nitac 14B and Cotac 744 had only several cells per transverse section. The microstructure of AG-170 often appeared cellular with boundaries resembling those shown in Fig. 10. This tendency towards cellularity made it difficult to distinguish between aligned and unaligned structures. Researchers at G.E.[22] have also observed this tendency and,

(a)

40 µm
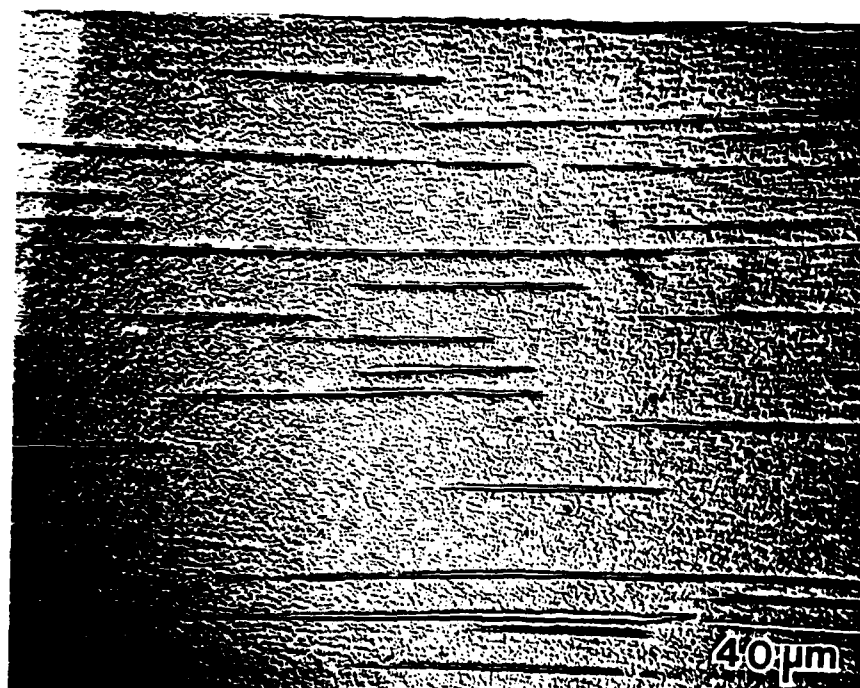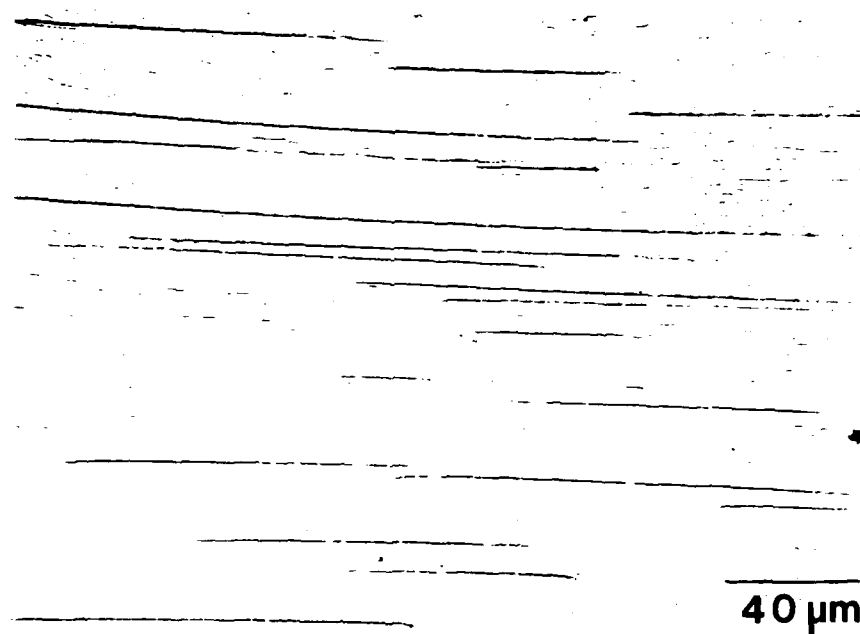
(b)

Fig. 9   Well-aligned, longitudinal microstructures.   (a)   Nitac 14B.
           (b)   Cotac 744.
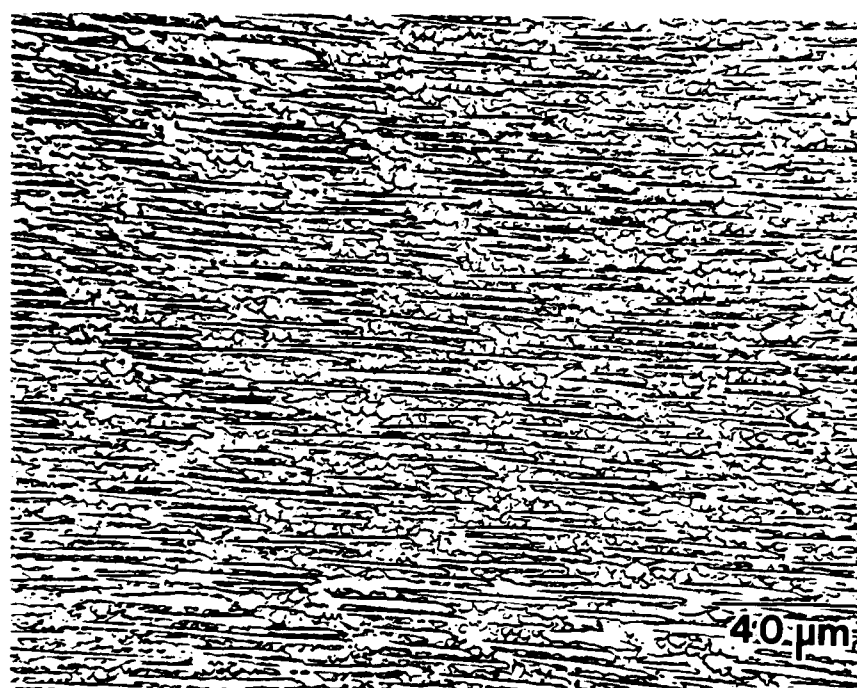
(c)

Fig. 9 Well-aligned, lonᵤitudinal microstructures. (c) AG-170.
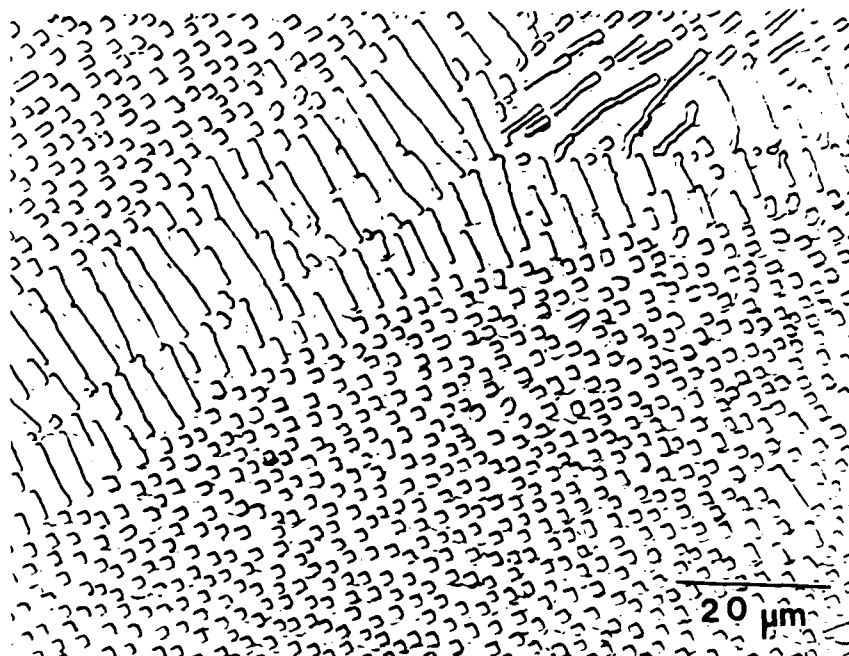
Fig. 10   Transverse view of cellular AG-170 showing breakdown in
           structure at the boundary.

therefore, have established a rating system for determining the degree of alignment in AG-170. However, the rating system depends upon an assumption of uniformity within the aligned section of the ingot. Our results cast doubt on this point.

Heat treatments were performed to alter the microstructure and, hence, increase the strength of these alloys. All three of the eutectics under investigation were responsive to conventional heat treatments. Heat treatments changed the size morphology and distribution of the γ'.

A two stage heat treatment was utilized in all cases. Partial solution treatment of Cotac 744 and Nitac 14B at 1200°C, followed by an ice brine quench, caused fine γ' particles to precipitate. These γ' particles are evident in Fig. 11a for Nitac 14B. An aging treatment of 4 hours in vacuum at 850°C was then given to both alloys. This temperature was sufficiently greater than the primary test temperature of 825°C. Aging was found to increase the uniform γ' distribution. Also, the gamma prime particles were observed to encase the cell boundaries, as illustrated in Fig. 11b.

TEM examination using diffraction revealed that heat treated structures of Nitac and Cotac to form a typical γ/γ' network. Fig. 12 shows the as D.S. and heat treated structures of Nitac 14B. These microstructures are also representative of Cotac 744. In the as D.S. condition, the microstructure consists of blocky γ' particles in the γ matrix (see Fig. 12a). The dislocations are concentrated in the γ phase. Solutionizing causes the γ phase area to increase, while the
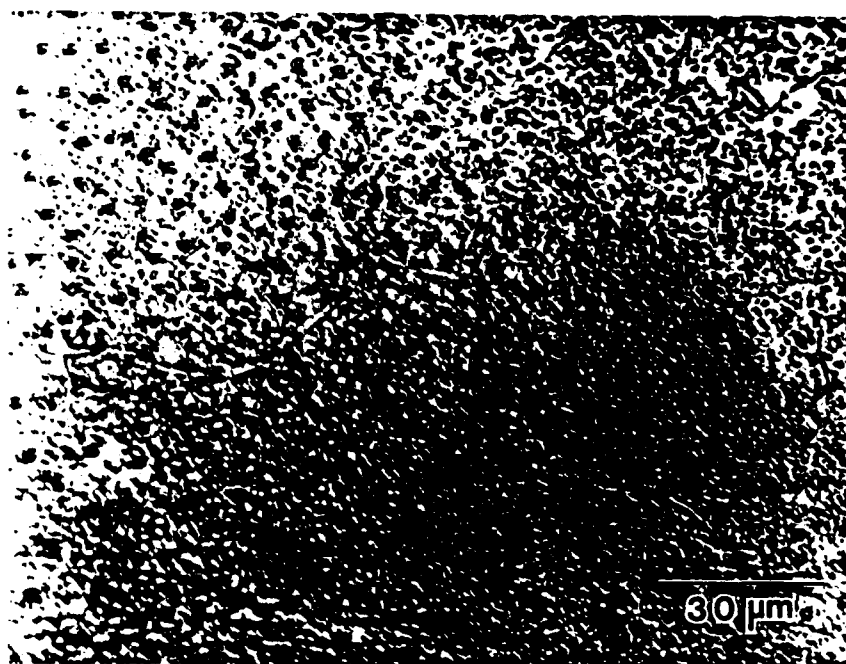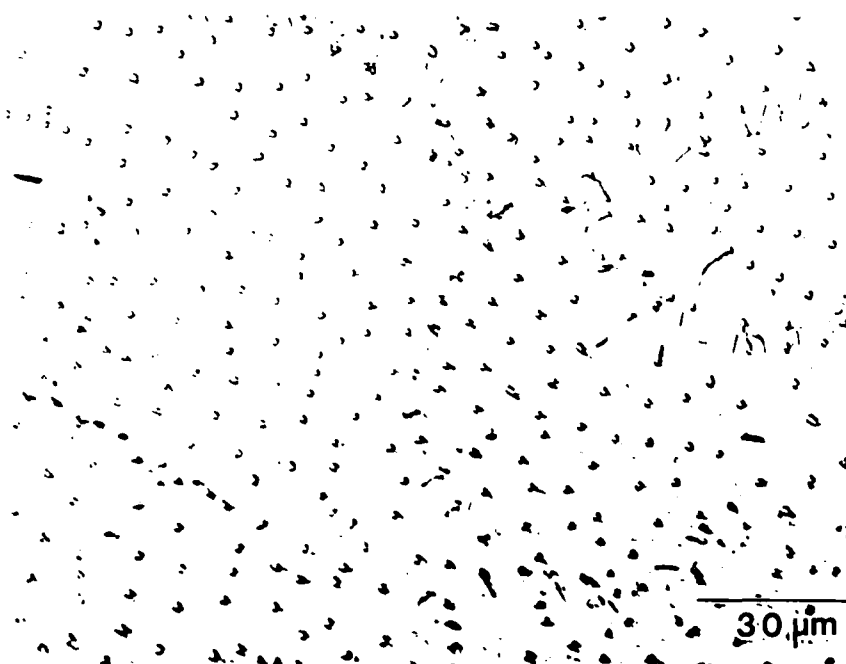
Fig. 11   Transverse microstructures of heat treated Nitac 14B.
           (a) Partially solutionized. (b) Aged.
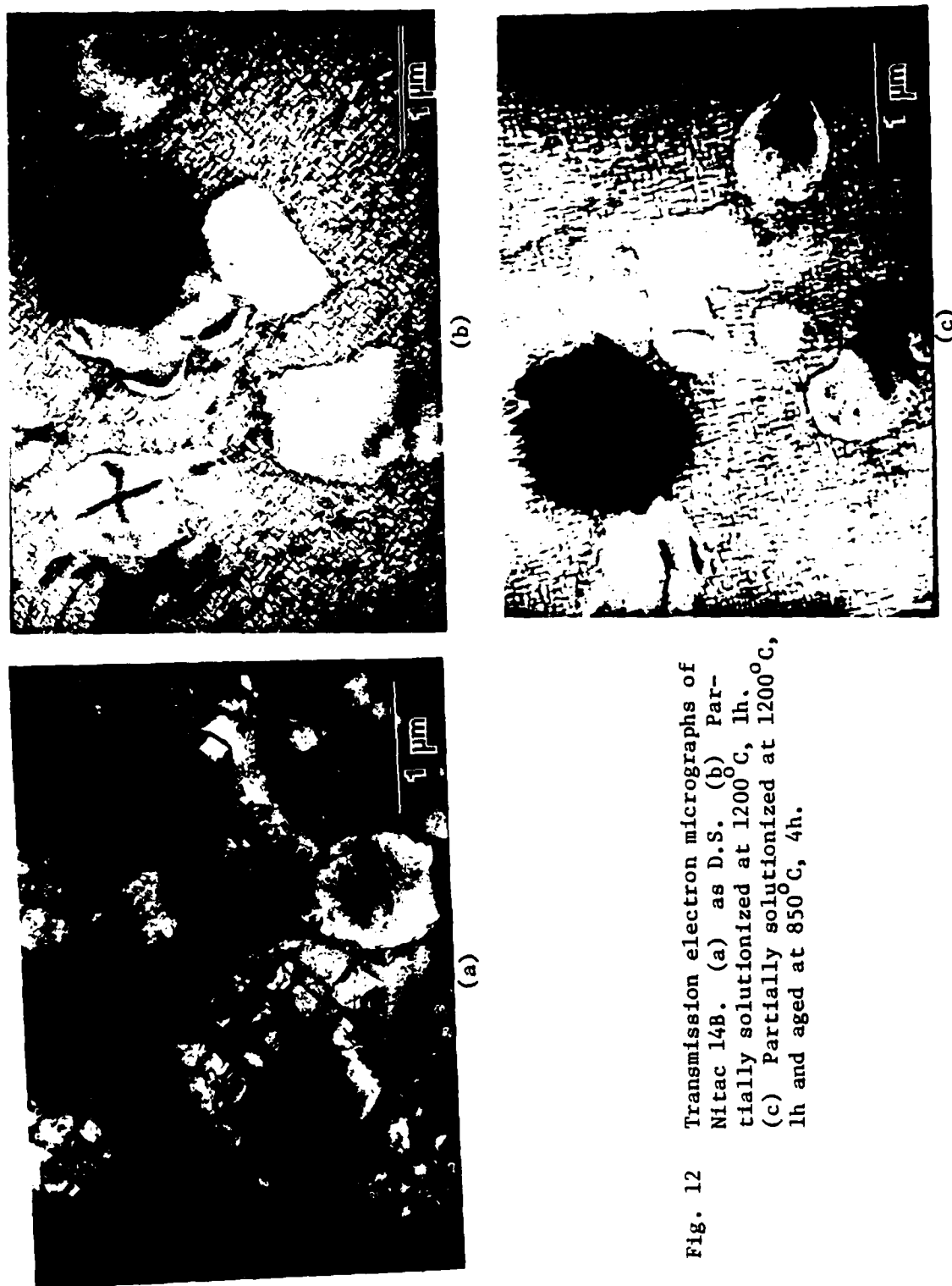
Fig. 12 Transmission electron micrographs of Nitac 14B. (a) as D.S. (b) Partially solutionized at $1200^{\circ}C$, 1h. (c) Partially solutionized at $1200^{\circ}C$, 1h and aged at $850^{\circ}C$, 4h.

overall structure remains typical of γ/γ'. Small squares of γ' phase are surrounded by γ phase as shown in Fig. 12b. Aging, even for as long as 24 hours, does not have a radical effect on the structure. The aged structure remains similar to the solutionized one. However, small precipitates were observed to form in the γ' phase as illustrated in Fig. 12c.

As mentioned earlier, AG-170 is noted for its strong response to heat treatments. This response was verified in the subsequent study. Significant changes in γ/γ' morphology occurred as a result of prolonged exposure at elevated temperatures.

The as D.S. microstructure of AG-170 is shown in Fig. 13a and consists of square molybdenum fibers in a γ' matrix, with the γ phase randomly distributed throughout the matrix. A two stage heat treatment was employed once again to change this morphology. Solutionizing at $50^{\circ}C$ below the melting point (i.e., $1300^{\circ}C$) for 4 hours caused the molybdenum fibers to transform from a rectangular to an octagonal shape. This transformation may be seen by comparing Fig. 13 a and b. Fig. 13b also illustrates the regular cubic γ' morphology which was attained after the solution treatment. A pure γ' phase now exists around each fiber, while the dark γ phase is interspersed among the γ' cuboids.

Aging in vacuum for 4 hours at $850^{\circ}C$ caused a new phase to precipitate. Fig. 13c depicts the precipitates which were formed in the γ' phase after a 24 hour aging treatment. The dark field image, Fig. 13d, gives an even clearer view of these elliptical precipitates.
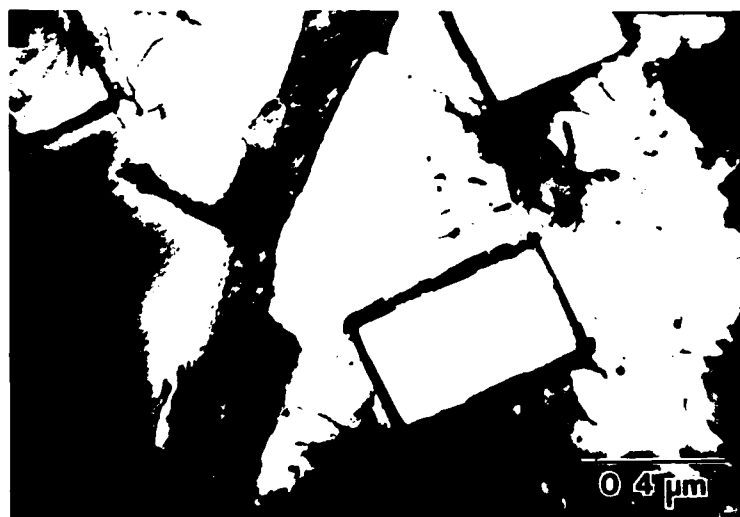
(a)

(b)

Fig. 13 Microstructures of AG-170. (a) As D.S. (b) Partially
solution treated at 1250°C, 4h, showing cuboidal γ/γ' net-
work and denuded zone around fibers.
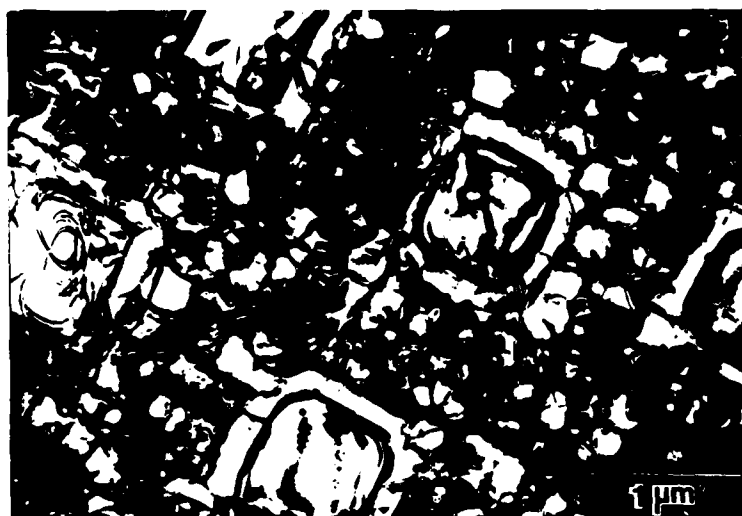
(c)

(d)

Fig. 13   Microstructures of AG-170. (c) Partially solutionized and
aged 4h at 850°C. (d) Dark field image accentuating Mo-
rich precipitates of (c).

The denuded zone around the fibers is observed to remain precipitate free. Ishii et al.[17] have observed similar structures for a heat treated AG-34 alloy. In their study they identified this elliptical precipitate as molybdenum rejected from γ'.

Heat treatments for each of the three aligned eutectics used in this fatigue study were chosen on the basis of optical and transmission electron microscopy. The results of hardness tests on each alloy after various heat treatments were used as an additional factor in the selection of optimum heat treating conditions.

Table II lists the results for Nitac 14B, Cotac 744 and AG-170. Solutionizing substantially increased the hardness in all cases. However, AG-170 showed the most significant increase after partial solution treatment. Its hardness increased by 26% over the as D.S. value. Subsequent aging at 850°C caused various hardness changes. For AG-170, aging for any length of time caused a hardness increase over the solutionized condition. Nitac 14B exhibited its minimum hardness after a 2 hour age while the hardness of Cotac 744 showed an initial drop after aging for 1 hour. Aging for longer time periods brought about a peak in hardness values. The three in-situ composites all achieved maximum hardness after 4 hours of aging. Thus, partial solution treatment followed by a 4 hour age was chosen as the optimum heat treatment condition.

Varying aging times did not cause considerable changes in microstructure. In fact, Nitac 14B showed hardly any structural changes. Cotac 744 and AG-170, however, exhibited slight variations in structure.

Table II

Vickers hardness values for Nitac 14B, Cotac 744 and

AG-170 in various heat treated conditions

CONDITION	VHN, 10 kg load		
	Nitac 14B	Cotac 744	AG-170
As D.S.	409	381	376
Partially Solution Treated*	477	419	473
Partially Solution Treated + 1h Age**	479	407	510
Partially Solution Treated + 2h Age	467	430	478
Partially Solution Treated + 4h Age	502	444	530
Partially Solution Treated + 16h Age	486	407	481

* Partial solution treatments for Nitac 14B and Cotac 744 consisted of heat treating in vacuum at 1200°C for 1 hour. AG-170 was partially solutionized in vacuum for 4 hours at 1250°C. Each was followed by an ice-brine quench.

** Aging treatments consisted of heat treating in vacuum at 850°C in all cases. This was followed by an ice-brine quench.

Greater γ' precipitation was seen in Cotac after 2 and 4 hours of aging. Maximum precipitation in AG-170 corresponded with the hardness peaks. Thus, maximum precipitation was observed after aging for 4 hours.

4.2 Fatigue Results

The results of high cycle fatigue testing of Nitac 14B, Cotac 744 and AG-170 will be presented as S-N plots in the following text. Each data point on the curves represents a single test. Arrows have been used to indicate test termination without failure. A considerable amount of scatter will be noted in several of the curves. This can be attributed to normal fatigue scatter, ingot to ingot fluctuations and microstructural defects which may have been produced during the solidification process.

4.2.1 Temperature Effects

The high cycle fatigue properties of the three nickel-base alloys at room temperature and 825°C are shown in Fig. 14. Nitac 14B appears to be superior at both temperatures. However, at room temperature little difference is noted among the three alloys near the fatigue limit. Fatigue strength showed a marked decrease as the test temperature was raised to 825°C. At this temperature there are distinct differences among Nitac 14B, Cotac 744 and AG-170 at all stress levels. Nitac 14B clearly reveals the highest fatigue resistance, AG-170 the lowest. The difference in stress level between these two alloys near the fatigue limit is approximately 20%.
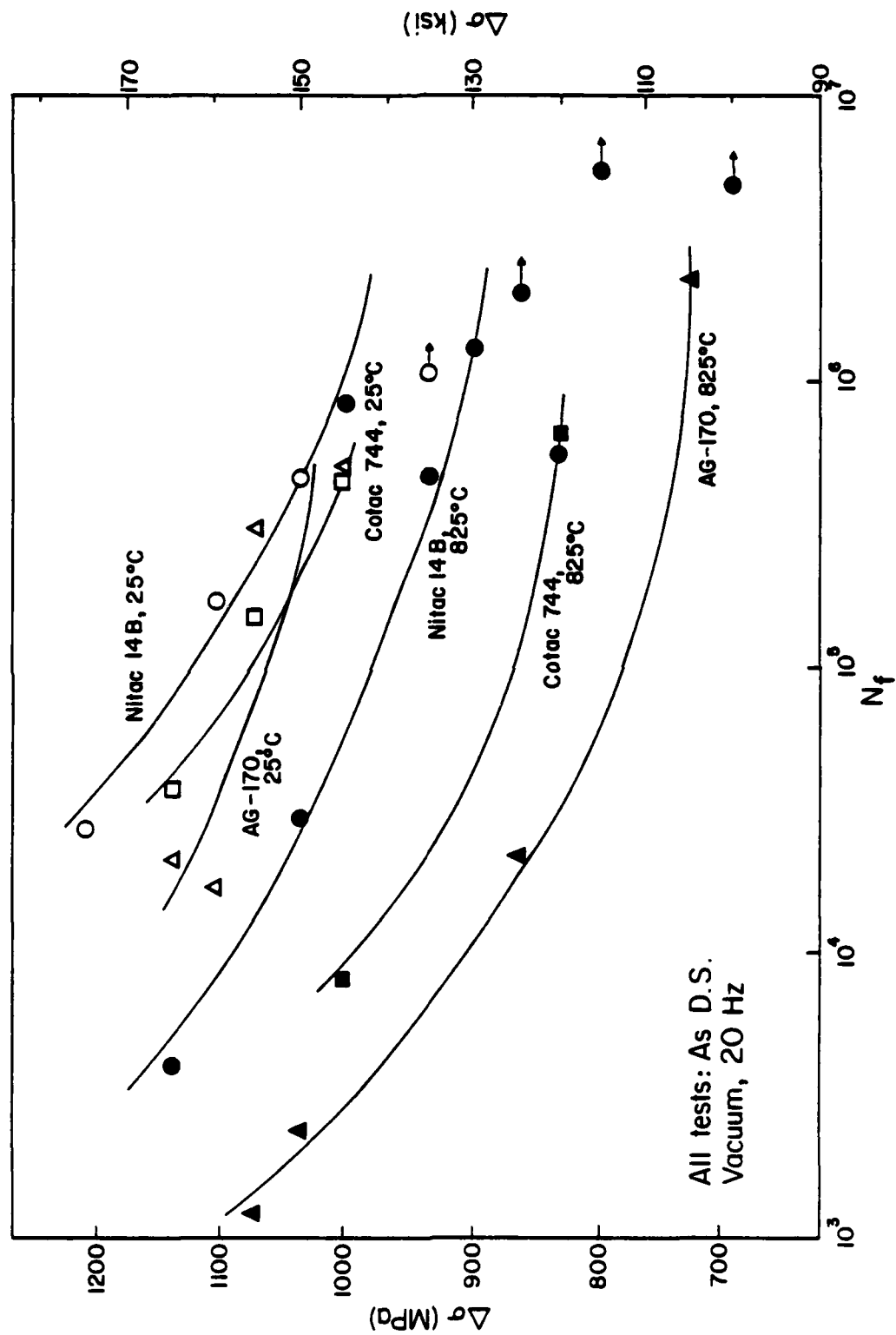
Figure 14 High cycle fatigue properties of the three nickel-base alloys at room temperature and 825°C.

Additional testing was conducted on Nitac 14B at temperatures up to 900°C. At a stress level of 1040 MPa (150 ksi), a near linear decrease was noted in fatigue life with increasing temperature. This effect is shown in Fig. 15.

4.2.2 Post Solidification Heat Treatment Effects

Heat treatment was found to have a significant effect on the fatigue properties of these three alloys, particularly at elevated temperature. A comparison of the room temperature fatigue properties of the three alloys in the aged condition is given in Fig. 16. Nitac 14B is no longer superior; AG-170 exhibits the most improved HCF life of the three after a solutionizing and aging treatment. Nitac 14B and Cotac 744 appear to have comparable lives following this treatment. Fig. 17 compares the results of heat treatment on the elevated temperature fatigue lives of Nitac 14B, Cotac 744 and AG-170. AG-170, previously found to display the worst 825°C fatigue properties in the as D.S. condition, shows the best S-N properties following aging. However, for fatigue lives exceeding 5×10^6 cycles, Nitac 14B is superior, Cotac 744 reveals the lowest fatigue resistance.

Heat treatment greatly enhanced the fatigue resistance of AG-170 at both 25°C and 825°C. Fig. 18 illustrates the significant improvement heat treatment had on the room temperature fatigue properties of AG-170. Partial solution treatment had little effect on fatigue life. Nevertheless, it did substantiate a vast improvement for cellular material where the fatigue life can be seen to increase by at least a factor
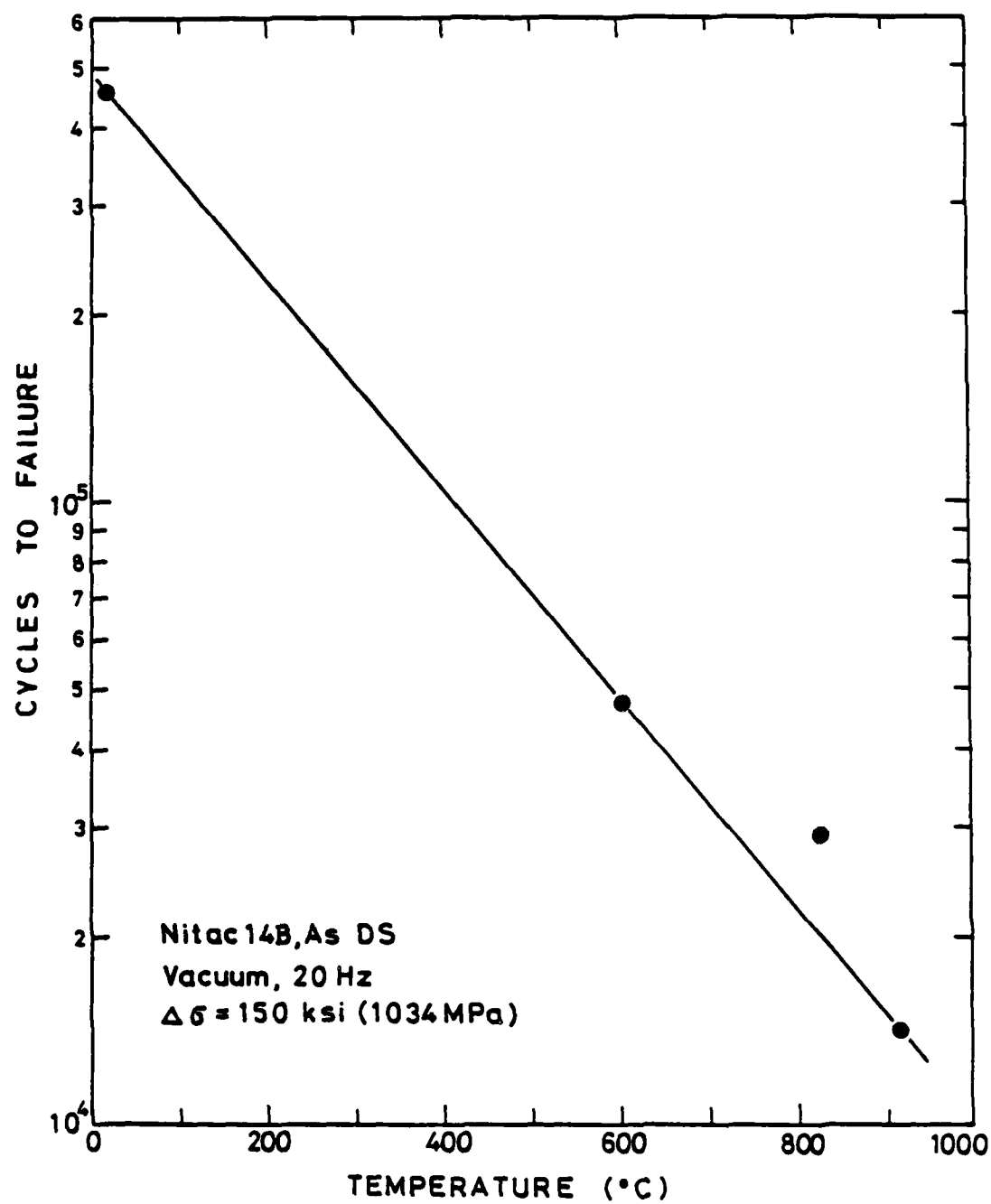
Fig. 15   Effect of temperature on the fatigue life of Nitac 14B
at constant $\Delta\sigma$.
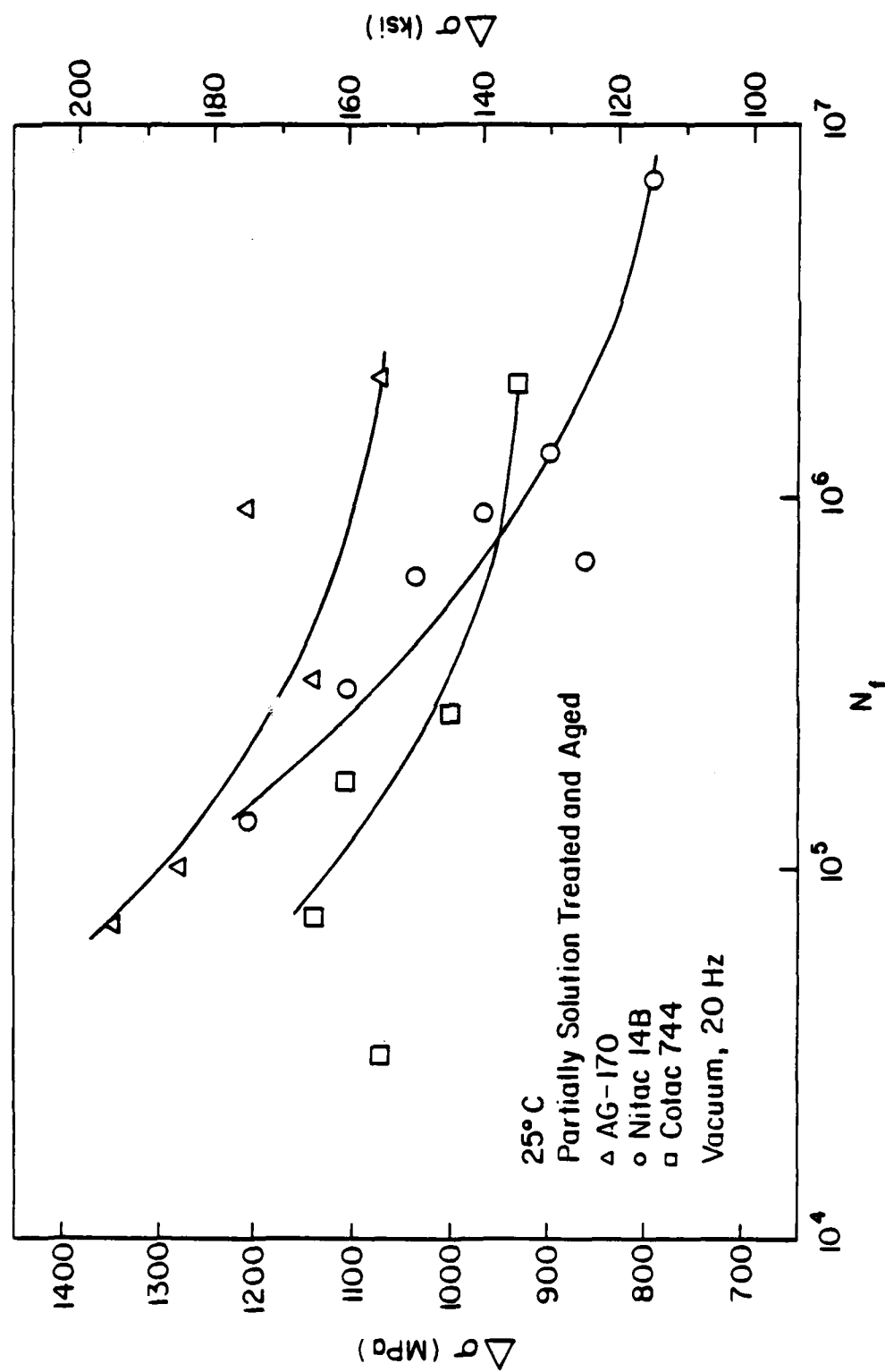
Fig. 16 Effect of heat treatment on the room temperature S-N properties of the three alloys.
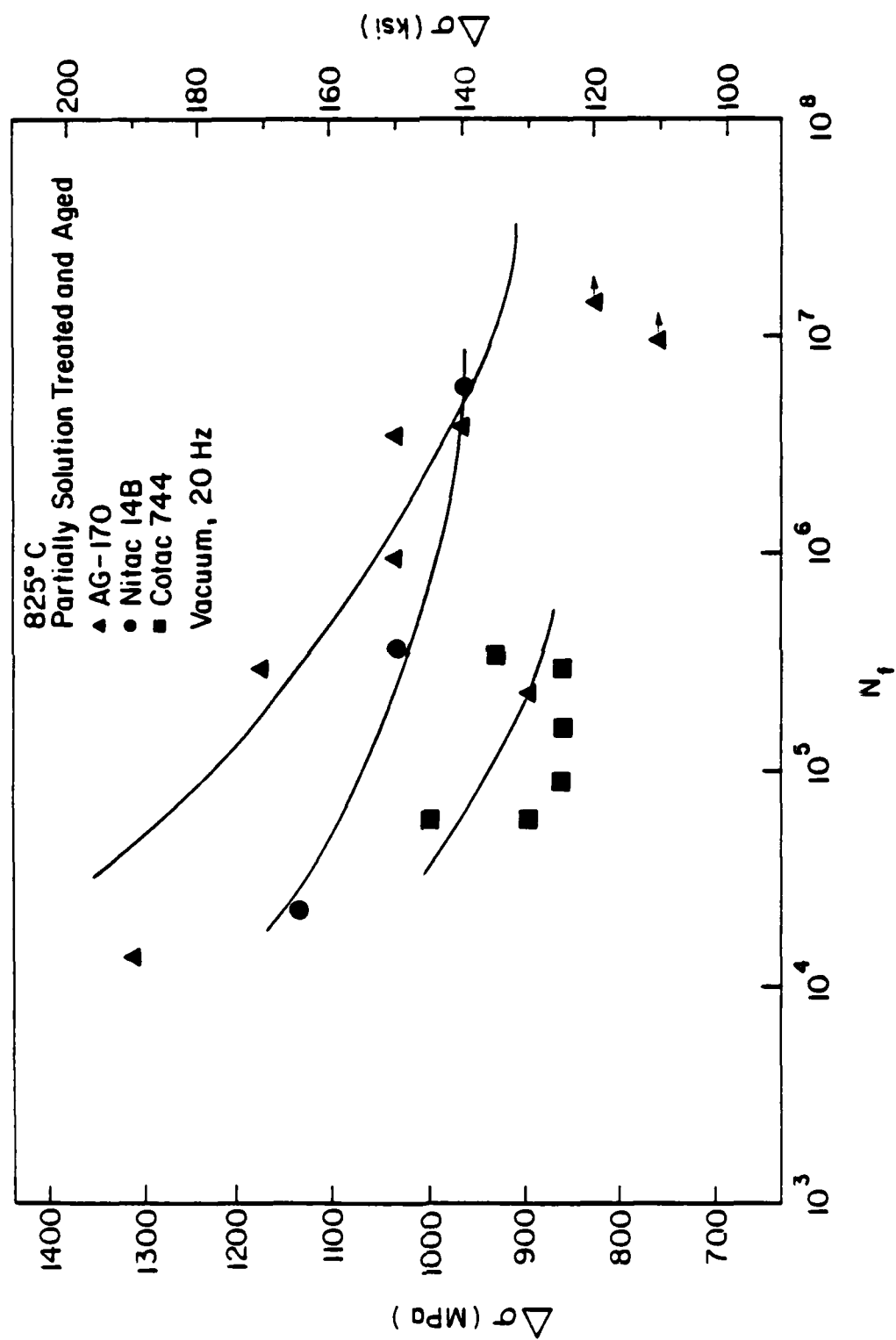
Fig. 17 Effect of heat treatment on the S-N properties of the three eutectics at 825°C.
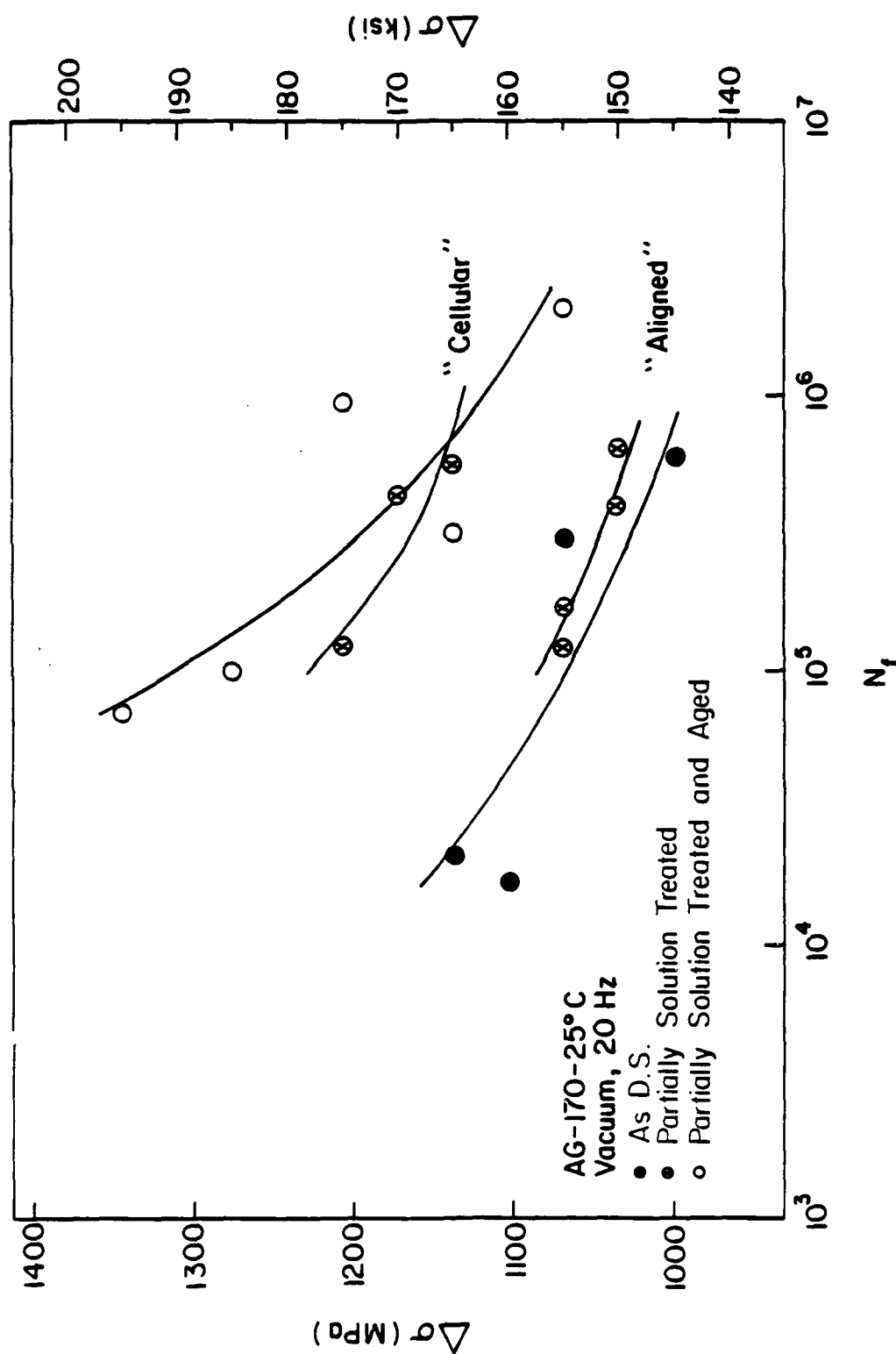
Fig 18 Effect of heat treatment on the S-N properties of AG-170 at 25°C. ("Cellular" material was distinguished by a lack of coherency across cell boundaries and fibers which differed in appearance from the usual rod-like structure.)

of 10. At high stresses, it is evident from this plot that aging had

an even greater effect than solutionizing. The aged material shows a

10% increase in fatigue limit over the as D.S. material. The most sig-

nificant effect on aging is observed at 825°C, as shown in Fig. 19.

From this plot, it can be seen that aging has improved the elevated

temperature fatigue resistance of AG-170 more than two orders of magni-

tude. The room temperature, as D.S. curve has been included for compar-

ative purposes. Comparing this curve with the 825°C plot for partially

solutionized and aged material proves the beneficial effect of heat

treatment at 825°C.

In the case of Nitac 14B, partial solution treatment resulted

in no significant increase in the room temperature HCF life. Subsequent

aging of the partially solutionized material slightly improved the 25°C

fatigue resistance at high stress levels. These results are illustrated

in Fig. 20. It should be noted that there is not a sizable heat treat-

ment effect on the fatigue behavior of Nitac 14B at ambient temperatures.

However, at 825°C the fatigue resistance of the heat treated material

has improved by an order of magnitude over the as D.S. state. The en-

tire heat treated S-N curve has been shifted to the right of the 825°C,

as D.S. curve. This can be viewed in Fig. 21, where the 25°C, as D.S.

results also are plotted. Heat treatments of 825°C specimens gave an

S-N curve approximately equivalent to the room temperature, as D.S. S-N

curve. Fatigue limits for these two conditions were almost identical.

Cotac 744 demonstrated little change in fatigue properties
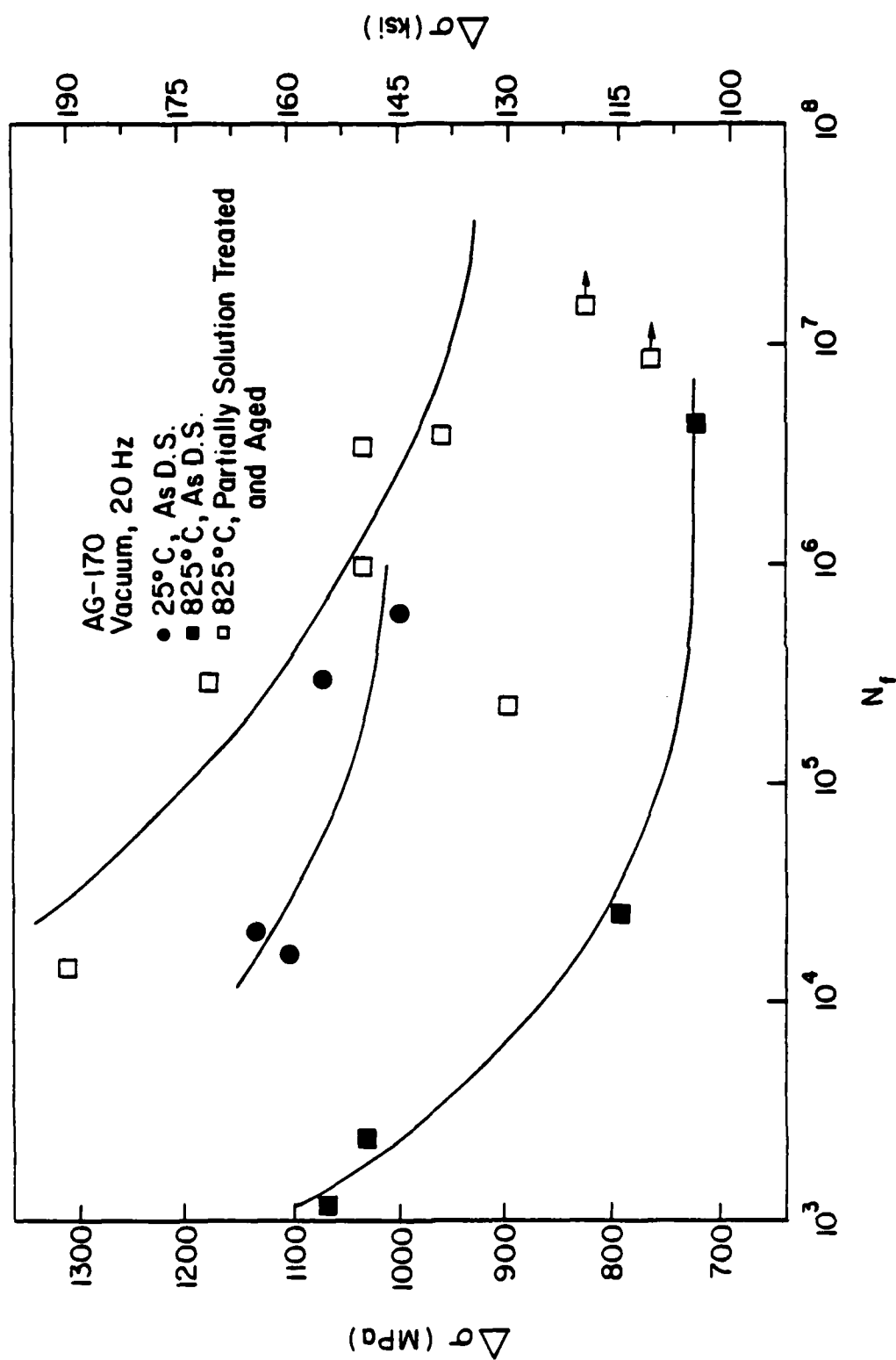
Fig. 19 Effect of aging on the S-N properties of AG-170 at 825°C.

NITAC 14B - 25°C
Vacuum, 20 Hz
• As D.S.
◇ Partially Solution Treated
○ Partially Solution Treated and Aged
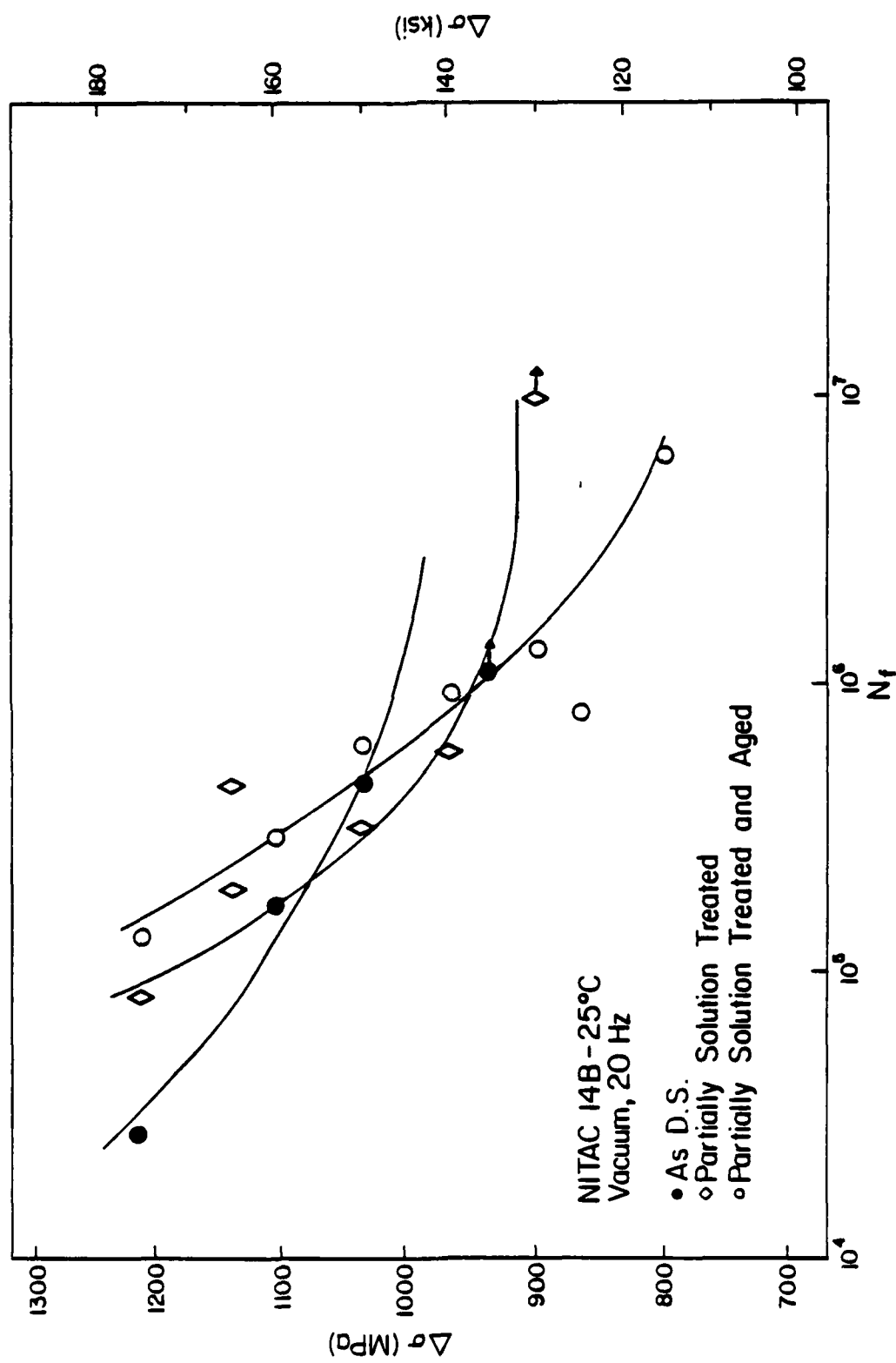
Fig. 20   Effect of heat treatment on the room temperature S-N properties of Nitac 14B.
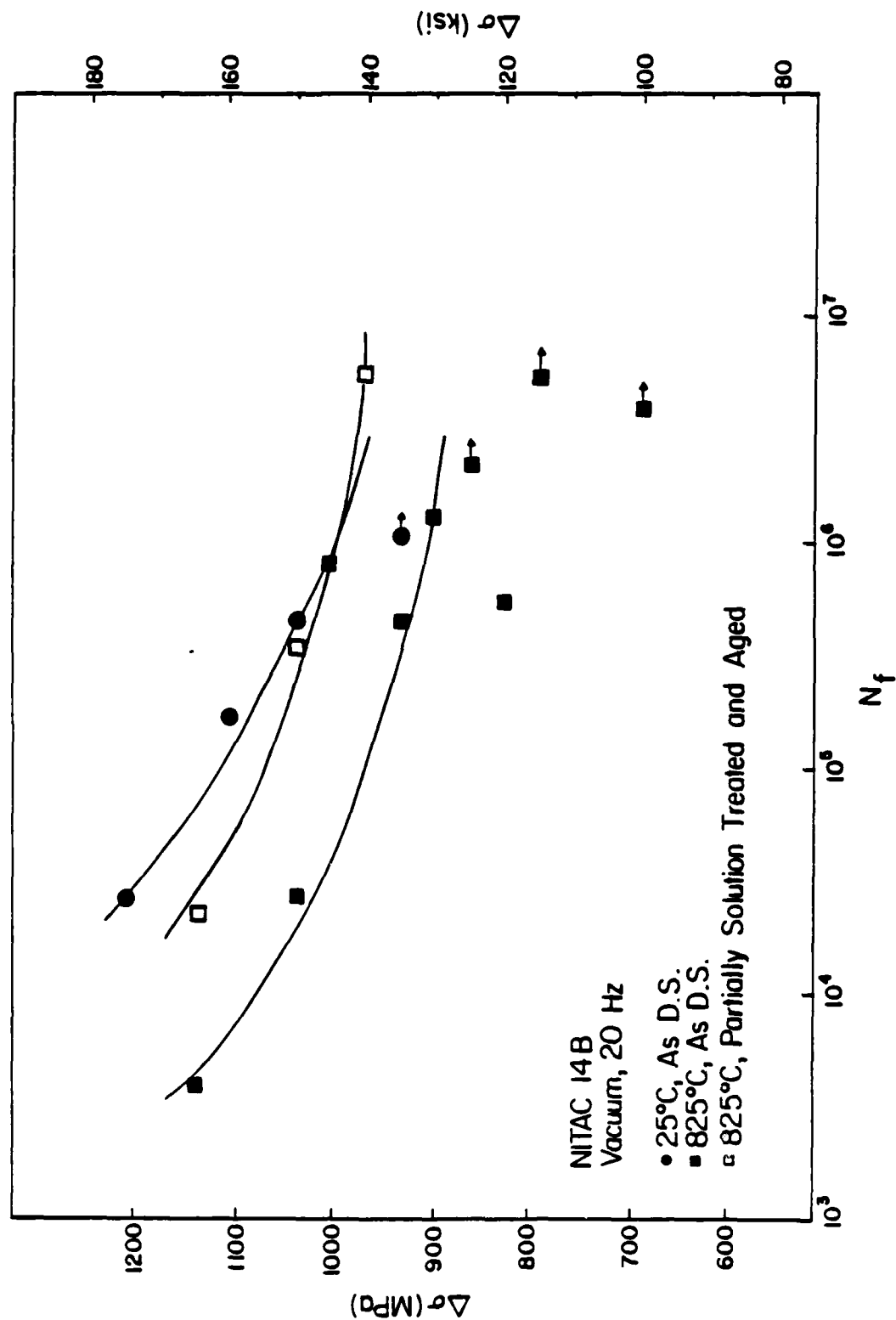
Fig. 21 Effect of aging on the S-N properties of Nitac 14B at 825°C.

following aging treatments. Fig. 22 displays the effects of aging on the 25°C and 825°C fatigue behavior of this alloy. Room temperature tests show little difference between the fatigue resistance of the aged and as D.S. material. Results of high temperature tests indicate a slight improvement after aging. However, it can be seen that several aged specimens had lives which fell on the 825°C, as D.S. curve. The Cotac specimen supply was depleted before a final conclusion could be formulated on the effects of heat treatment at 825°C. Further tests on aged material need to be conducted at 825°C before a more definitive statement can be made on heat treatment effects on this alloy.

4.2.3 Frequency Effects

Fig. 23 shows the effects of frequency on aged Nitac 14B at 825°C in vacuum. Reducing the test frequency from 20 Hz to 2 Hz caused little change in fatigue life. However, a pronounced influence of test frequency on the S-N curve is noted at lower frequencies. Decreasing the frequency from 2 Hz to 0.02 Hz produces a reduction in N_f of at least 1000 times at a constant stress. For example, at a stress level of 965 MPa the number of cycles to failure decreased from 6×10^6 at 2 Hz to 8.5×10^4 at 0.2 Hz and finally to 1.1×10^3 at 0.02 Hz.

Additional tests on as D.S. Nitac 14B at 825°C in vacuum revealed little difference in fatigue life at 20 Hz and 2 Hz. Fig. 24 gives the results of these tests, which were performed at two different stress levels.
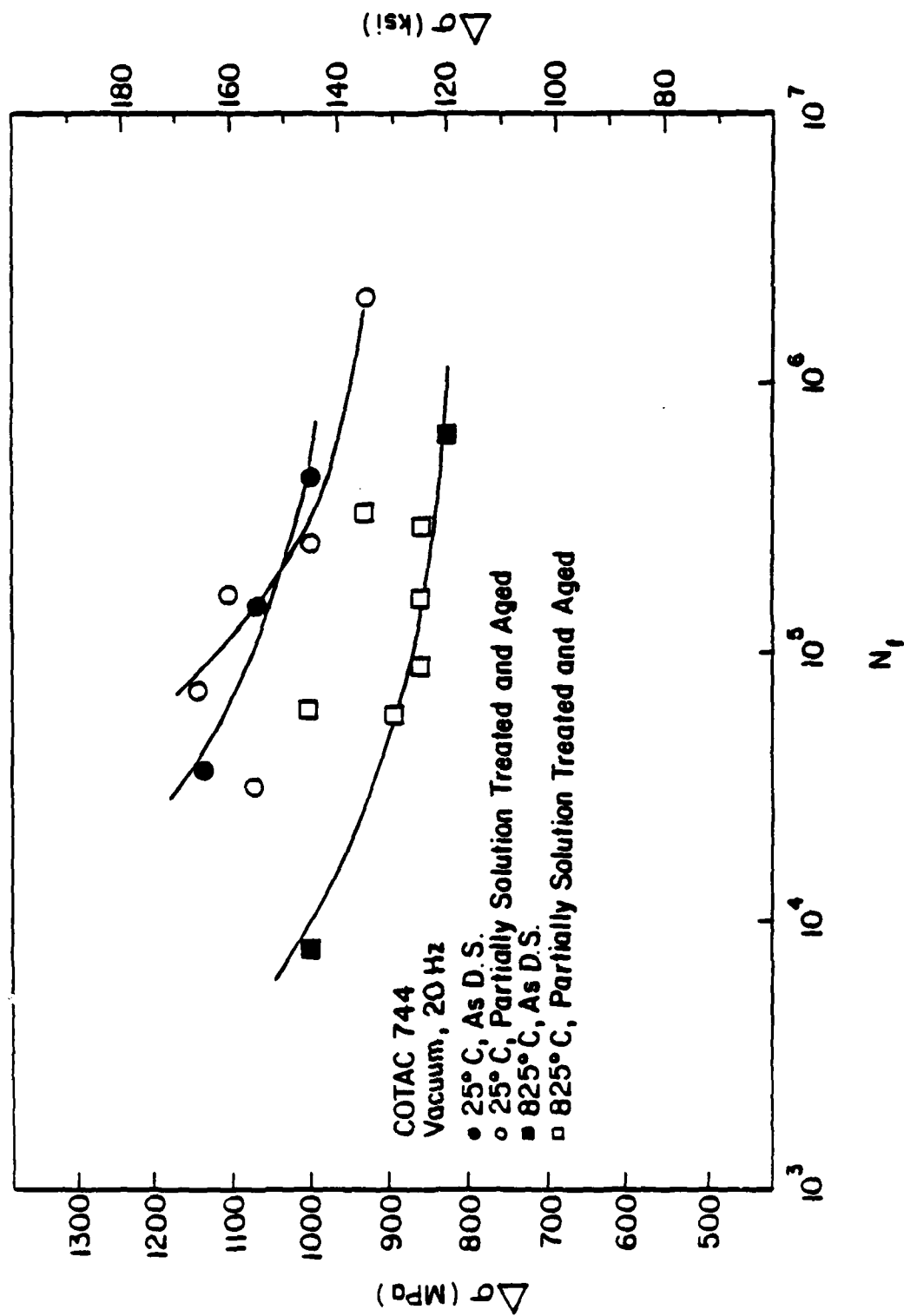
Fig. 22   Effect of heat treatment on the S-N properties of Cotac 744 at 25°C and 825°C.
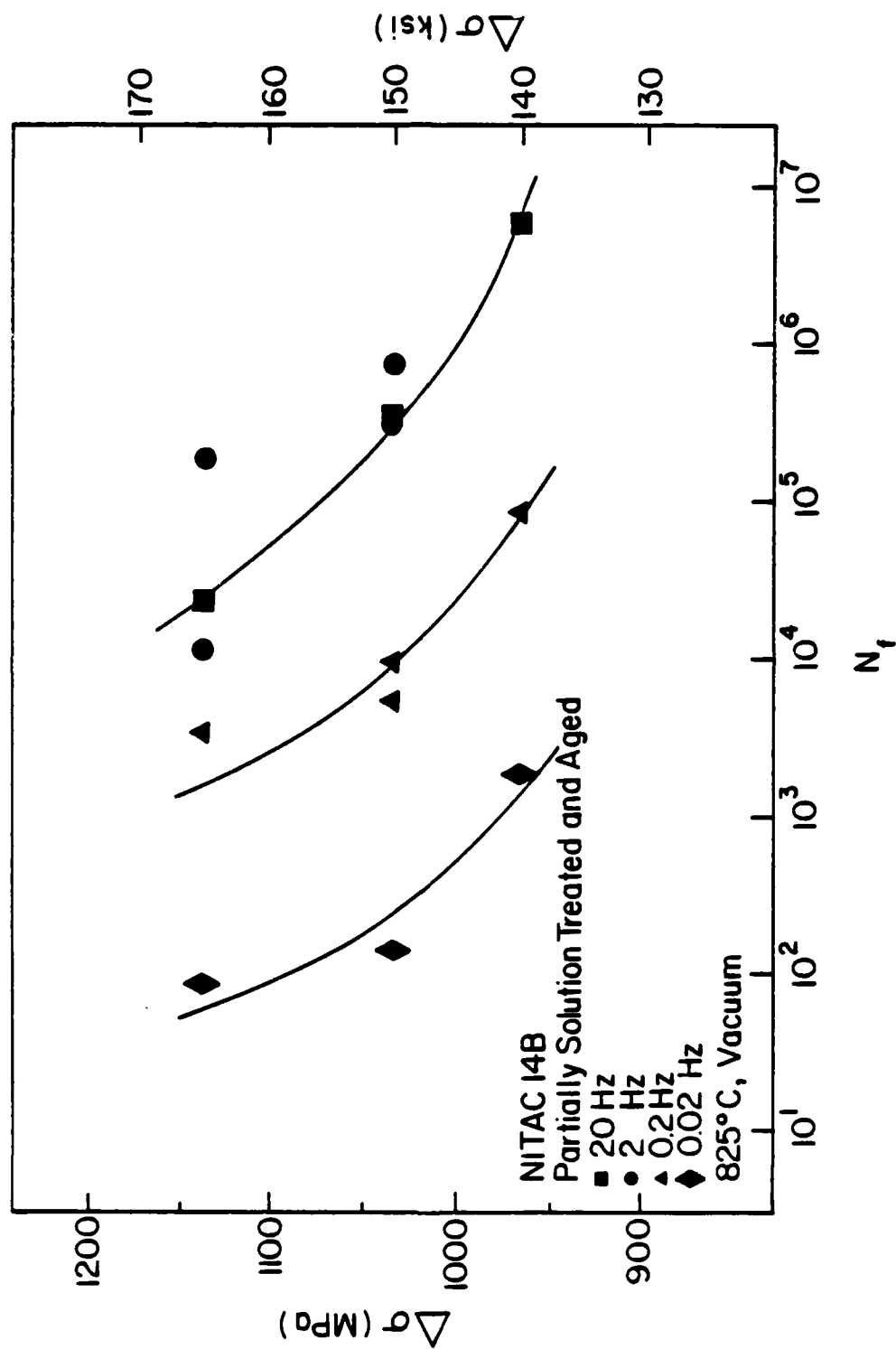
Fig. 23 Effect of frequency on the S-N curve of aged Nitac 14B at 825°C.
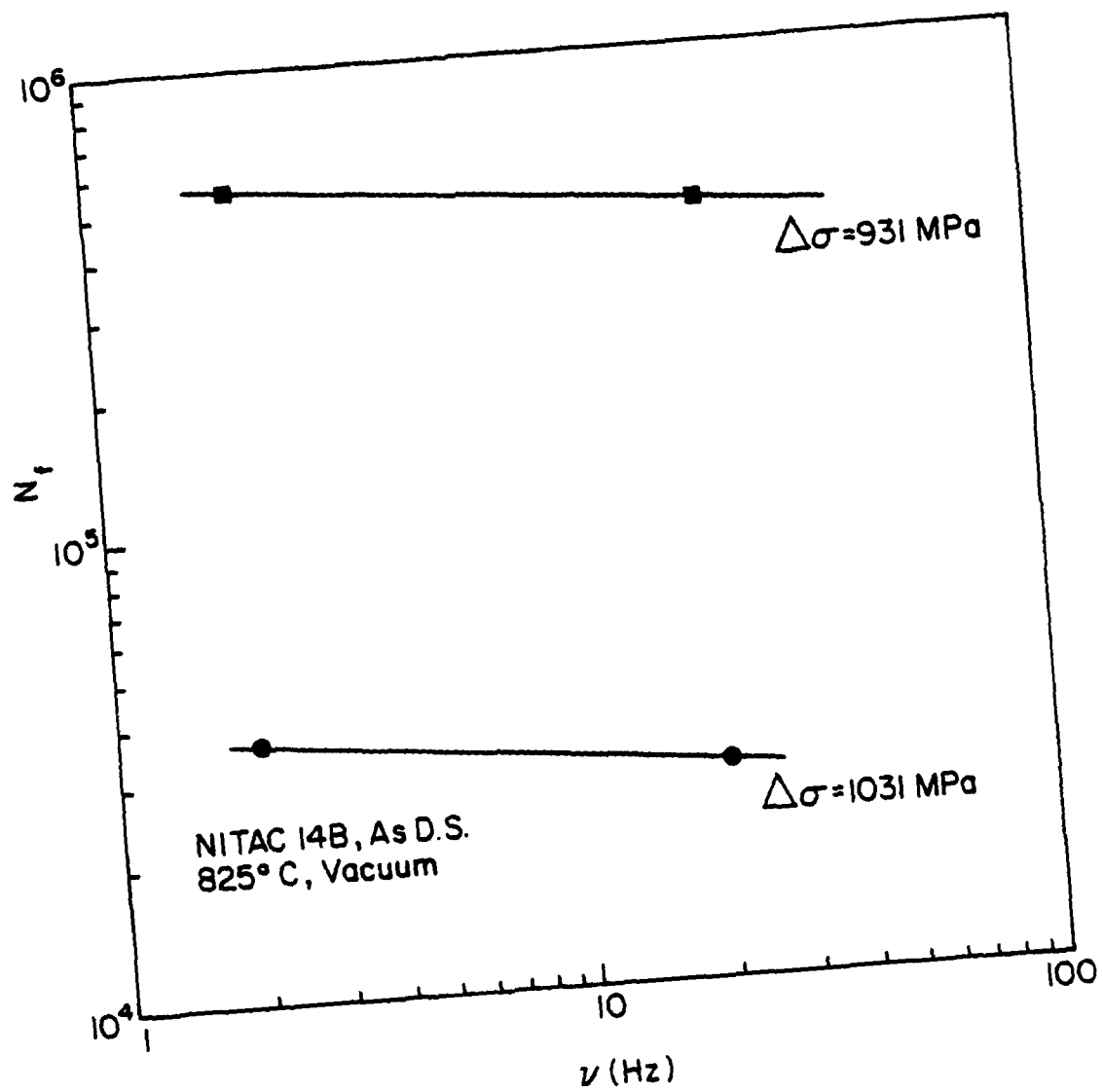
Fig. 24 Effect of frequency on the fatigue life of as D.S. Nitac 14B at 825° C.

4.3 Metallographic, Fractographic and TEM Observations of

Fatigue Failures

4.3.1 Temperature Effects

Fatigue failures of the three alloys at room temperature generally revealed three distinct regions: an initiation site, a fatigue crack propagation zone, and a tensile overload region. These regions are readily identified in Fig. 25 where they are labelled I, F and O. Nitac and Cotac have easily distinguishable zones, unlike AG-170 where the regions are not well-defined.

At 25°C, fatigue cracks in all of the as D.S. alloys initiated at the specimen surface. Fig. 26 depicts a representative surface initiation site in Cotac 744 at $\Delta\sigma = 1000$ MPa after 4.5×10^6 cycles. Upon careful examination, Stage I cracking is visible in both Fig. 25 and 26. AG-170 also shows evidence of Stage I cracking in the vicinity of the surface initiation site. Fig. 27a illustrates a surface initiation site for a specimen stressed at 1100 MPa. Crack propagation can be seen to be along crystal planes. These planes are magnified in Fig. 27b for easier viewing.

This type of crystallographic cracking is characteristic of low temperature fatigue fractures in these alloys. Further evidence of crystallographic cracking was found after close inspection of the sides of the gage section. Fibers were observed to crack along slip bands and follow specific crystallographic planes in Nitac 14B and Cotac 744. AG-170, reinforced by ductile Mo fibers, did not show any

Fig. 25   Fracture profile of room temperature fatigue failure of
           Nitac 14B illustrating three distinct regions: I - initia-
           tion site, F - fatigue zone, O - overload zone.
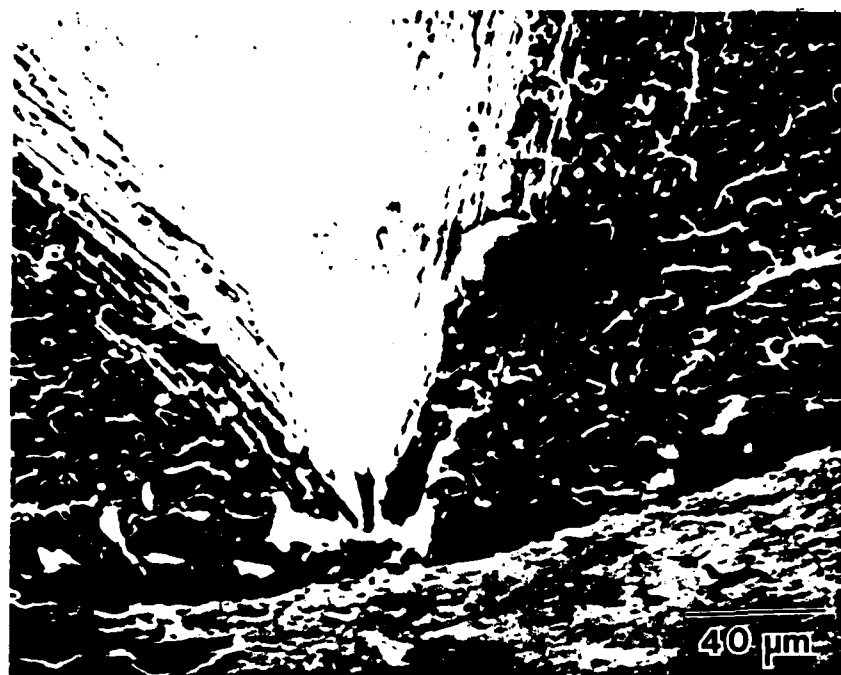
Fig. 26   Surface initiation site in Cotac 744, fatigue tested at 25°C.

(a)

(b)

Fig. 27   Characteristic (a) surface origin and (b) Stage I cracking
for an AG-170 specimen tested at 25°C and $\Delta\sigma$ = 1100 MPa.

surface cracks. These features are shown in Fig. 28.

Although the initial stages of fatigue cracking were thought
to occur by Stage I cracking in all of the alloys, the fatigue zones
varied in appearance. The fatigue zone was faceted in AG-170. Cotac 744
showed a fatigue zone which was flat with shallow dimples, while the cor-
responding regions in Nitac 14B were dimpled. The fatigue zone is the
area of slow crack growth. As the crack front advances into the speci-
men, the mode of cracking changes to Stage II where the crack propagates
normal to the tensile axis. The final fracture occurs by a tensile
overload. Fig. 29a illustrates a dimpled overload zone typical of Nitac
and Cotac. The fibers have fractured by cleavage and are within ductile-
appearing, equiaxed, matrix dimples. Fracture is by a void growth and
coalescence mechanism. In AG-170, however, no dimples are present (see
Fig. 29b). Failure occurs by interfacial debonding and fiber pullout.

Fracture surfaces at $825^{\circ}C$ in each of the as D.S. alloys
showed little difference from those of specimens tested at $25^{\circ}C$. At
$825^{\circ}C$, cracks initiating at the surface were only identified unambigous-
ly in Nitac 14B (see Fig. 30a). However, AG-170 revealed signs of sur-
face initiation like that shown in Fig. 30b. Many of the as D.S. AG-170
specimens which were fatigue tested at $825^{\circ}C$ did not provide useful data
due to the presence of dendrites on the fracture surface, as shown in
Fig. 31. Note the breakdown in microstructure in the vicinity of the
dendrites in Fig. 31b. Defects in microstructure, in these dendrites,
were thought to arise from improper solidification techniques and
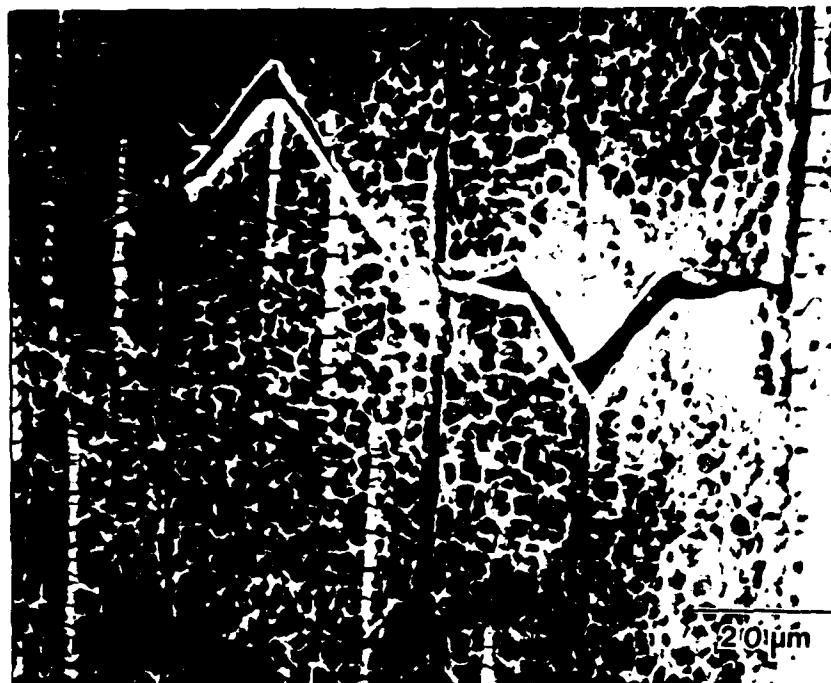
(a)
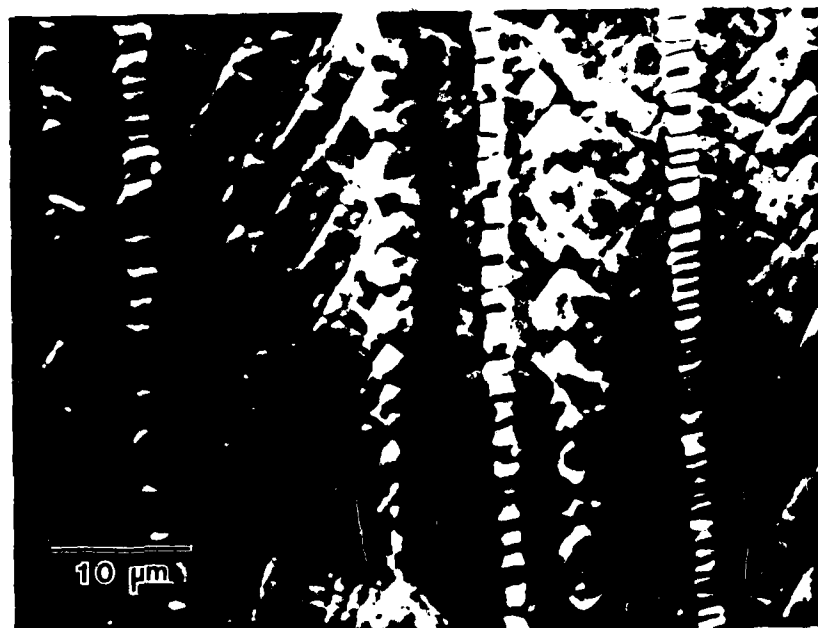
(b)

Fig. 28   Side surfaces of (a) Nitac 14B, (b) Cotac 744, after room
temperature fatigue, showing crystallographic cracking only
for the carbide-reinforced eutectics.

(c)

Fig. 28 (c) Side surfaces of AG-170 after room temperature fatigue, showing crystallographic cracking only for the carbide-reinforced eutectics.
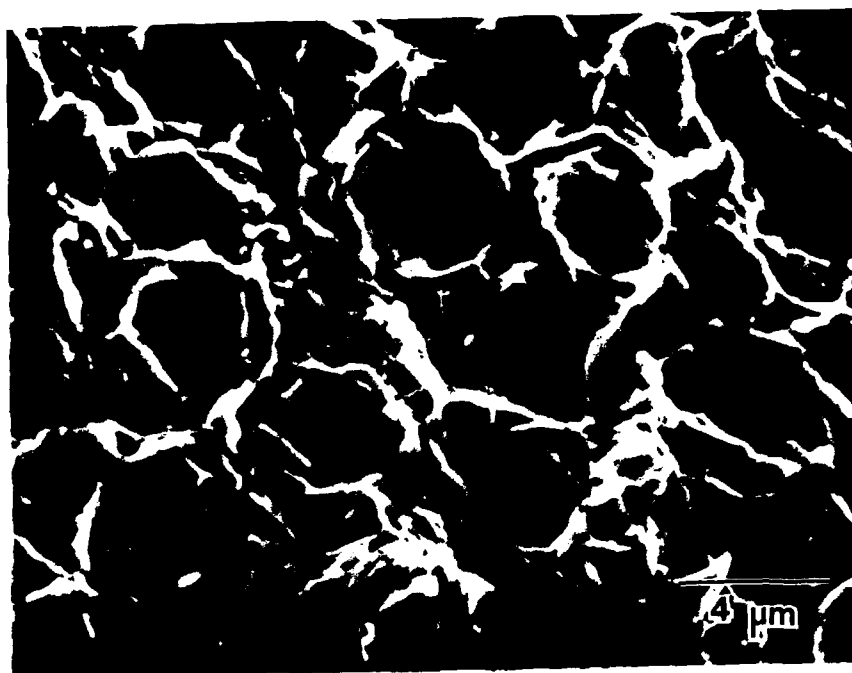
(a)

(b)

Fig. 29   SEM fractographs of typical overload regions in (a)   the
carbide-reinforced eutectics (Cotac 744, in this instance)
and (b) AG-170.
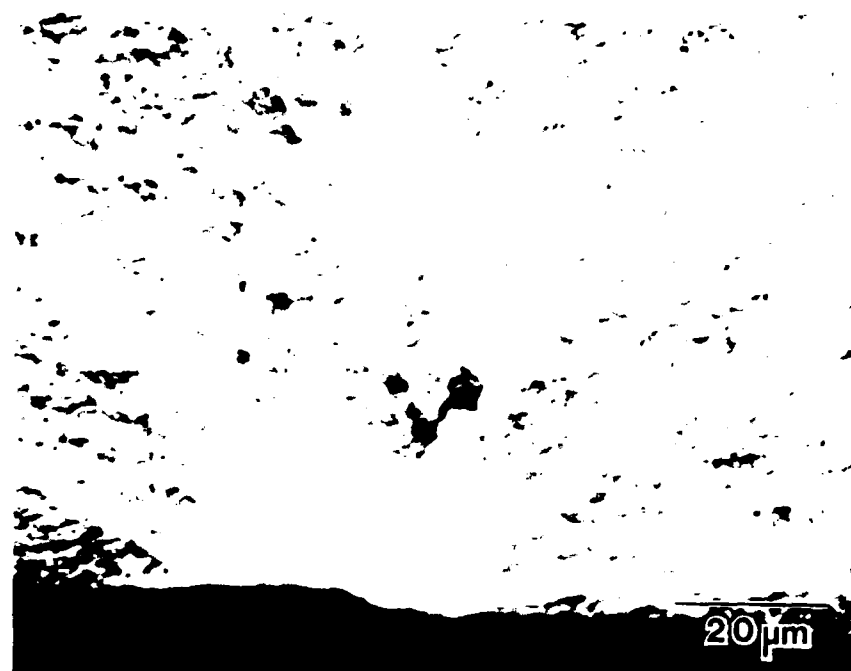
(a)

(b)

Fig. 30 Surface initiation sites in (a) Nitac 14B and (b) AG-170 at 825°C.
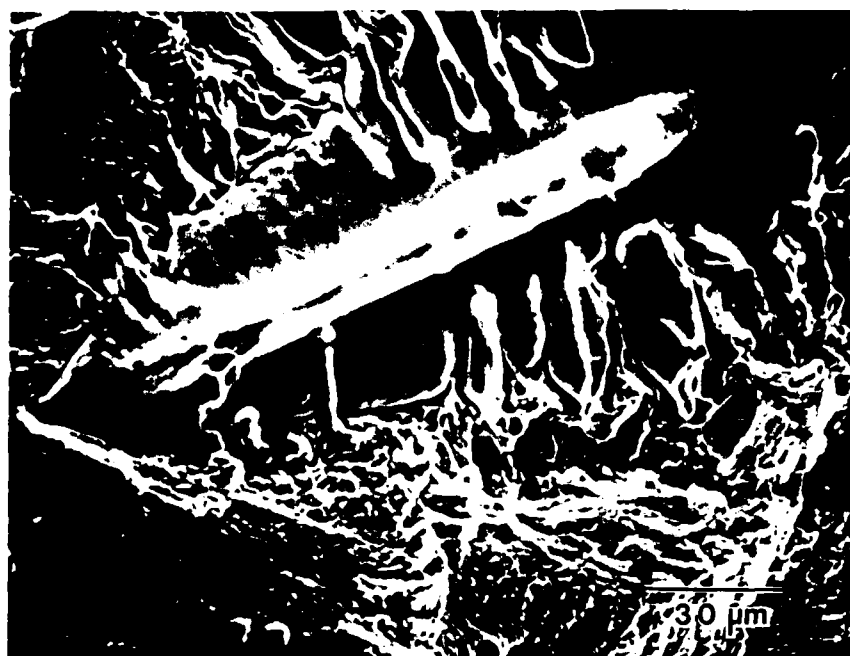
(a)
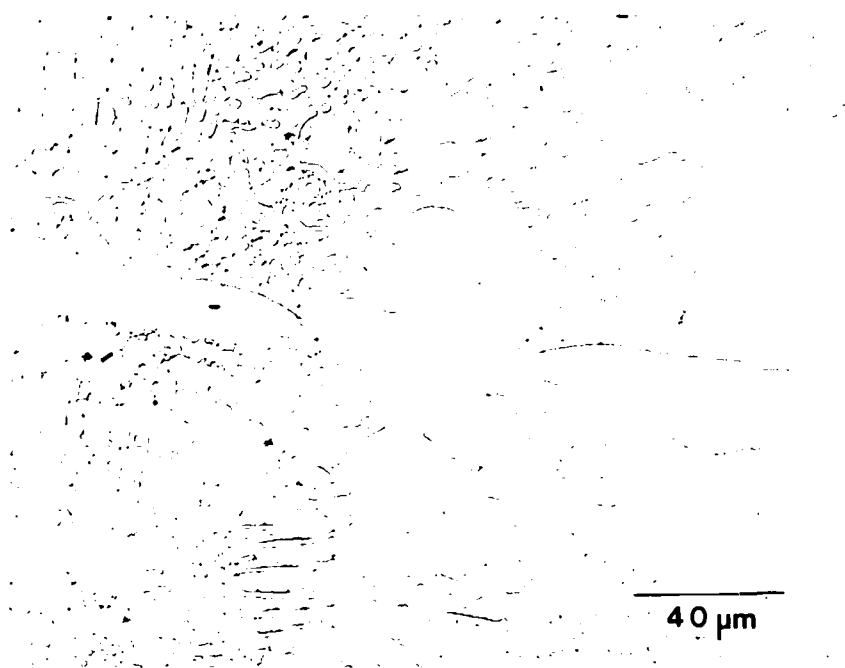
(b)

Fig. 31 Dendritic defects in an AG-170 specimen, tested at 825°C and
$\Delta\sigma = 862$MPa. (a) SEM fractograph shows the dendrite on the
fracture surface. (b) Microstructural breakdown.

inadequate $\frac{G}{R}$ ratios.

Nitac 14B and Cotac 744 readily revealed fibers cracks such as those shown in Fig. 32. In AG-170, only one specimen exhibited fiber cracks. The fatigue zones were similar in appearance to those at 25°C; representative fatigue zones are shown in Fig. 33. Nitac 14B (Fig. 33a) and Cotac 744 displayed dimpled fatigue zones, as previously noted. AG-170 (Fig. 33b) once again exhibited a faceted fatigue zone. However, at 825°C the fatigue zone occupied a smaller fraction of the fracture surface than was observed at ambient temperature. Overload regions, having features like those of Fig. 29a and b, were found over the remainder of each fracture surface.

Fatigue of Nitac 14B, at both room temperature and 825°C, generated a characteristic dislocation substructure. Fig. 34a and b shows this substructure after high cycle fatigue at 25°C and 825°C, respectively. Comparison should be made with the as D.S. structure of Nitac 14B shown in Fig. 12a. The dislocation density appears to have increased during fatigue, particularly near the fibers. The specimen fatigued at 25°C (Fig. 34a) exhibits dislocation entanglement in the γ phase, which is similar to the behavior observed in the as D.S. material (Fig. 12a). However, there is also some deformation in the γ' phase of the fatigued material. Also, dislocation activity in the fibers is visible at 25°C.

Relatively little difference can be noted between the dislocations in the γ/γ' matrix of the material tested at 25°C (Fig. 34a) and at 825°C (Fig. 34b). A slight rearrangement of the dislocation structure
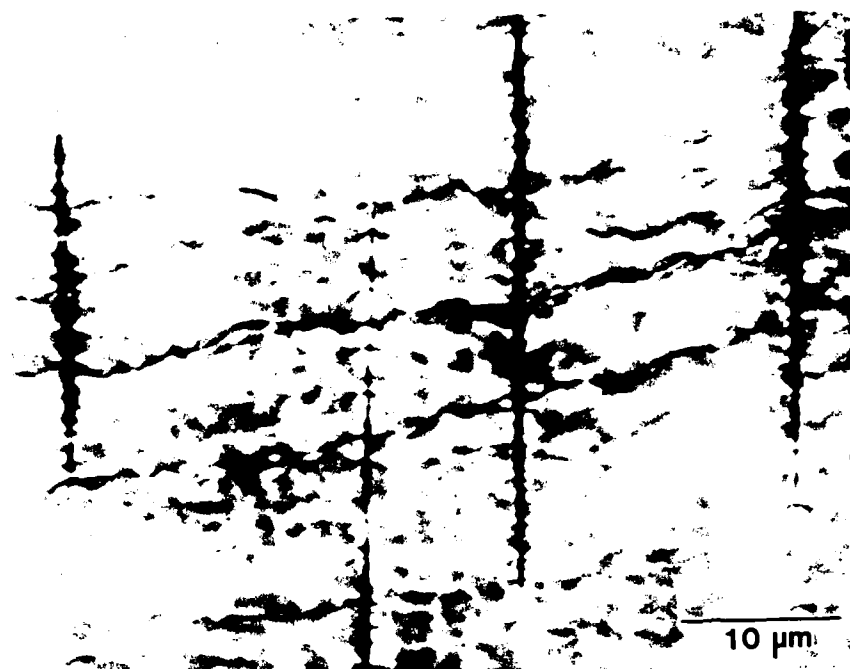
(a)
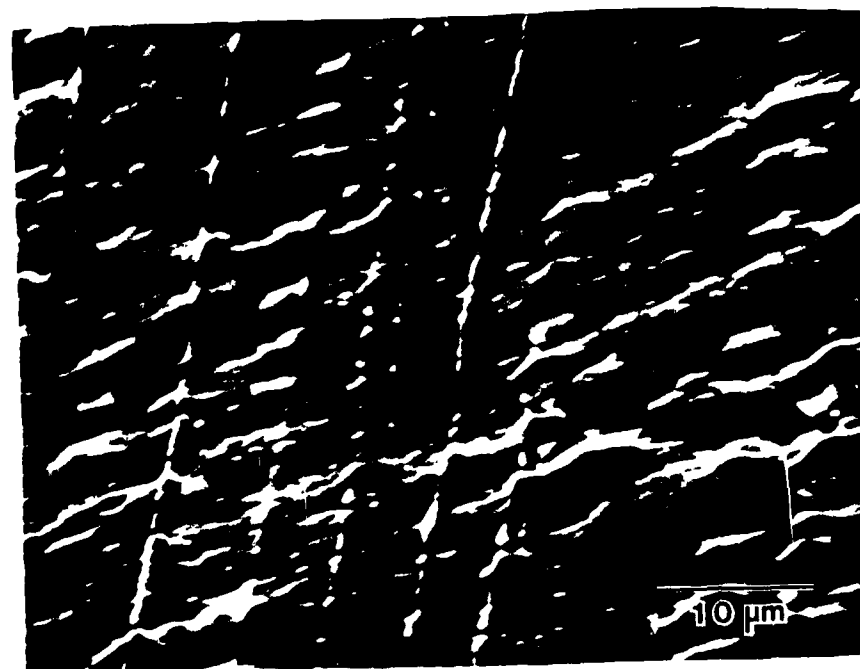
(b)

Fig. 32 Fiber cracks on the side surface of (a) Nitac 14B, and
(b) Cotac 744 after high temperature fatigue tests.
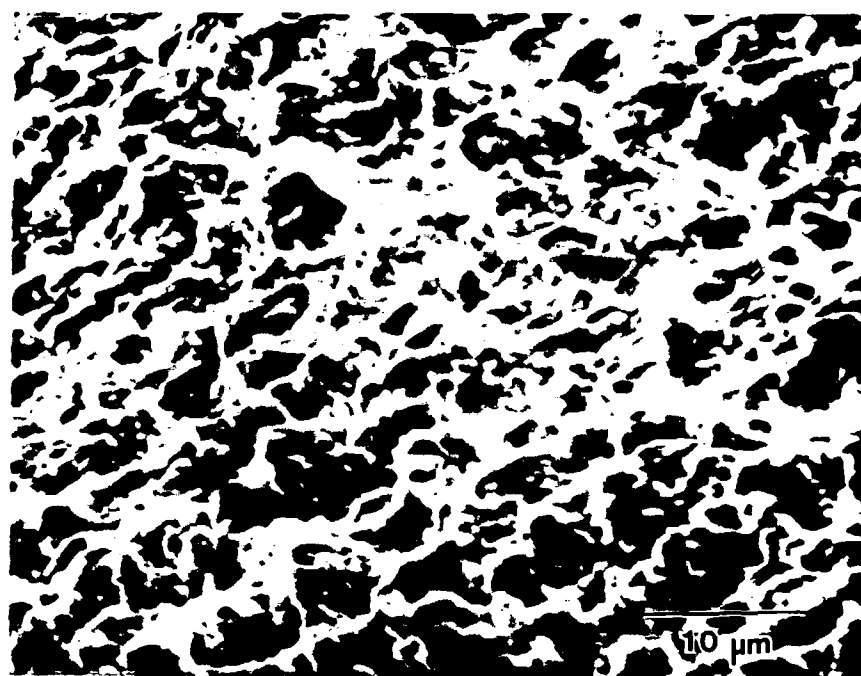
(a)
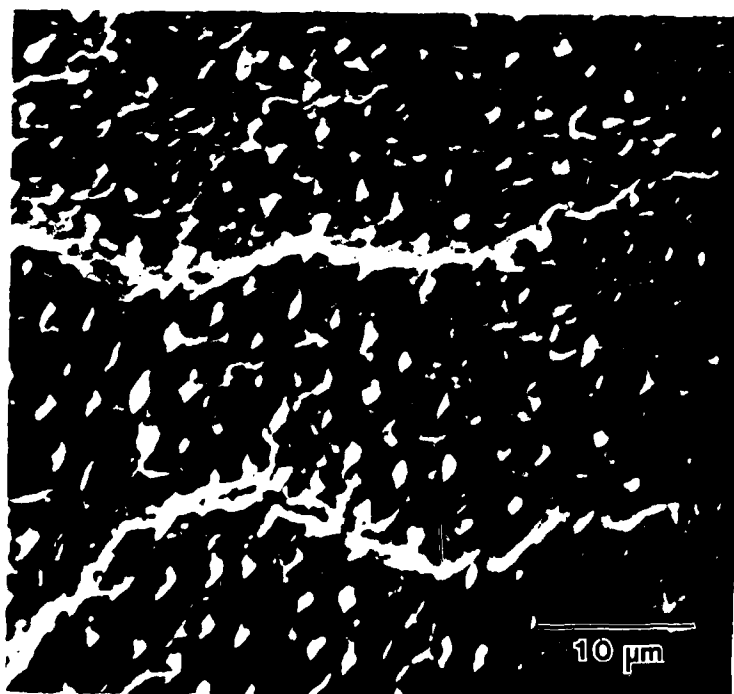
(b)

Fig. 33   Fatigue zones of (a) Nitac 14B and (b) AG-170 following
cyclic failure at 825°C.
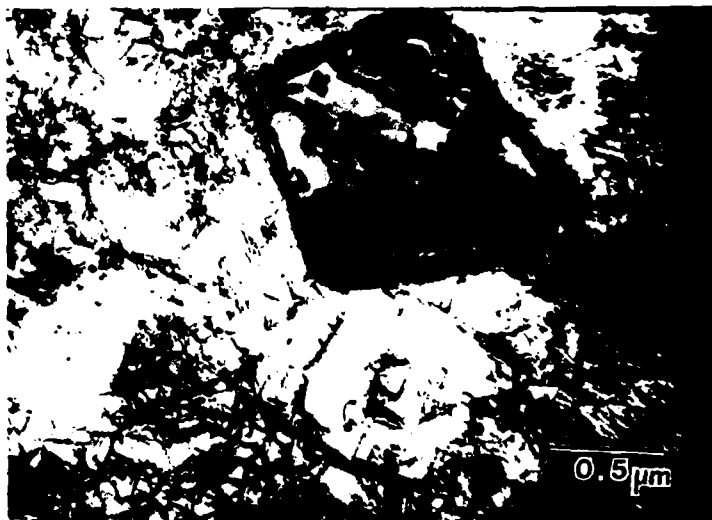
(a)
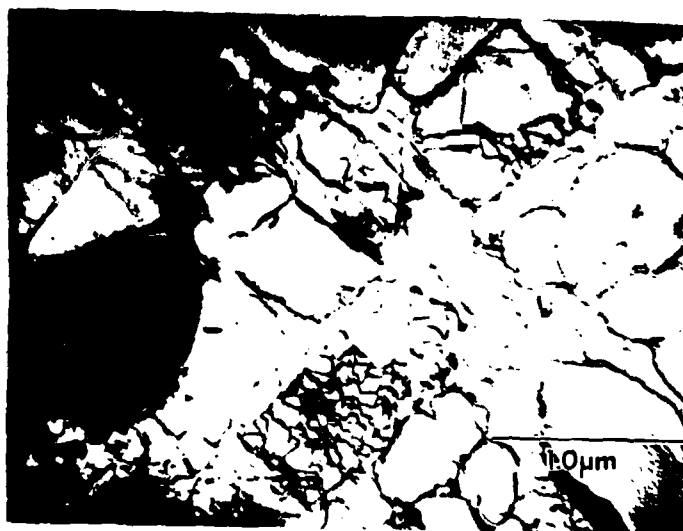
(b)

Fig. 34   Dislocation substructures in as D.S. Nitac 14B after high
cycle fatigue. (a) 25°C. (b) 825°C.

in the γ phase occurs at 825°C. The formation of a cell structure has begun, but the density of dislocations in the γ' phase is still very low.

Cotac 744 displayed approximately the same dislocation substructure after fatigue at 25°C and 825°C. However, no dislocation activity was observed in the fibers.

The greatest effect of fatigue cycling on substructure was seen in AG-170. Dislocation substructures generated after fatigue at 25°C and 825°C are illustrated in Fig. 35. The as D.S. structure (see Fig. 13a) has a low density of dislocations, especially in the Mo fibers and the γ' matrix. Stressing has caused a remarkable increase in the dislocation densities of these phases. Many dislocation intersections and much tangling is observed. At 825°C, precipitates in the Mo fibers are visible. Fig. 35c shows an enlargement of the fiber on the lower right of Fig. 35b. Similar precipitates have been observed by Jackson et al.[16] and by Pearson and Lemkey.[73] These precipitates may contain Mo, Ni and Al. Dark field imaging of diffraction spots proved insufficient for positive identification. However, it did deny the possibility of γ' (Ni_3Al).

4.3.2 Post Solidification Heat Treatment Effects

4.3.2.1 Tests of Partially Solutionized Material. Solution treated fatigue specimens of Nitac 14B tested at 25°C did not differ greatly in appearance from the as D.S. specimens. This was not unexpected since the S-N curves fell within the same scatterband.
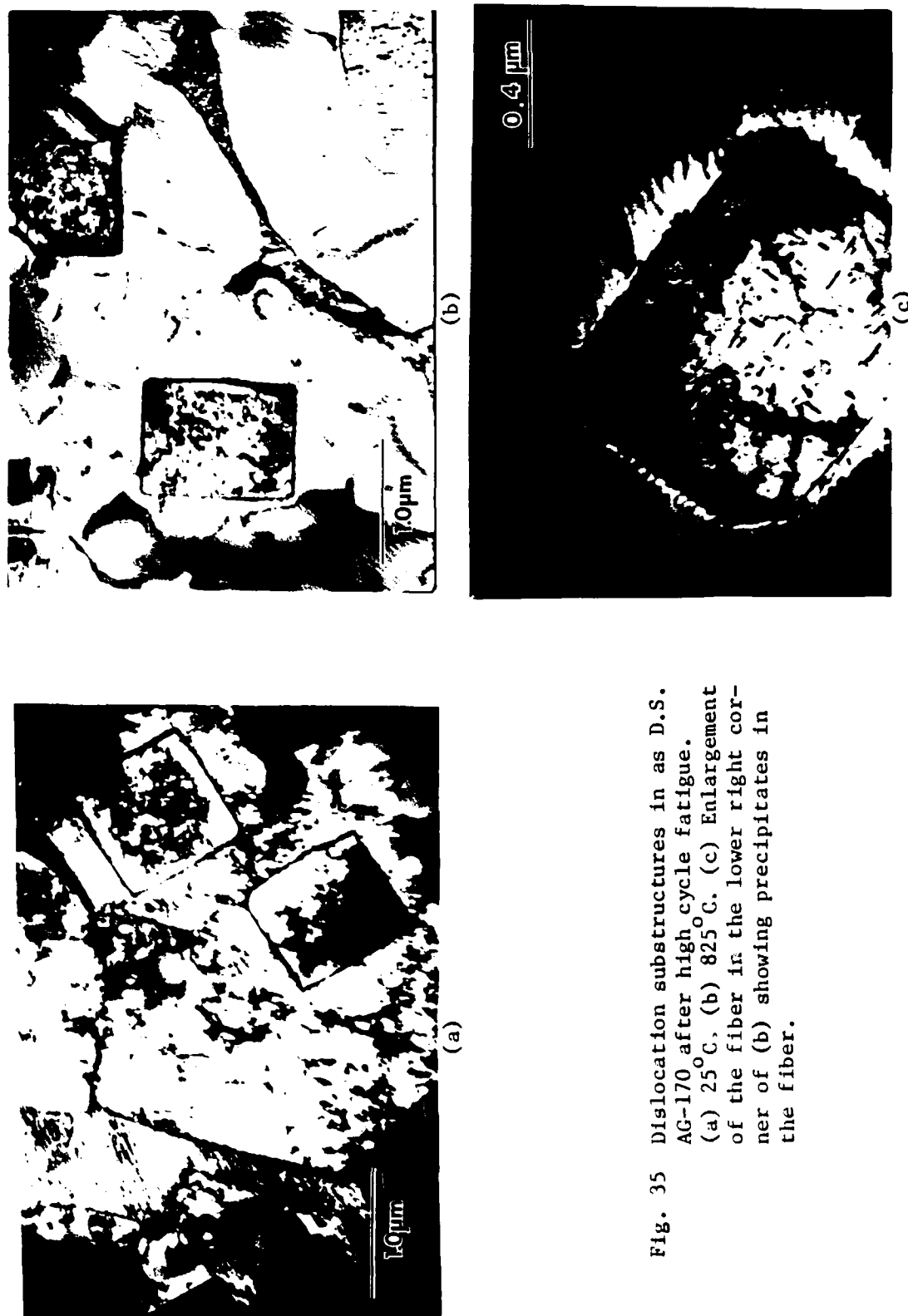
Fig. 35 Dislocation substructures in as D.S. AG-170 after high cycle fatigue. (a) 25°C. (b) 825°C. (c) Enlargement of the fiber in the lower right corner of (b) showing precipitates in the fiber.

A view of the overall fracture surface of Nitac 14B is shown in Fig. 36a. Note the similarities between this specimen and the as D.S. specimen pictured previously in Fig. 25. The three regions (i.e. initiation site, fatigue zone, and overload zone) are again easily differentiated. However, the overload zone appears to occupy a larger fraction of the fracture surface. The fracture is more angled than the as D.S. material, with the fracture angle approaching 45° from the stress axis.

The fatigue zone of solution treated Nitac is flatter than in as D.S. Nitac. It contains shallow dimples which house cleaved TaC fibers, as shown in Fig. 36b. Other fractographic features remain identical to the as D.S. material. Stage I cracking is still observed. Crystallographic cracking has even been viewed on the side surfaces of fractured specimens (see Fig. 36c). The overload zone, though larger, is dimpled as before. However, the dimples are no longer equiaxed. Cleaved, as well as split, fibers are present within the dimples of Fig. 36d.

AG-170 also was tested in the partially solution treated condition at room temperature. Results fit on two, separate S-N curves as depicted in Fig. 18 of the preceding section. The difference between the two curves has been attributed to the presence of imperfect microstructures in several samples. Specimens incorporating many cells with imperfect alignment at cell boundaries were deemed cellular. A transverse cellular microstructure, typical of solution treated AG-170
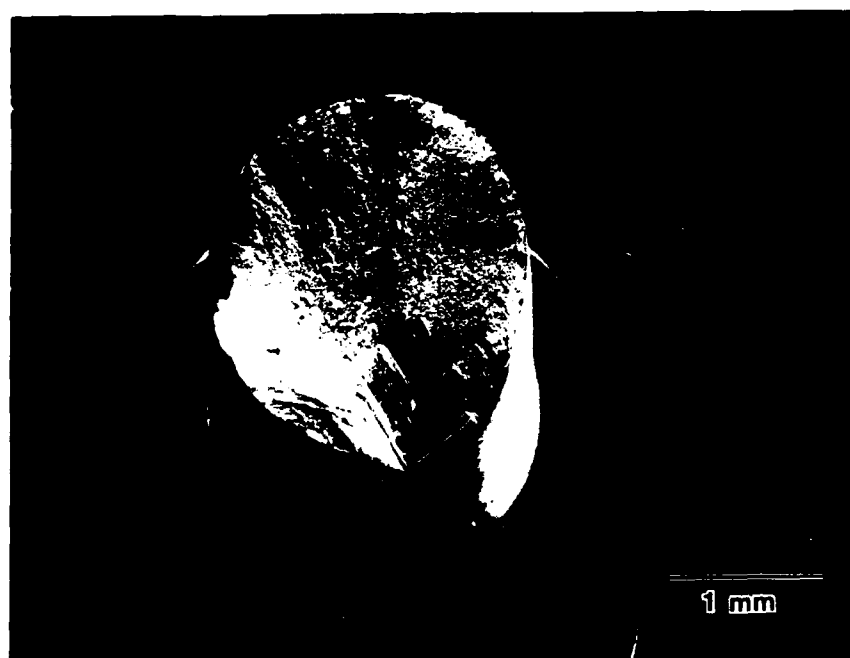
(a)
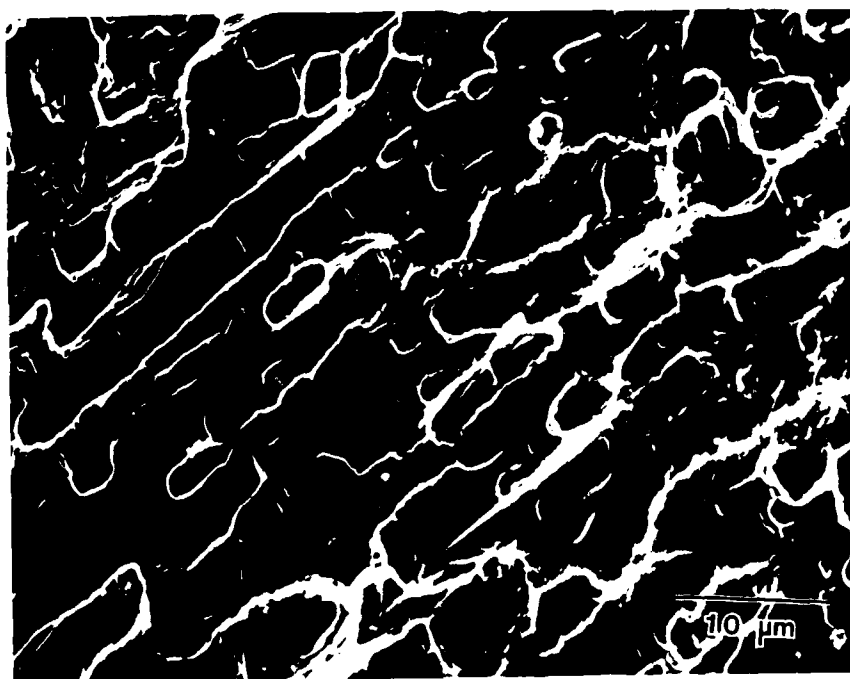
(b)

Fig. 36 SEM fractographs of partially solution treated Nitac 14B, tested at 25°C. (a) Overall fracture surface. (b) Flat fatigue zone.
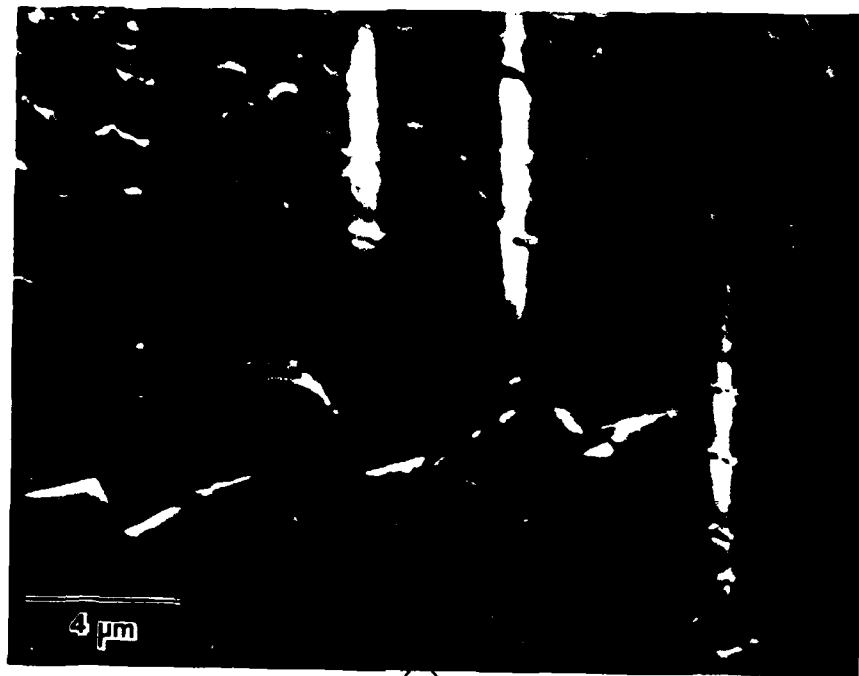
(c)
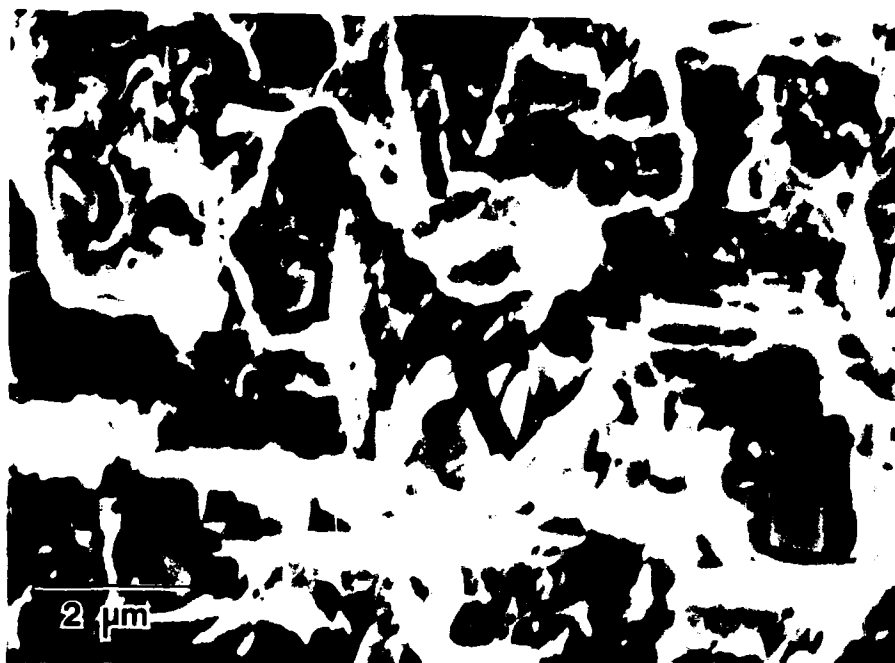
(d)

Fig. 36 SEM fractographs of partially solution treated Nitac 14B,
tested at 25°C. (c) Crystallographic surface cracks.
(d) Overload region.

END

FILMED

DTIC

	1.0	4.5	2.8	2.5
	1.1	5.0 5.6 6.3 4.0	3.2 3.6	2.2 2.0
				1.8
	1.25	1.4		1.6
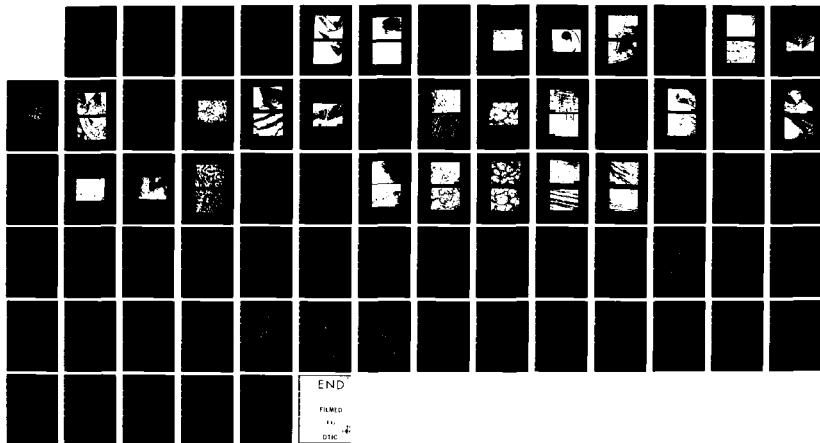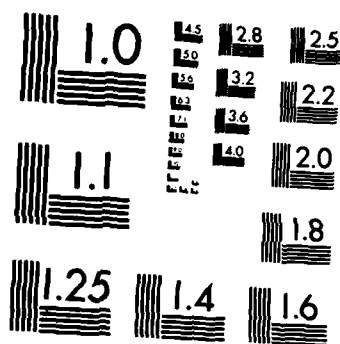
MICROCOPY RESOLUTION TEST CHART
NATIONAL BUREAU OF STANDARDS-1963-A

specimens tested at 25°C, is illustrated in Fig. 37. The lack of co-
herency across the boundary is evident. The fibers are no longer rod-
like. Aligned microstructures, even if they possessed a few cell boun-
daries, exhibited a continuity of structure across the boundary. For
example, Fig. 38a shows a cell boundary in an aligned specimen tested
at 25°C. There is not a total breakdown of structure at the boundary.
The remainder of the specimen displayed a typical aligned microstructure
like that shown in Fig. 38b.

Solution treated specimens with aligned microstructures had
fractographic features similar to as D.S. samples. Fractures were al-
ways surface initiated, like the one shown in Fig. 39a. Multiple sur-
face initiation sites were occasionally observed. Also, more secondary
cracking was exhibited than in the as D.S. failures. Some of these
cracks are pictured in Fig. 39b.

Fractographs of cellular specimens differed slightly. Once
again multiple surface initiation sites were found. However, river
patterns were seen to emanate from the fracture origin. Crystallograph-
ic cracking was more evident than in the aligned microstructures.
Fig. 40a illustrates a surface initiation site for a specimen which
fractured after 6×10^5 cycles at a stress of 1138 MPa. Fig. 40b is an
enlargement of the right side of the initiation region, proving that
cracks are propagating in a Stage I mode.

Crack branching has occurred, diverting the crack into cell
boundaries. Obviously, cell boundary cracking is more prevalent in
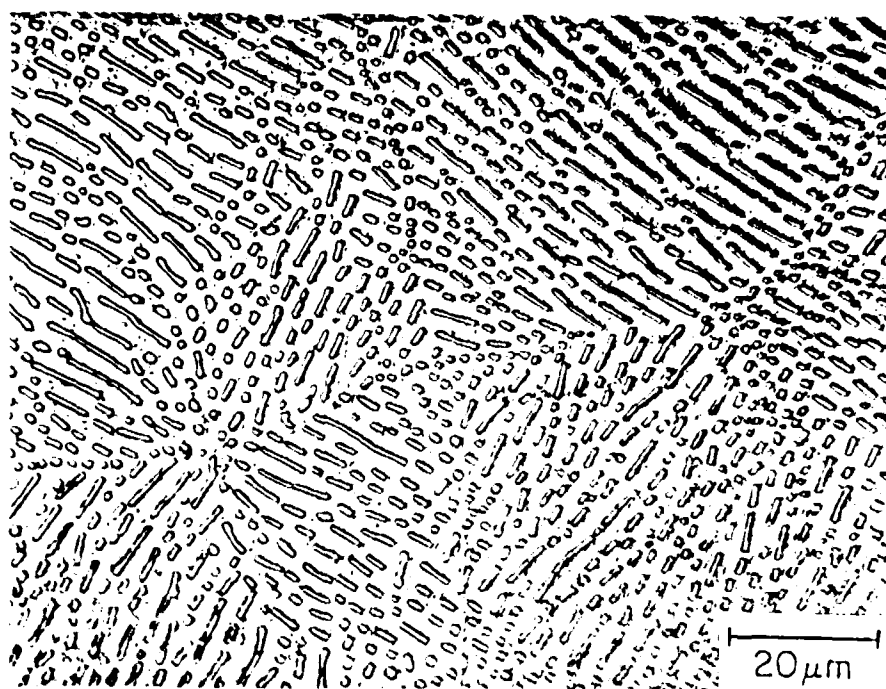
Fig. 37 A characteristic "cellular" microstructure of a partially
solution treated AG-170 specimen fatigued at room tempera-
ture.
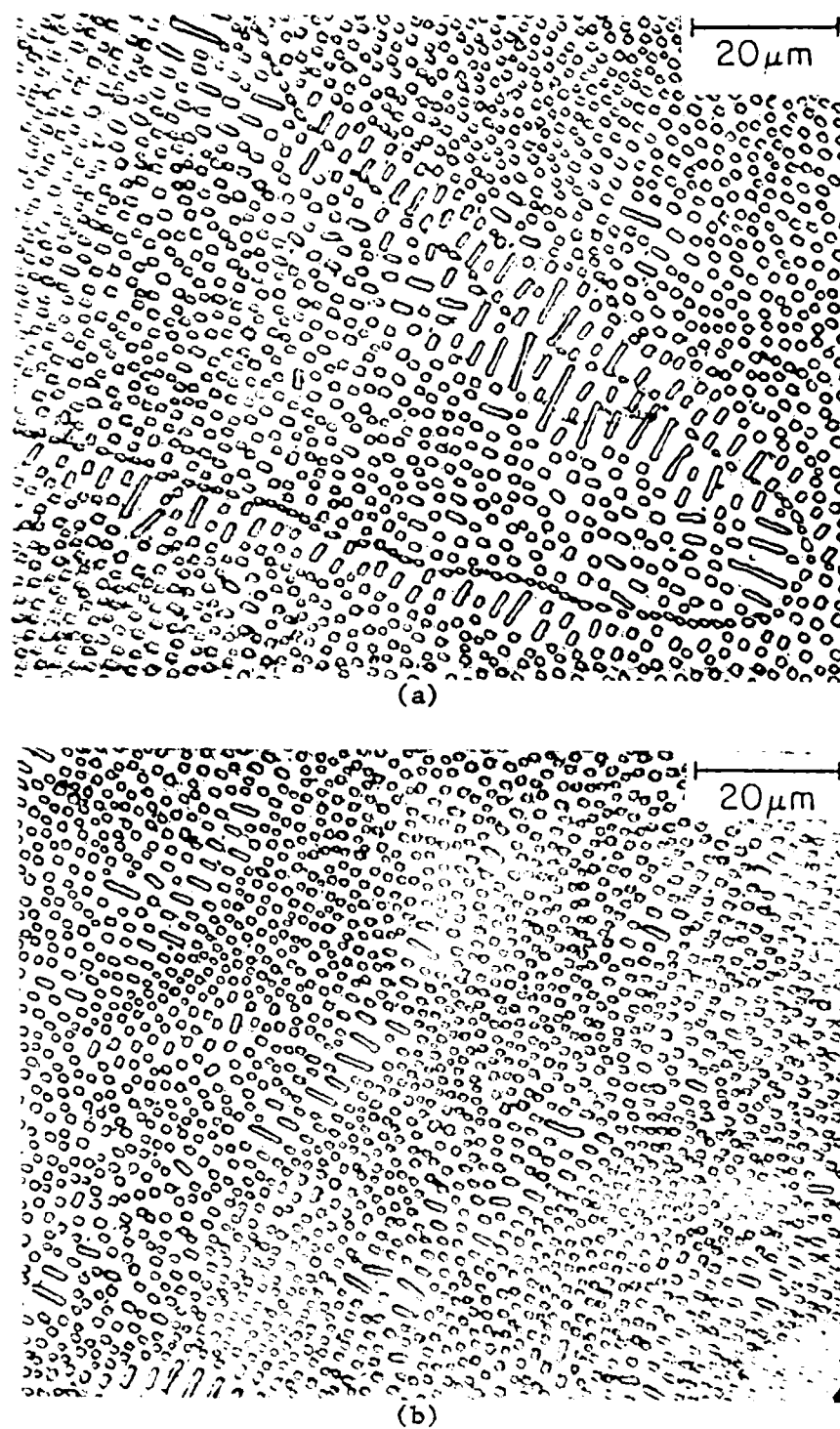
Fig. 38 Representative microstructures of "aligned" AG-170 in the
partially solutionized condition. (a) Cell boundary showing a
continuity of structure across the boundary. (b) Typical
aligned region.

(a)

(b)

Fig. 39 SEM Fractographs of "aligned", partially solution treated
        AG-170, tested in fatigue at 25°C and $\Delta\sigma = 1034$ MPa.
        (a) Surface initiation site. (b) Secondary cracks.
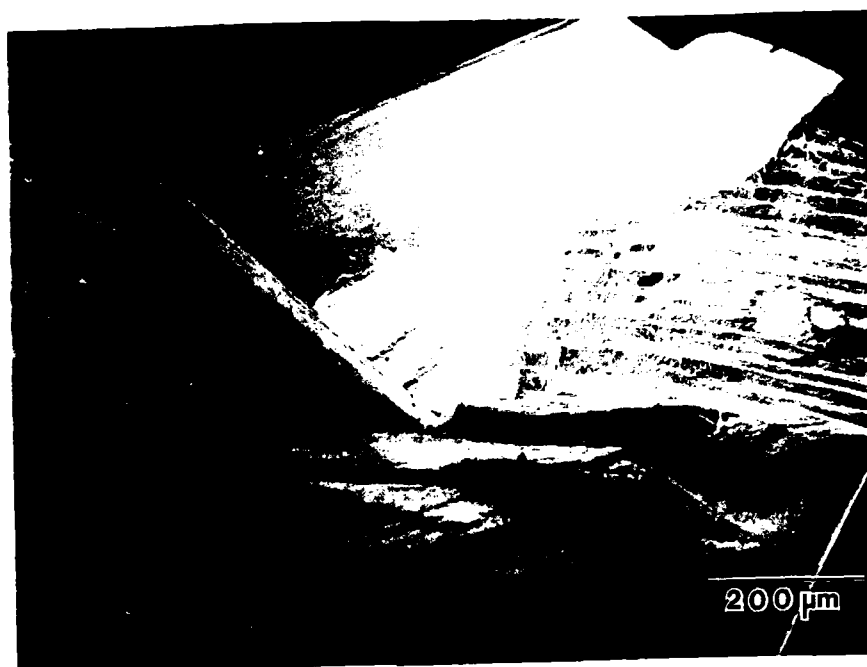
(a)
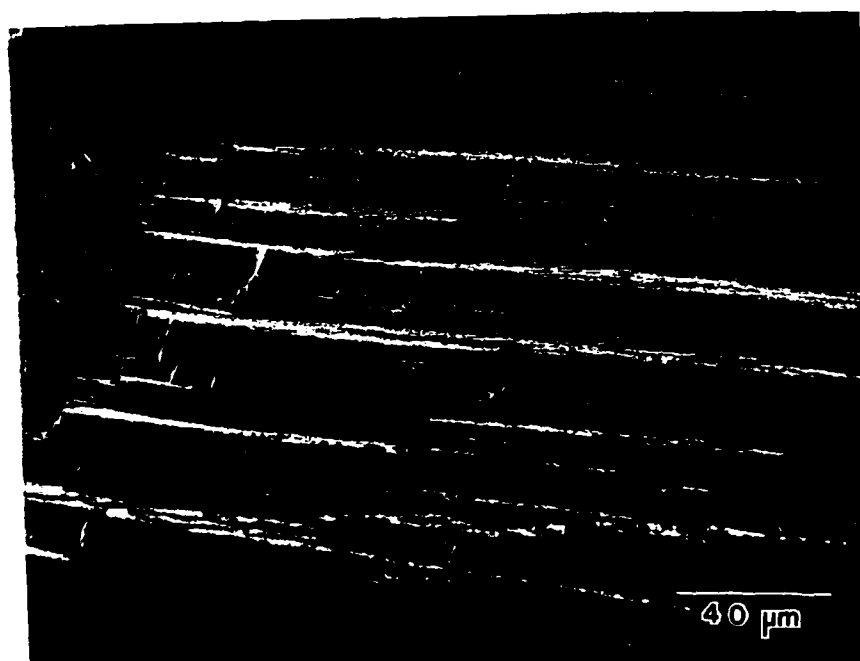
(b)

Fig. 40 SEM fractographs of "cellular", partially solution treated
AG-170 after fatigue at $25^{o}C$. (a) Surface initiation and
Stage I cracking. (b) Crystallographic cracking.

material which possesses a cellular microstructure. Fig. 41 gives a high magnification view of the inside of one of these crack walls. The overload zones which encompass these secondary cracks remain faceted. The fibers have necked and broken in a chiselpoint, similar to the fibers in the overload zone of the as D.S. material (see Fig. 29b).

No tests were performed at 825°C on partially solutionized material. In effect, testing at this temperature would cause aging. Thus, the results would be analogous to those for solutionized and aged material tested at 825°C.

4.3.2.2 25°C Tests of Aged Material. The fracture surfaces of aged Nitac 14B specimens tested at 25°C are quite similar to those of other Nitac specimens stressed at room temperature. Fractures of aged Nitac samples were characterized by a three stage failure. Note the resemblance of the fracture profile of aged Nitac 14B shown in Fig. 42 to other room temperature Nitac fractures already pictured. (See Figs. 25 and 36a for comparison.)

Fractures were usually surface initiated, as shown (Fig. 43). However, a crack in one of the aged specimens was traced to an internal origin. Fig. 43a displays this internal initiation site. River lines indicating the direction of propagation can be seen emanating from the crack source. A closer view of the initiator (Fig. 43b) confirms it is an impurity particle, consisting of two phases. The parent phase appears to be a ceramic phase,[74] while the second phase is crystalline and marked by the presence of dendrites.
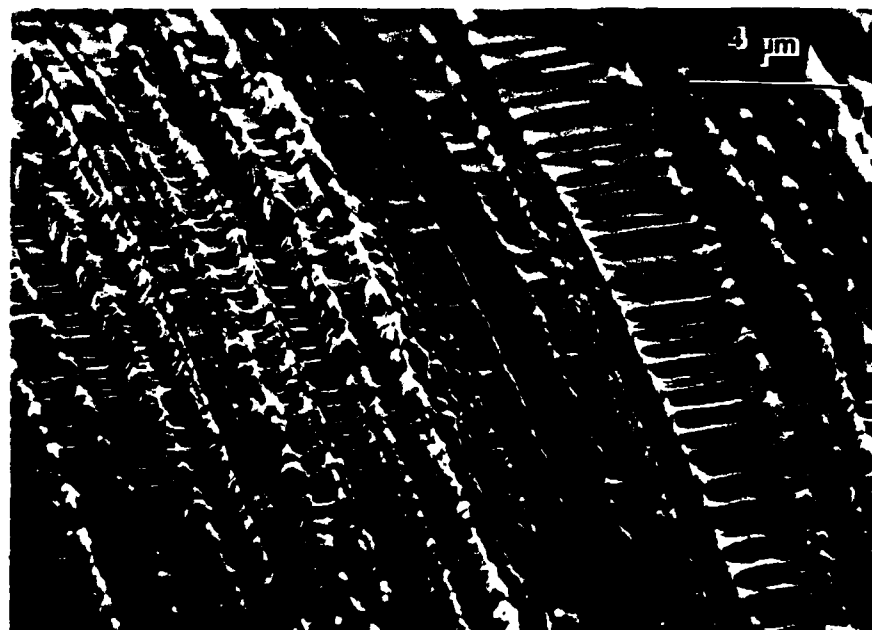
Fig. 41   View of the crack wall of a longitudinal, cell boundary crack.

Fig. 42   Typical fracture surface of aged Nitac 14B, tested at room
           temperature, illustrating the usual three stage failure.
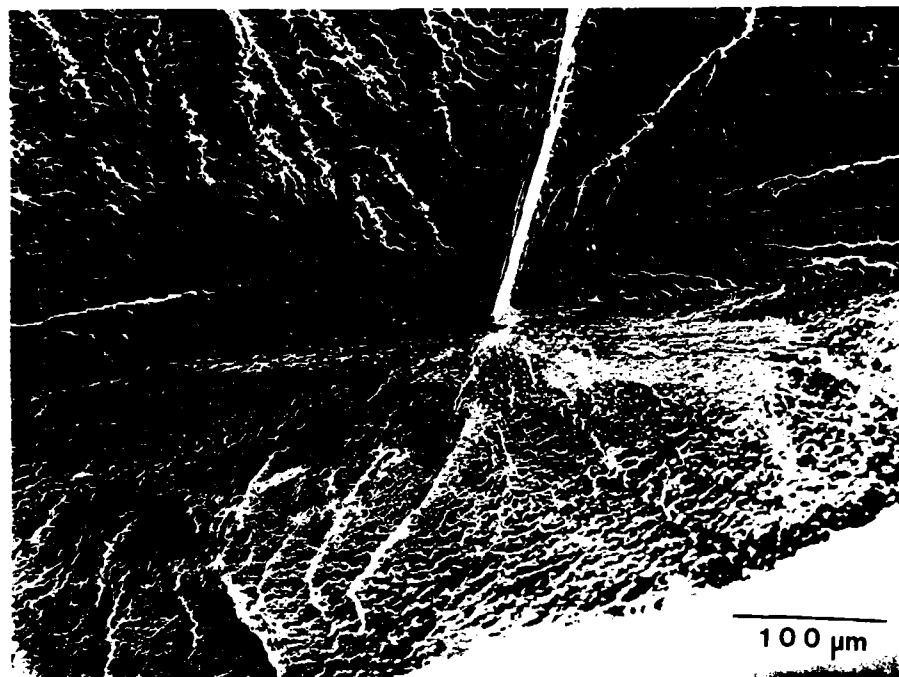
(a)
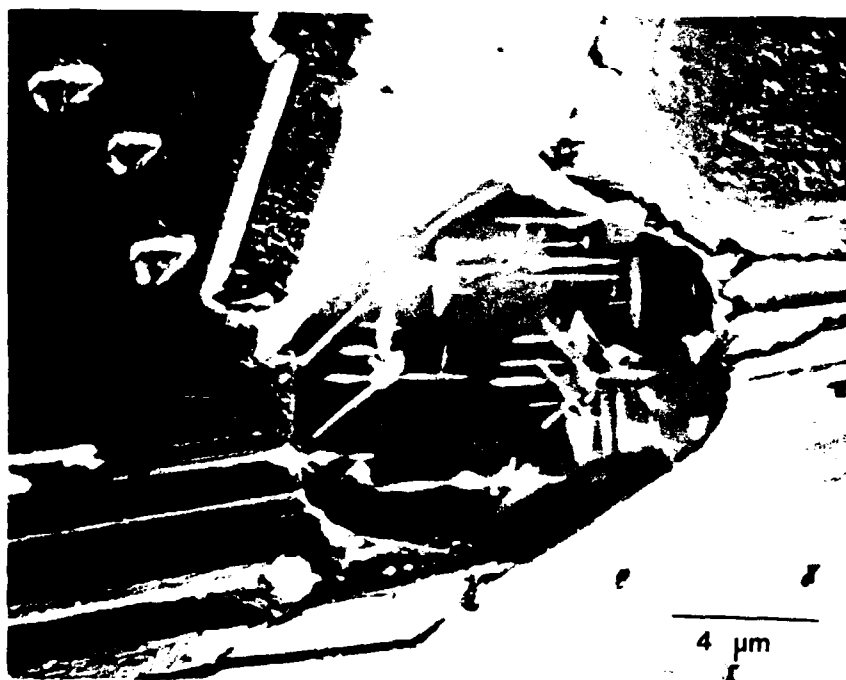
(b)

Fig. 43   Impurity-initiated origin in a room temperature fatigue speci-
men   of aged Nitac 14B.   (a) Internal initiation site.
(b) Two-phase impurity, consisting of ceramic and crystalline
phases.

All of the aged Nitac 14B, room temperature specimens exhibited extensive Stage I cracking. This is evident even for the impurity-initiated fracture. Observe the slip band cracks in the vicinity of the origin of Fig. 43b. This type of cracking was most prevalent in the surface initiated fractures. Fig. 44a illustrates Stage I cracks found near the surface origin. Both of the aforementioned figures also give a reasonable view of the fatigue zone. Like before, it is relatively flat with shallow dimples. The overload zone also remains dimpled. However, the dimples are not as shallow as previously observed. Fig. 44b shows cleaved fibers in shallow dimples in the overload zone.

Aged Cotac 744 specimens tested at $25^{o}C$ showed little change from as D.S. fractures at that temperature. Surface initiation, accompanied by Stage I cracking, was once again observed. Fig. 45 is representative. The fracture was not as planar as the room temperature as D.S. failure. This is even apparent in the fatigue zone. Examination of this area revealed shallow dimples. However, the surface was not flat.

Considerably more grain boundary cracking has been observed in the aged alloys. Inspection of the transverse microstructure of a specimen which had been tested at a stress level of 931 MPa yielded a cellular structure as shown in Fig. 46. This was not unforeseen in view of the large amount of cell boundary cracking noted in this sample. Fig. 47 depicts a few of these internal cracks. Steep grain boundary walls clearly encompass the more ductile transgranular dimpled region.
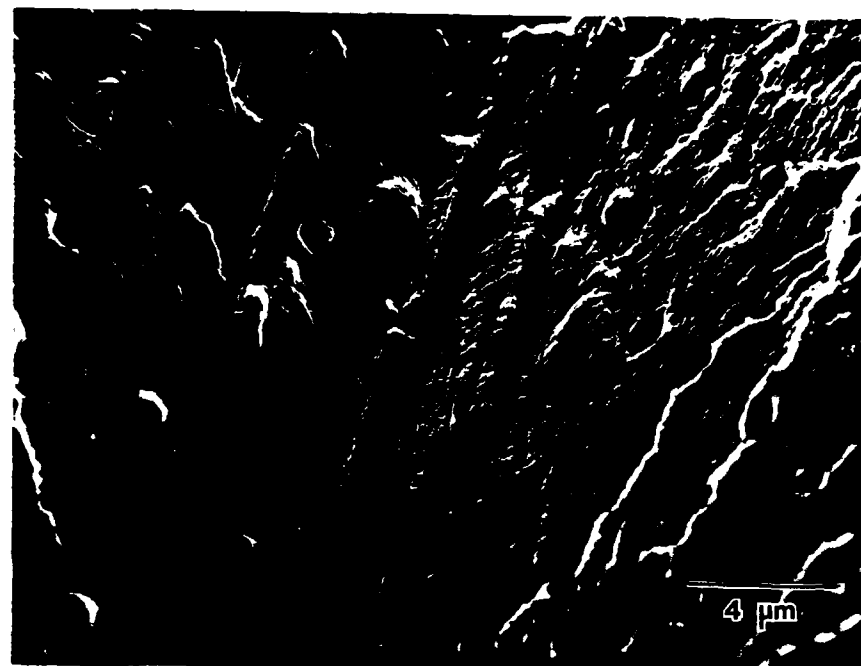
(a)
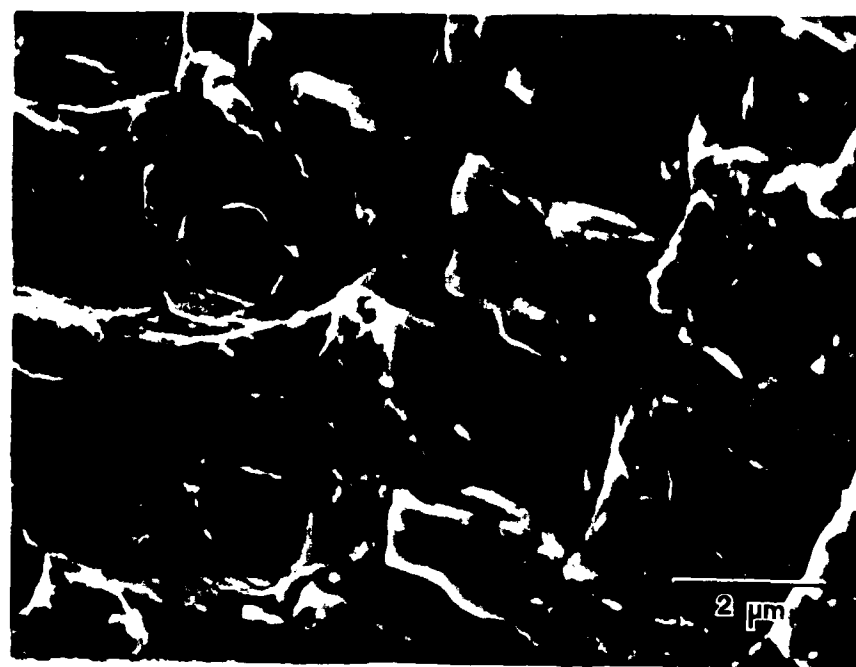
(b)

Fig. 44 SEM micrographs of a fatigue failure in aged Nitac 14B at 25°C.
(a) Stage I cracking in the fatigue zone. (b) Shallow
dimples in the overload region.

Fig. 45   Surface initiation and Stage I cracking in aged Cotac 744, tested at 25°C.

Fig. 46   Transverse microstructure of aged Cotac 744 following high
cycle fatigue at room temperature. Note the cellular appear-
ance.

(a)
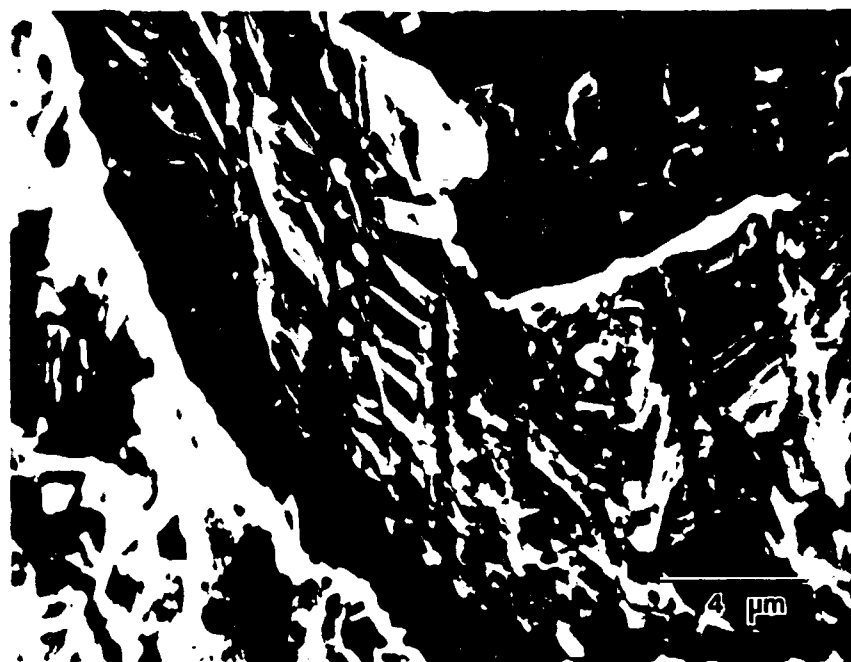
(b)

Fig. 47   Grain boundary cracking in the sample shown in Fig. 46.
         (a) Steep grain boundary cracks. (b) Magnified view of the
         crack wall.

A closer view of the grain boundary wall is pictured in Fig. 47b. It is clear that the fibers have fractured. Yet fine dimples, indicative of nonbrittle fracture, exist in the immediate vicinity of the crack.

Fiber cracking has also been noted in the void coalescence region of aged Cotac 744. However, longitudinal fiber cracks are revealed in the overload zone. Fig. 48 illustrates the large number of split fibers which form voids. Final failure is by eventual linkage of these voids.

Significant differences were observed in the fractographic features of aged AG-170 tested at 25°C when compared with the as D.S. and solutionized fractures. Fractures were no longer sharply faceted. The crack appeared to originate at a surface initiation site. Propagation proceeded outward and was seen to follow a terraced crack path. Fig. 49a illustrates the regular array of terraces found on the fracture surface. Crystallographic cracking occurs as the crack advances (see Fig. 49b). Careful examination of this fractograph reveals that the longitudinal cracks on the surface are due to interface debonding. An enlargement of one of these cracks, Fig. 49c, shows the achievement of a clean break with the ductile, Mo fibers remaining intact. The surrounding regions display cleaved fibers suggesting fiber pullout and interface debonding as the failure mechanism.

4.3.2.3 825°C Tests of Aged Material.

The effect of aging on the high temperature S-N curves for Nitac, Cotac and AG-170 was shown earlier in Figs. 19, 21, and 22. An improvement in fatigue life was
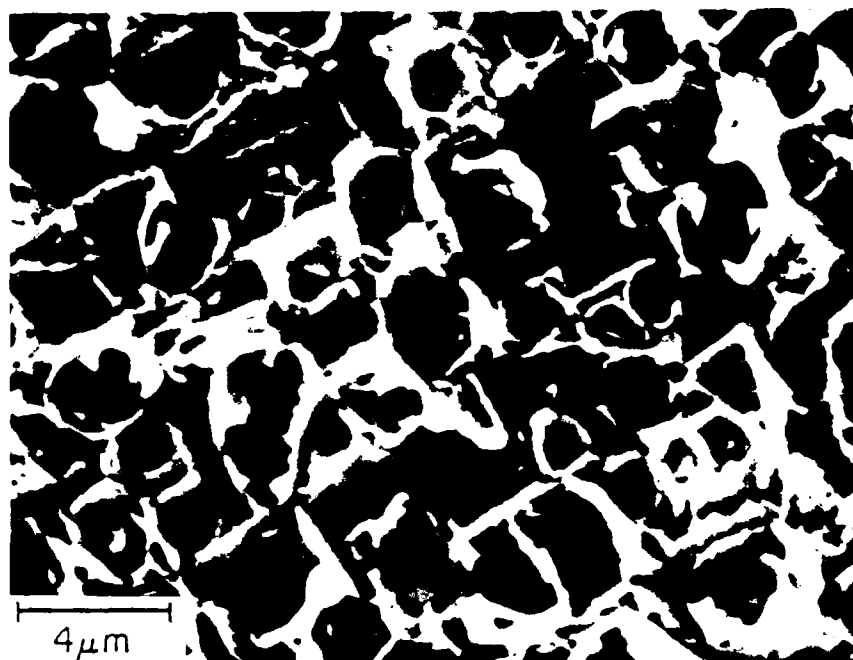
Fig. 48   Overload zone in an aged Cotac 744 specimen after room temperature fatigue failure. Note the large number of voids resulting from split fibers.

(a)

(b)
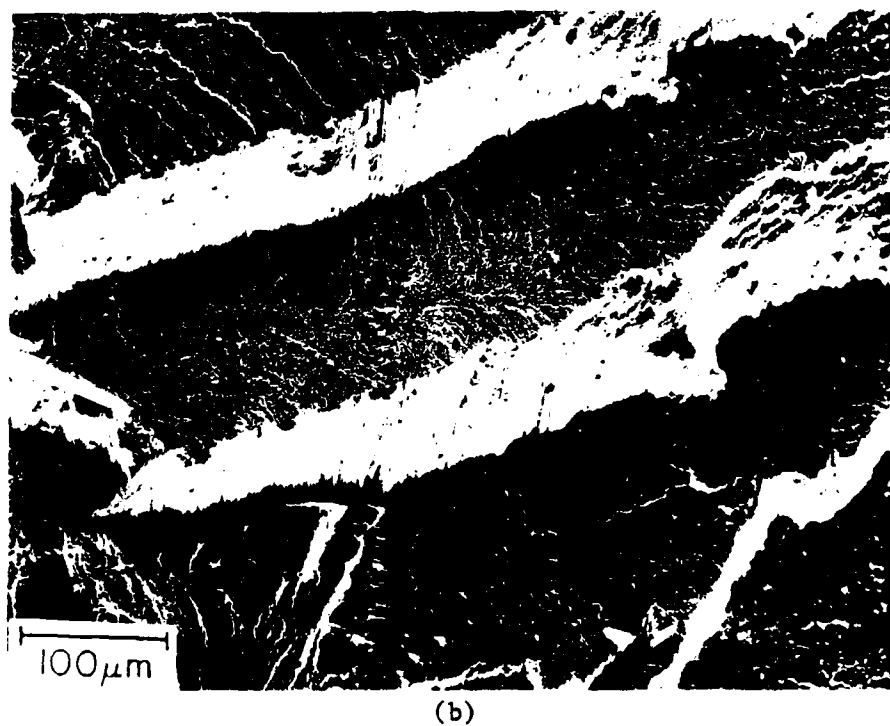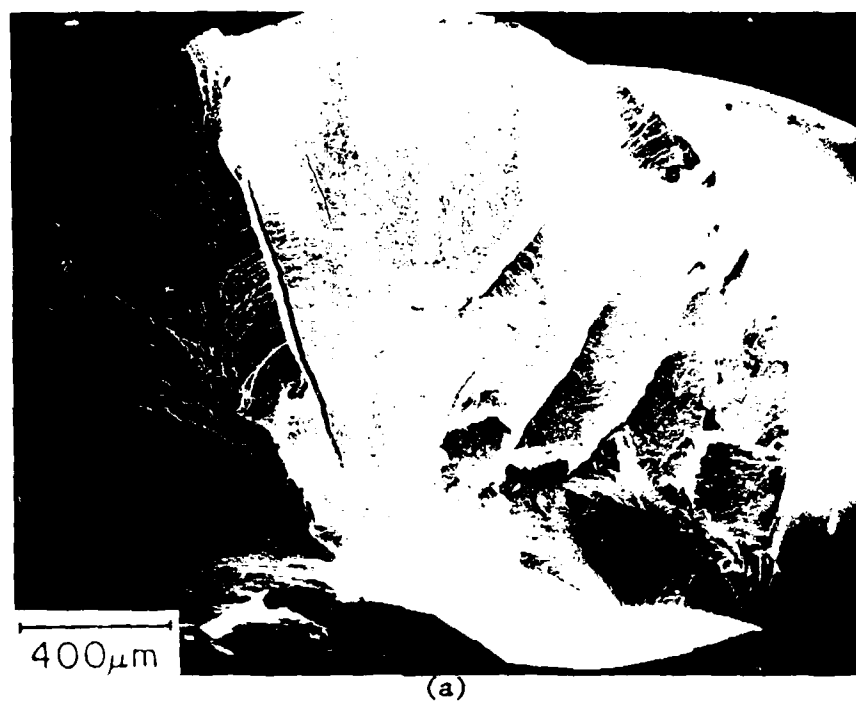
Fig. 49 SEM fractographs of aged AG-170, tested in fatigue at 25°C
and $\Delta\sigma$ = 1138 MPa. (a) Overall fracture surface illustrating
propagation along parallel steps. (b) Terraced crack path.

20μm
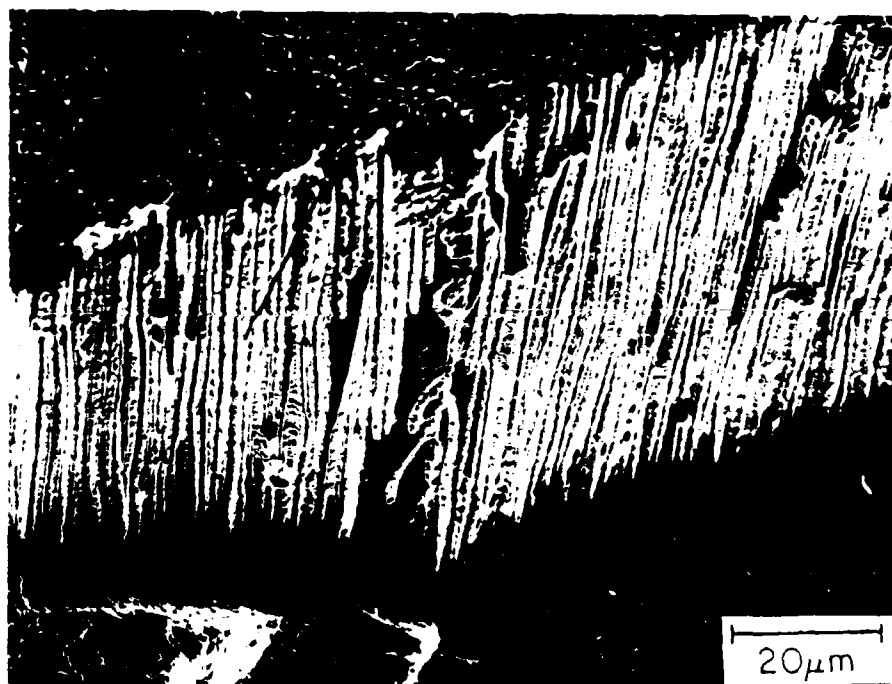
(c)

Fig. 49 SEM fractographs of aged AG–170, tested in fatigue at 25°C and $\Delta\sigma$ = 1138 MPa. (c) Debonded interface with fibers intact.

noted in all cases. Thus, major changes in the 825°C fracture appearance of as-grown and heat treated specimens are not unexpected.

Aged Nitac 14B showed surface initiation sites, similar to the 25°C and 825°C as D.S. specimens. However, other variations prevailed. The fatigue zone in the vicinity of the crack origin was flat. Yet it displayed progressive markings emanating from the dimples. Fig. 50a depicts this information. It is apparent that these fibers did not fail simply by cleavage. Rather, multiple slip systems were operating.

Proceeding further away from the initiation region, the fatigue zone loses its planarity. A coarse surface containing cleaved fibers has evolved. Fig. 50b illustrates this outer fatigue zone. Note the raised appearance of some fibers while others are depressed. All of the fibers gradually become depressed as the overload zone is approached. Dimples, much deeper than those observed in 825°C as D.S. fractures, have been found. These dimples are pictured in Fig. 51 where ridges can be seen extending away from the fibers.

Surface structure was markedly altered from the as D.S. material. Referring to Fig. 32a, transverse cracks were observed in surface fibers of the as-grown specimens. Greater surface activity was demonstrated in the aged condition. Aged Nitac 14B revealed more pronounced fibrous cracking along well-defined slip bands. (see Fig. 52a) Matrix cracking was also found in several of the specimens. Fig. 52b illustrates this effect where longitudinal, as well as transverse, fiber cracks are found.
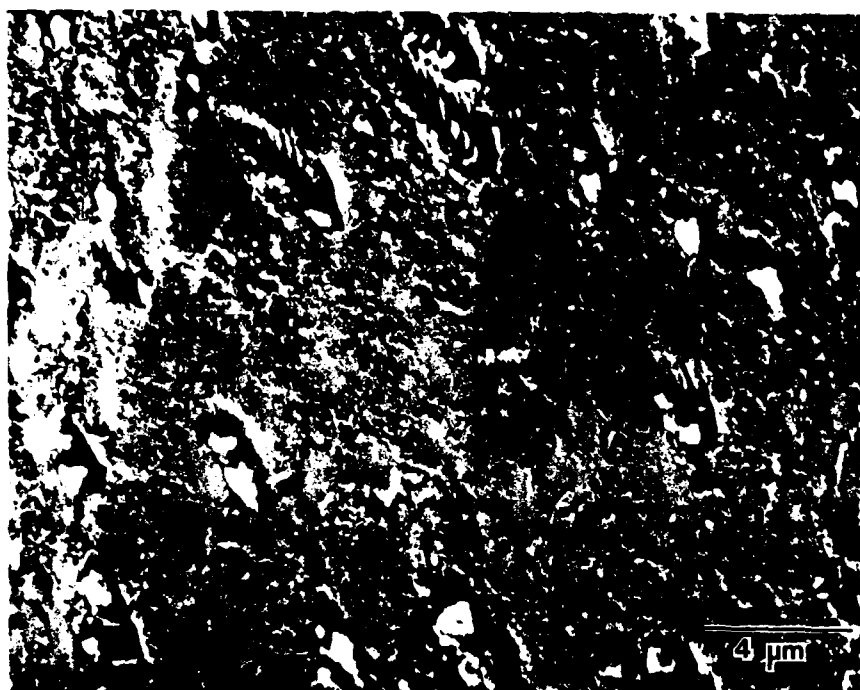
(a)

(b)

Fig. 50   Fatigue zone in aged Nitac 14B after high cycle fatigue at
elevated temperature. (a) Flat region near surface origin.
(b) Outer fatigue zone.
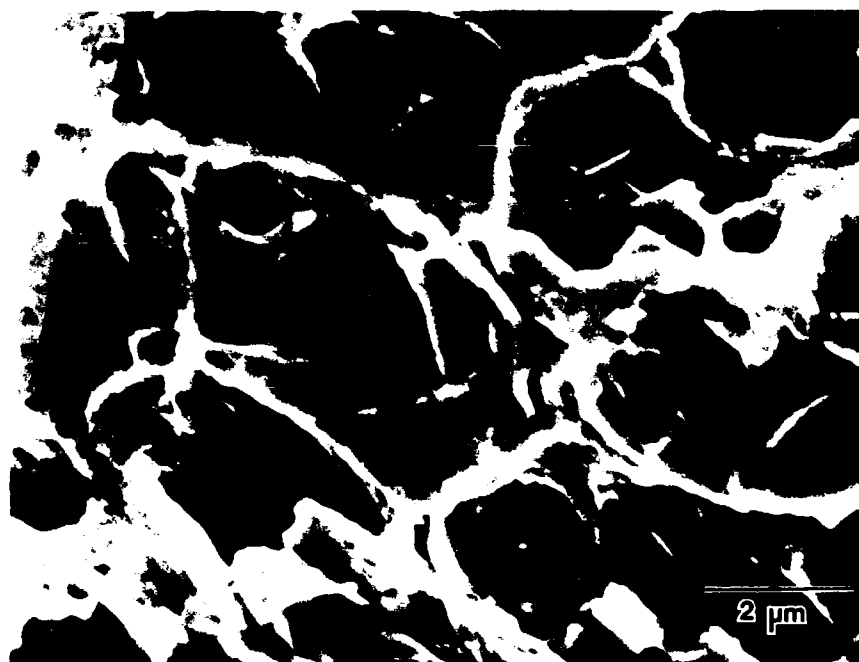
Fig. 51   Dimpled overload region in aged Nitac 14B, 825°C.
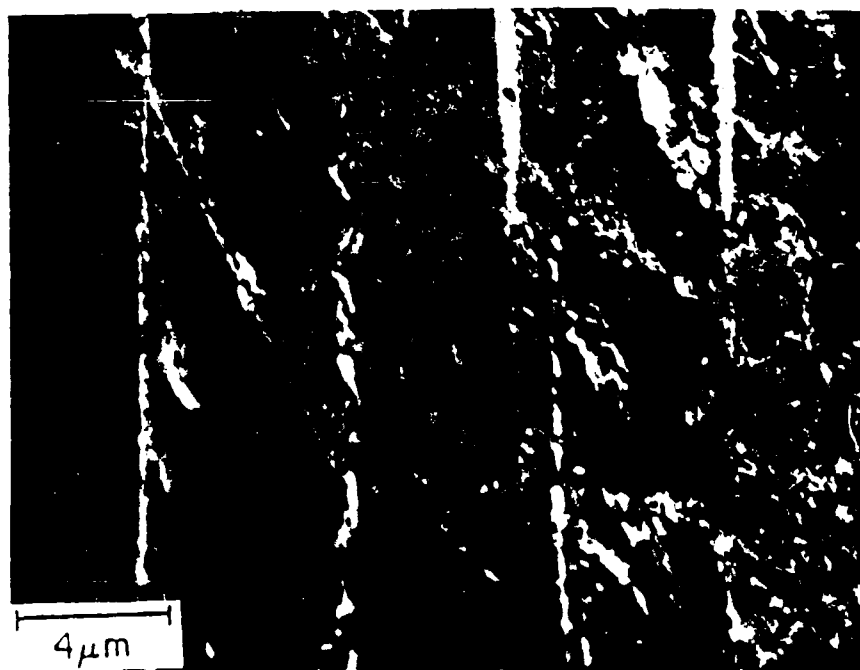
Fig. 52 Surface activity in aged Nitac 14B following cyclic stressing
at 825°C. (a) Slip band cracking. (b) Matrix cracking,
plus longitudinal and transverse fiber cracking.

Cotac 744 demonstrated a more angular fracture in the aged condition. The crack origin was difficult to distinguish. However, an internal initiation region was observed in a particular specimen stressed at 1000 MPa for 51 minutes. Fig. 53a depicts this internal origin. The fatigue zone in this case was very flat with shallow dimples. (see Fig. 53b) Generally, fatigue zones were dimpled and displayed a large amount of internal cracking.

Fig. 22 reveals that a single curve cannot be drawn through the $825^{\circ}C$ data for the aged material. This fluctuation in fatigue properties has been attributed to microstructural variations. The two specimens which demonstrated an increase in life subsequent to aging were found to have cellular structures. Fig. 54 shows a representative cellular microstructure for these samples. The other specimens revealed well-aligned structures. Thus, the mechanism is the same as that previously stated for P.S.T. AG-170 tested at $25^{\circ}C$ (see 4.3.2.1). Many cell boundaries hinder the crack propagation rate.

AG-170 demonstrated the most substantial increase in $825^{\circ}C$ fatigue life due to aging. Therefore, it is not surprising that its fracture profile also changed significantly as a result of aging.

The fracture surfaces of aged specimens showed many facets. The fracture was traced to an internal initiator. Internal initiation regions resembled the one shown in Fig. 55a. Note the severe angularity of the fracture. The initiation may have originated at cell boundaries where there was a breakdown of structure. Enlargement of an internal
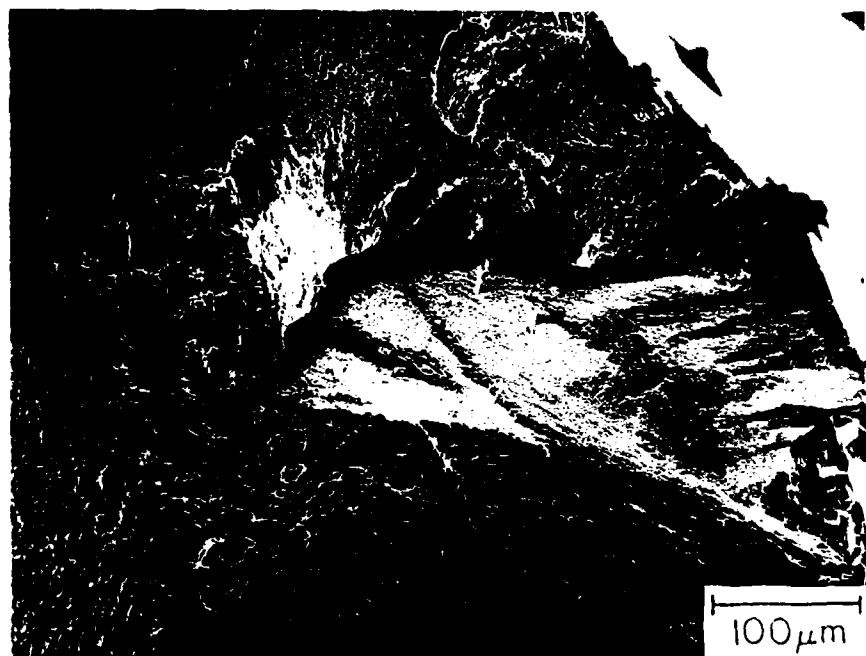
(a)
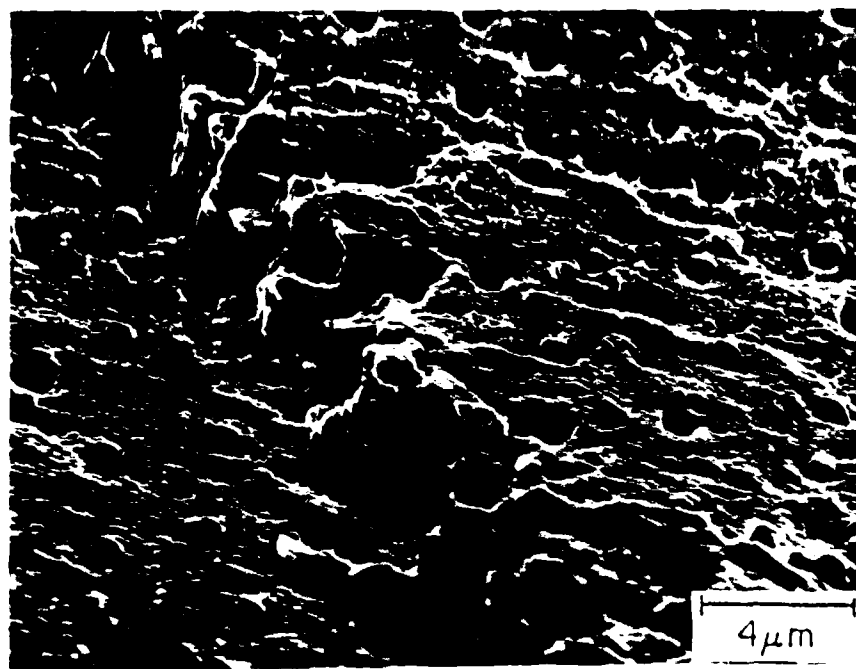
(b)

Fig. 53   SEM fractographs of aged Cotac 744, tested in fatigue at 825°C
and $\Delta\sigma = 1000$ MPa.   (a) Internal origin.   (b) Flat fatigue zone
with shallow dimples.
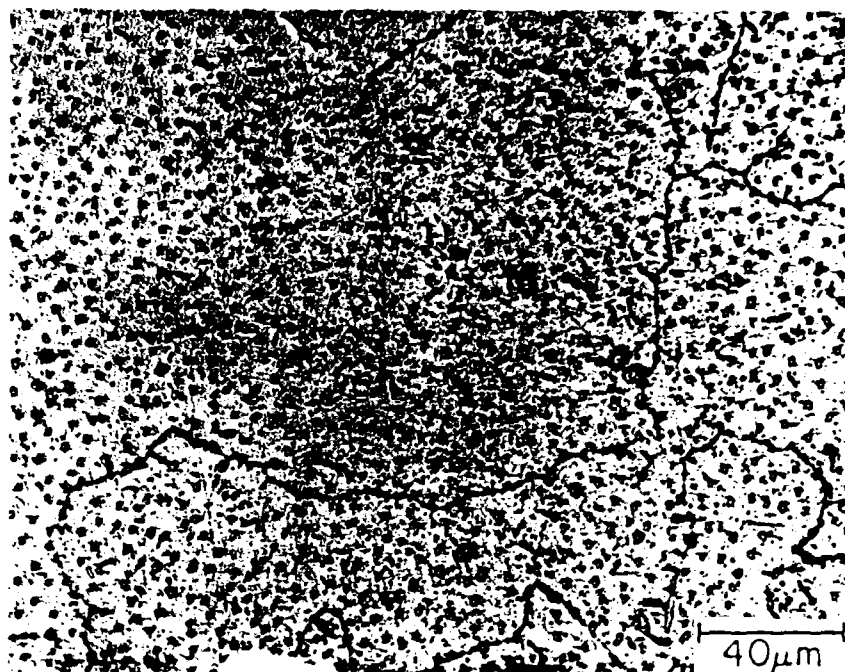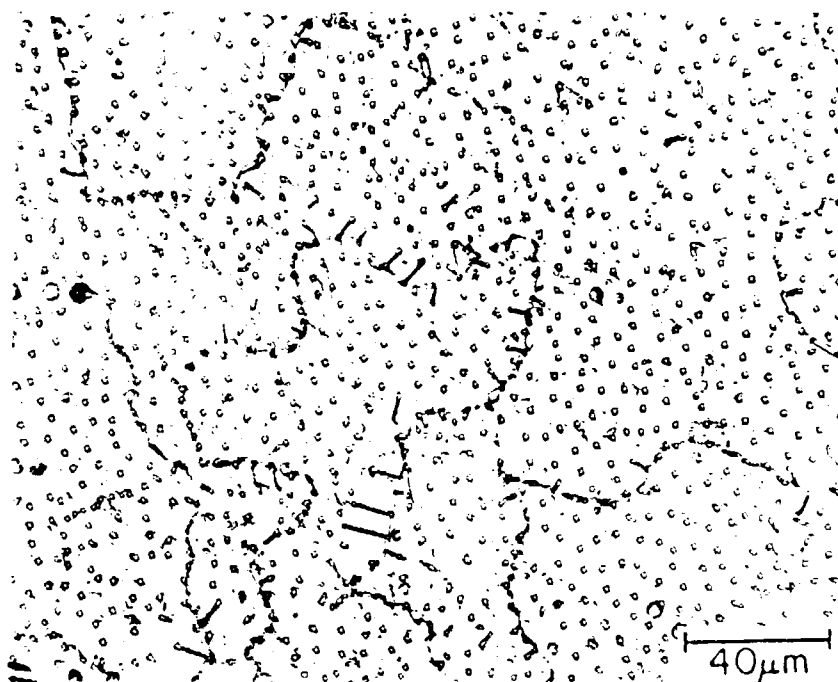
Fig. 54   Transverse microstructure of aged Cotac 744 following high
cycle fatigue at 825°C. Note the cellular appearance.
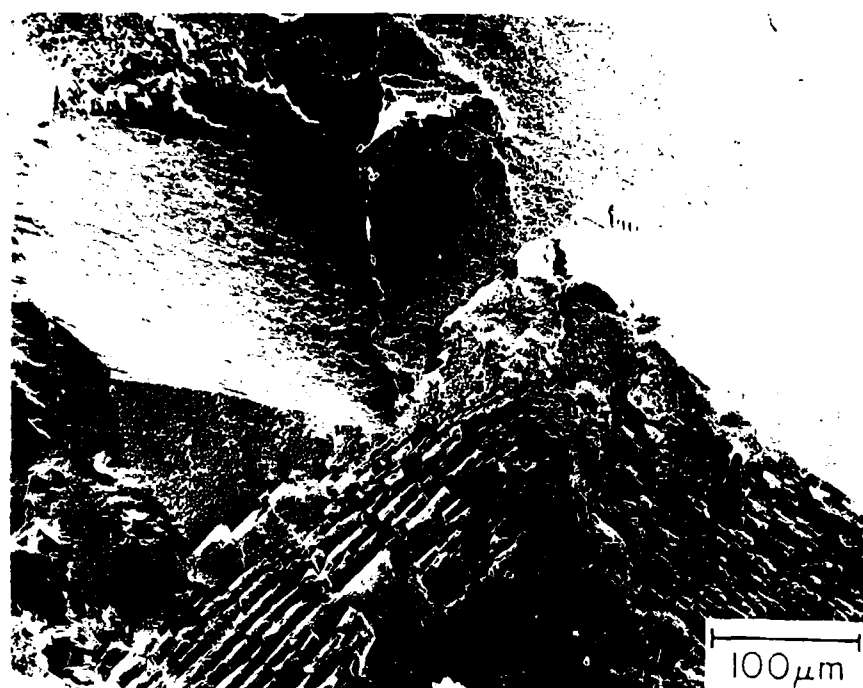
(a)
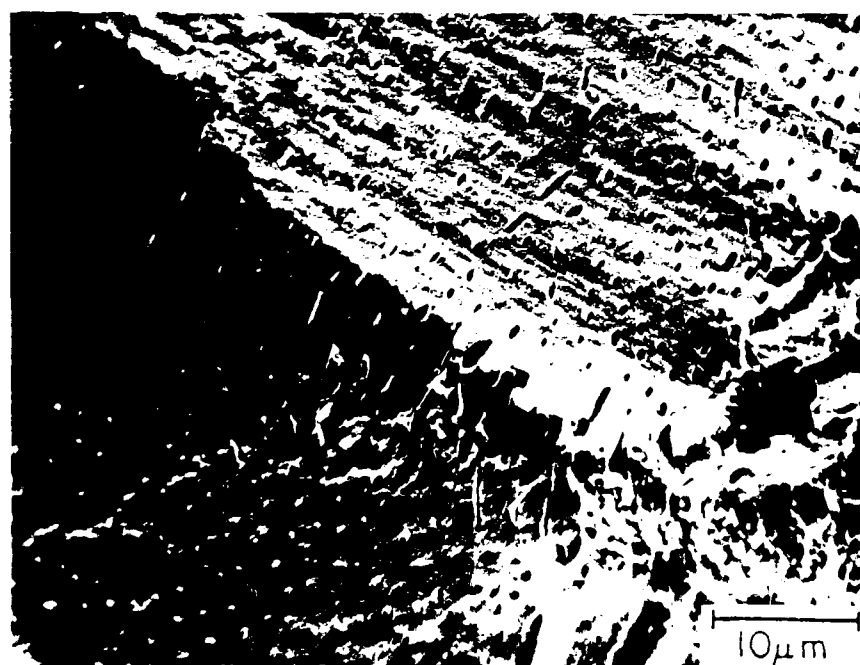
(b)

Fig. 55   SEM fractographs of aged AG-170 after fatigue testing at 825°C.
(a)   Internal initiation region.   (b)   Structural breakdown at
a colony boundary in the vicinity of the initiation region.

initiation region in another specimen (Fig. 55b) supports this hypothesis. The internal origin was always recognized by adjacent regions of terraced cracking. These can be easily identified in Fig. 55a. A higher magnification fractograph (Fig. 56) denies this as Stage I cracking. Stage II cracking, marked by well-defined striations, was observed near the origin in one of the specimens. These striations are shown in Fig. 57.

Difficulties were encountered in differentiating the fatigue and overload zones. However, observation of the outlying regions showed areas of severely necked fibers like those pictured in Fig. 58a. Also, the Mo fibers were found to show progressive markings similar to those observed for TaC in the aged Nitac alloy. These resemblances can be noted by comparing Fig. 58b and Fig. 50a.

4.3.3 Frequency Effects

Reduction of the 825°C test frequency from 20 Hz to 0.02 Hz caused significant changes in the fracture mode. Specimens no longer displayed distinct fracture regimes. The fracture surfaces of low frequency samples were essentially featureless. Fig. 59a shows a typical low frequency fracture profile. The identification of an initiation site was not easily accomplished. Some features characteristic of surface initiation were observed. However, these were too nebulous to be used for confirmation.

Fatigue zones were not found in aged Nitac 14B tested at frequencies of 2, 0.2 and 0.02 Hz. Unlike the specimens stressed at 20 Hz,
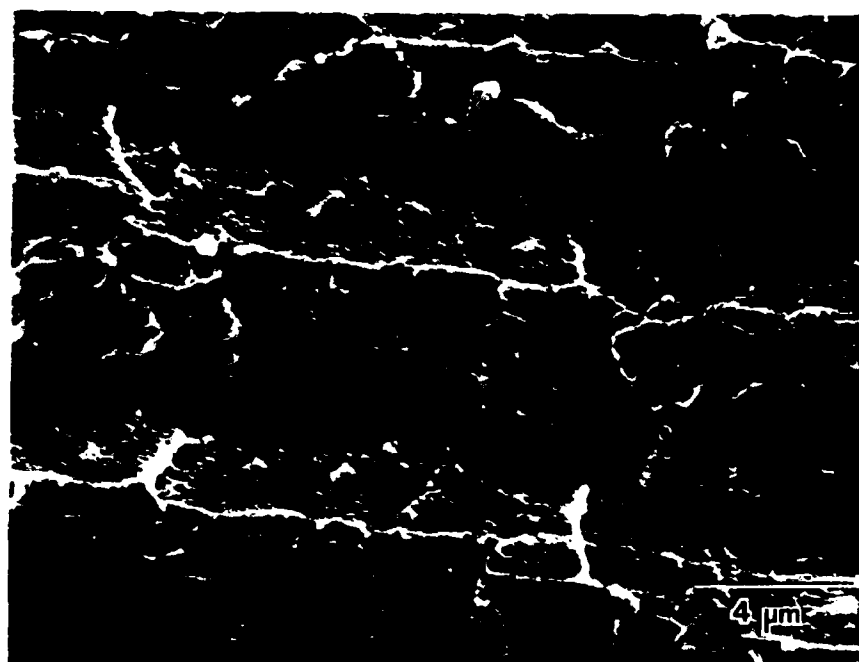
Fig. 56   Terraced cracking in the initiation region.
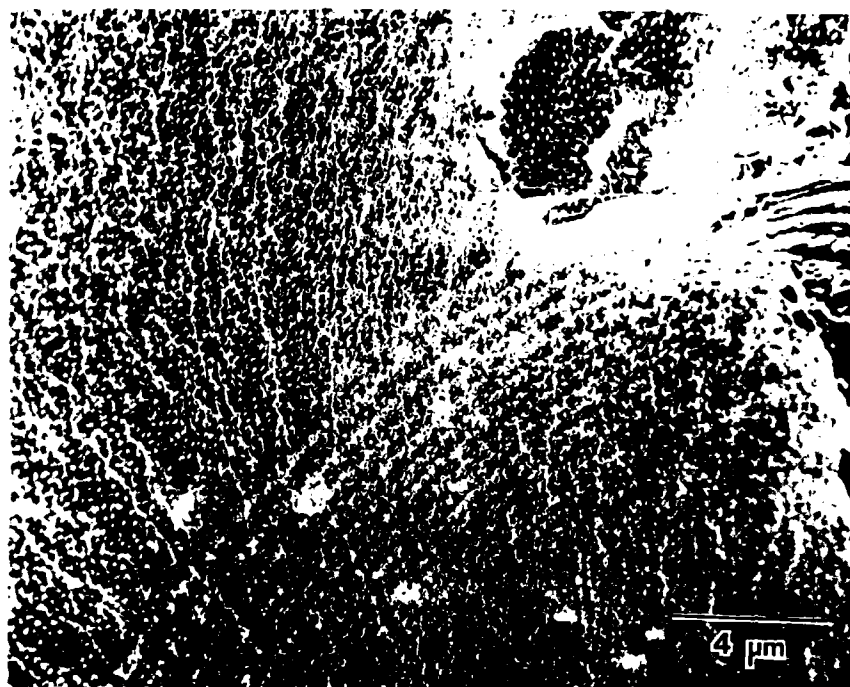
Fig. 57   Striations in an aged AG-170 specimen tested at 825°C and
Δσ = 1034 MPa.
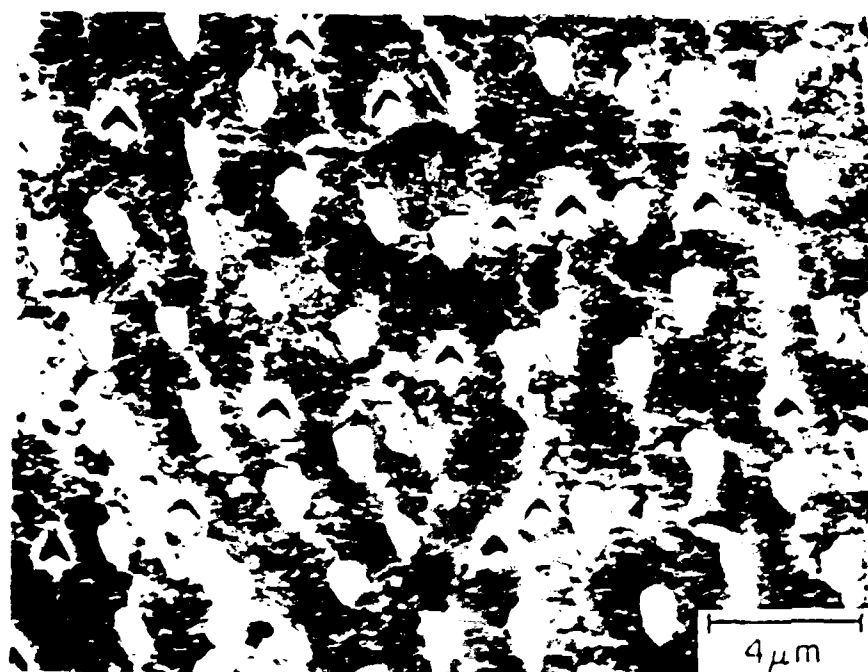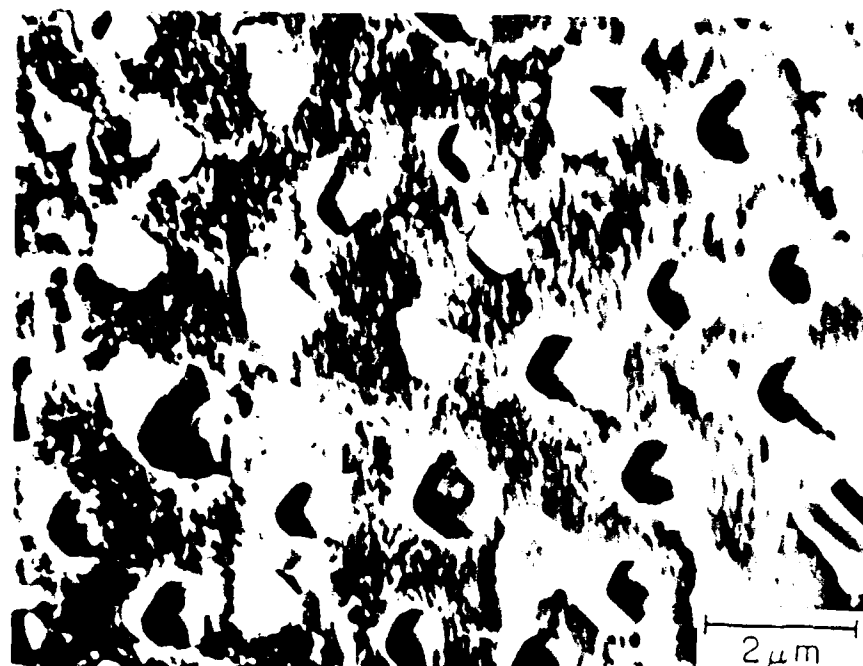
Fig. 58 Overload regions in aged AG-170 fatigue fracture. (a) Sever-
ly necked fibers. (b) Progressive slip markings extend from
fibers.

the fracture surfaces of low frequency specimens consisted almost entirely of dimpled overload regions. Void growth and coalescence is the mode of fracture. Final failure takes place by shear along active slip planes at an angle of 45° to the stress axis. Thus, fracture surfaces of low frequency specimens exhibited characteristic shear lips similar to the one pictured in Fig. 59b.

The dimpled regions are compared in Fig. 60. At the same magfication, the dimples were seen to increase in size from 2.5 μm to 7.5 μm as the frequency decreased. This is most apparent upon direct comparison of the extremes, Fig. 60a and Fig. 60d. A cycling frequency of 2 Hz caused little change in the S-N curve from 20 Hz. Hence, the dimple sizes of the 20 Hz and 2 Hz samples were approximately equal. The increase in dimple size upon lowering the cyclic frequency, plus the absence of well-defined fatigue and overload fracture zones, suggests a cyclic creep mechanism may be operating.

Extensive surface activity was also noted at reduced frequencies. Fig. 61 compares the surfaces of aged Nitac 14B at 20, 0.2 and 0.02 Hz. At a frequency of 20 Hz, fibers were observed to crack along planar slip bands on the surface (Fig. 60a). Fibers still cracked in the 0.2 Hz specimen. However, slip became wavier as shown in Fig. 61b. Further away from the fracture, small voids were found in the matrix. These voids were seen to linkup and cause fiber cracking. The effect was most spectacular at 0.02 Hz. Fig. 61c illustrates wavy slip on the specimen surface. Cracked fibers appeared serrated due to the action

of wavy slip. Larger voids were revealed on the sides of the gage sec-
tion (Fig. 61d) closer to the fracture surface. These observations are
also additional evidence of creep damage.
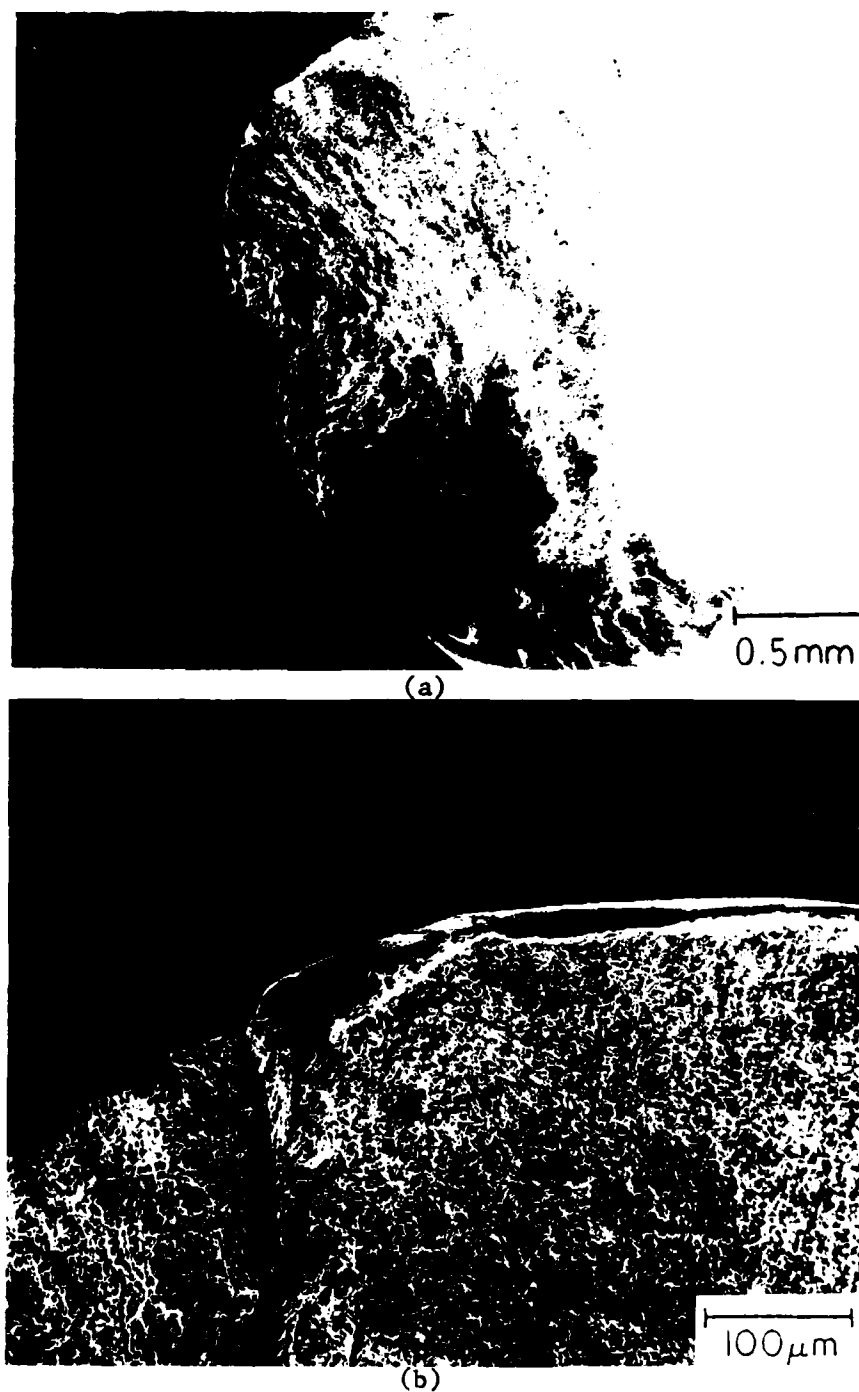
Fig. 59   SEM fractographs of aged Nitac 14B, tested at low frequency and
825°C. (a) Featureless fracture surface of specimen tested at
$\Delta\sigma$ = 1138 MPa and ν = 0.02 Hz. (b) Characteristic shear lip
on a specimen tested at $\Delta\sigma$ = 1034 MPa and ν = 2 Hz.
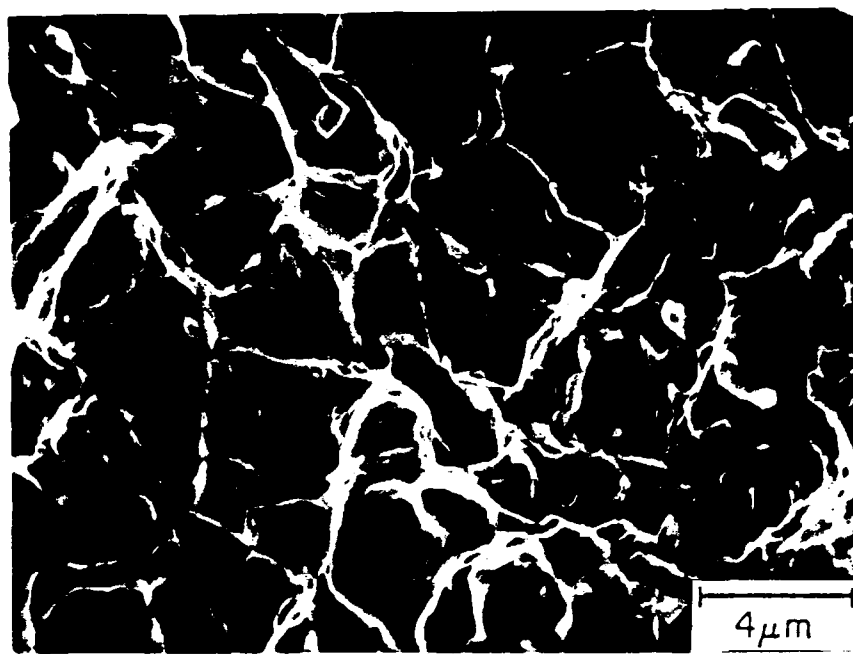
(a)
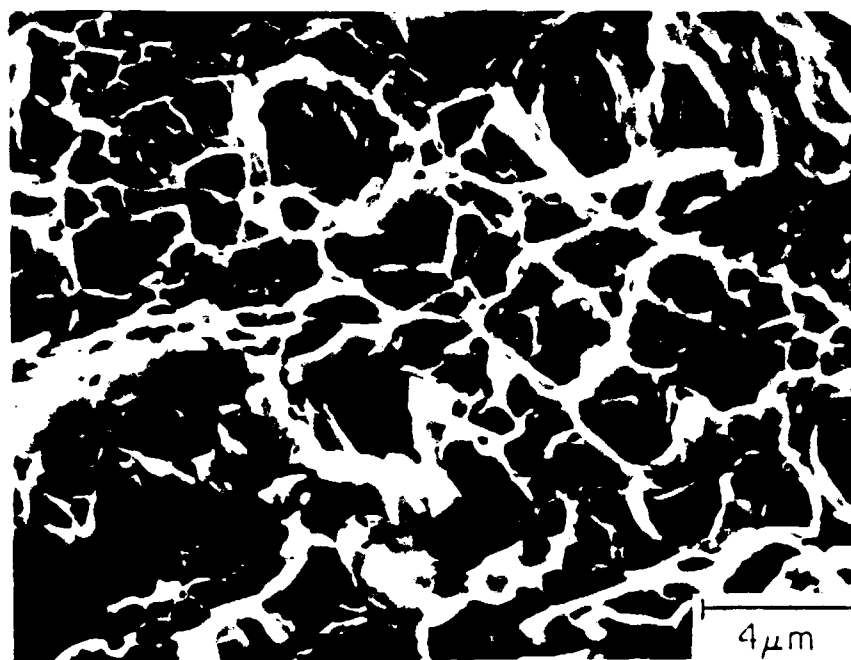
(b)

Fig. 60   Dimpled regions in aged Nitac 14B, tested at 825°C and
           $\Delta\sigma$ = 1034 MPa.   (a)   20 Hz.   (b) 2 Hz.
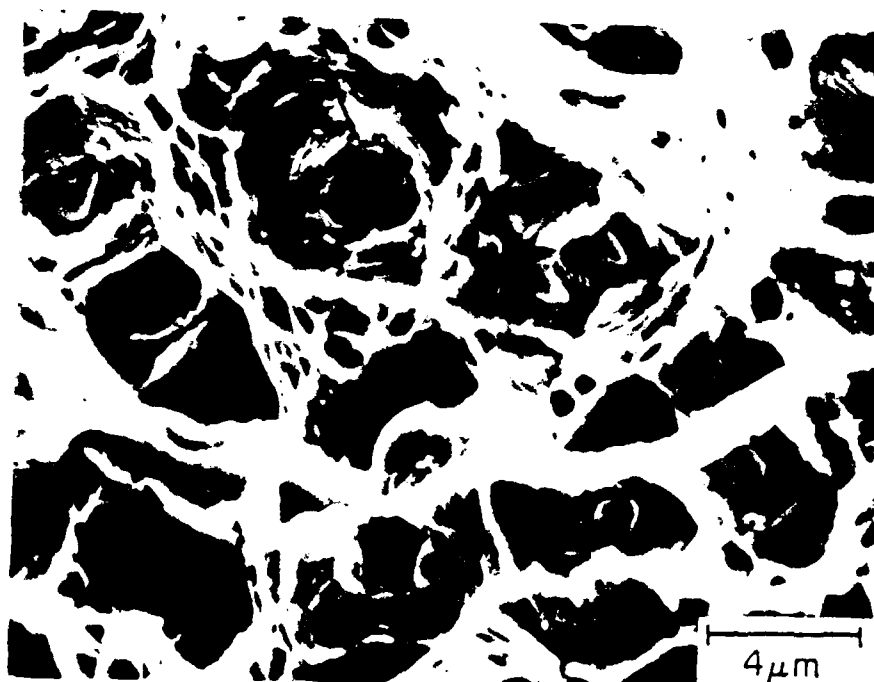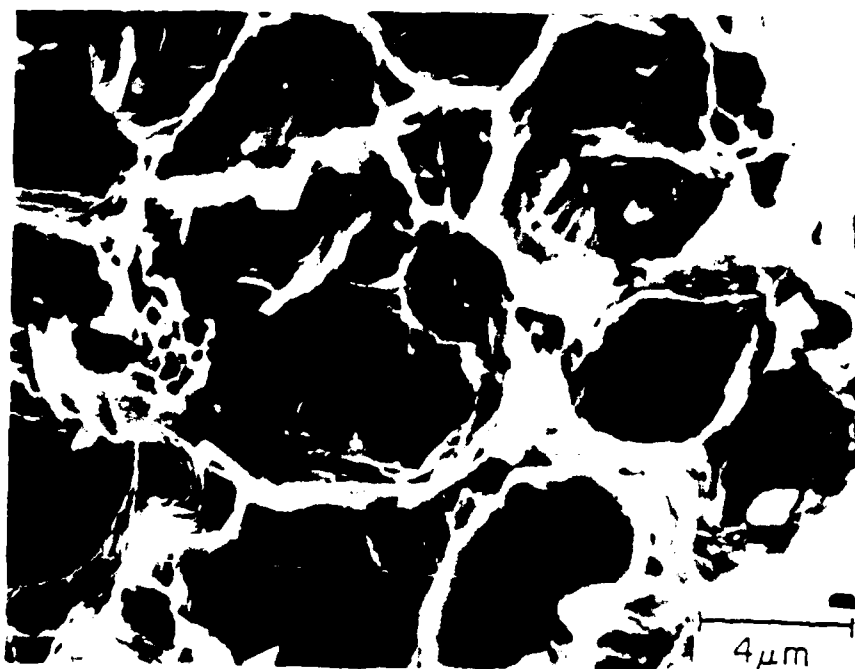
Fig. 60 Dimpled regions in aged Nitac 14B, tested at 825°C and
$\Delta\sigma$ = 1034 MPa. (c) 0.2 Hz. (d) 0.02 Hz. Note the in-
crease in dimple size with decreasing frequency.
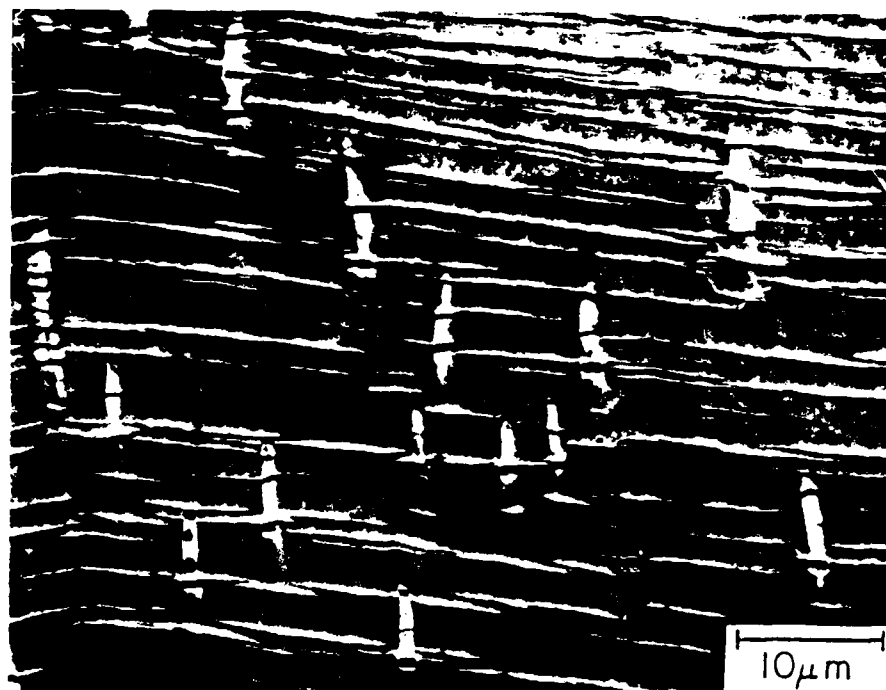
(a)
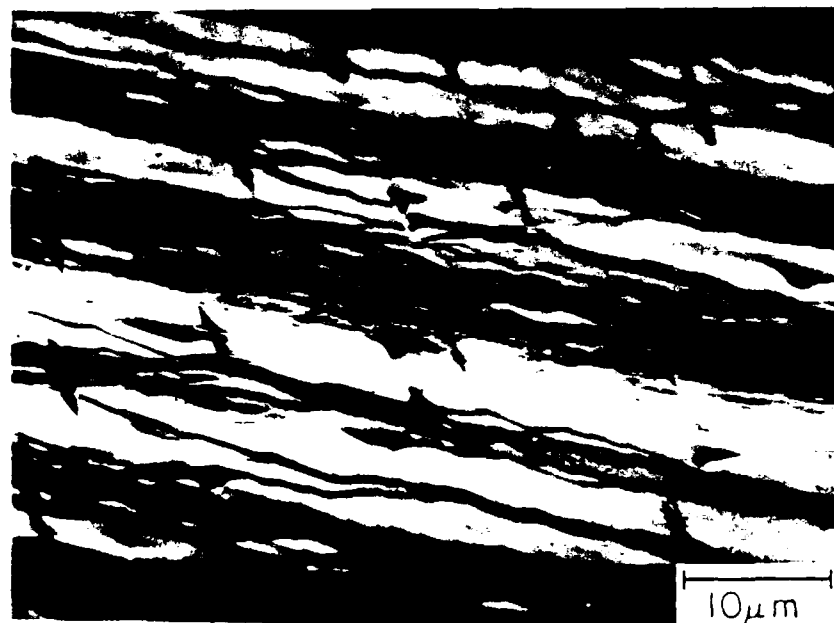
(b)

Fig. 61 Surface activity in aged Nitac 14B, tested at 825°C and
varying frequencies. (a) Planar slip at 20 Hz. (b) Wavy
slip at 0.2 Hz.
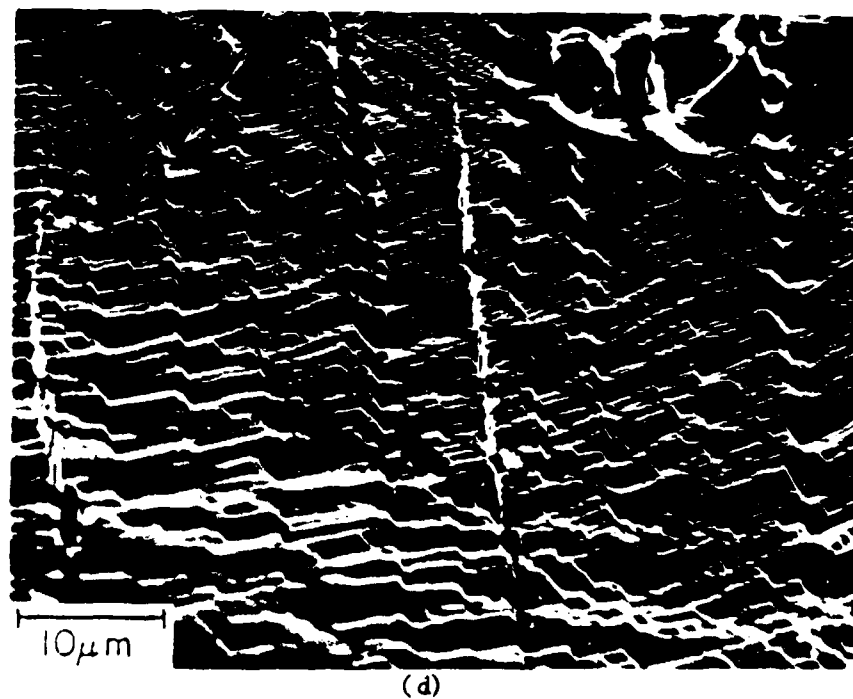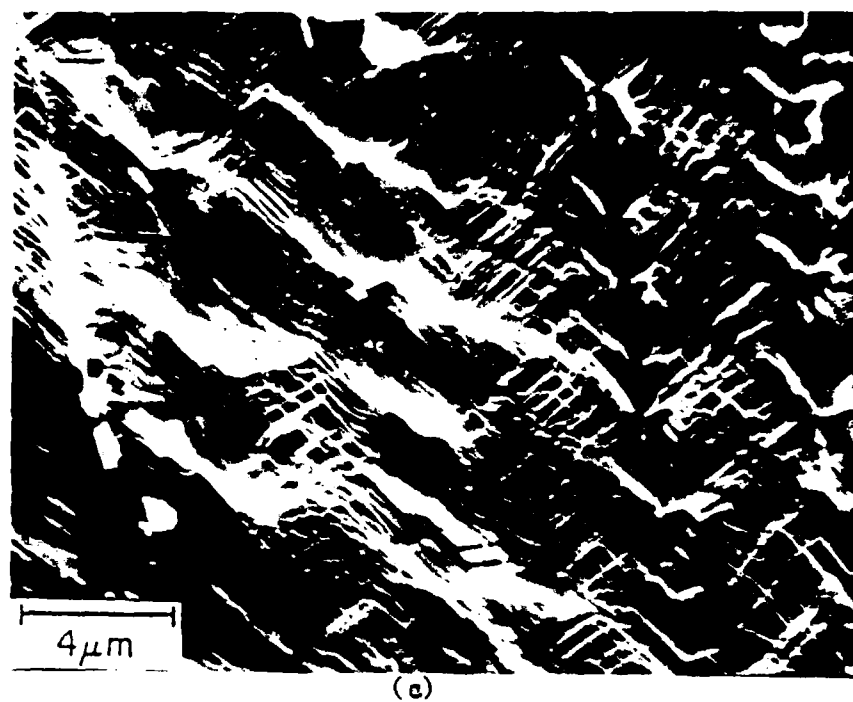
Fig. 61   Surface activity in aged Nitac 14B, tested at 825°C and
varying frequencies. (c) Wavy slip and void linkup at
0.02 Hz. (d) Lower magnification view of (c) showing
extensive slip activity.

PART 5

DISCUSSION

The mechanisms of fatigue damage for directionally solidi-
fied eutectics are different than for homogeneous materials. The
existence of more than one phase creates a complex microstructural
state of damage over a large volume instead of a few major cracks.
Several detailed investigations of the fatigue mechanisms of aligned
eutectics have already been conducted in our laboratory.[1,4,20,29,30,
51] This discussion focuses on failure modes in three stronger eu-
tectic alloys. In cases where earlier damage models are not suitable,
new mechanisms have been proposed to explain the fatigue behavior.

5.1 Temperature

The three advanced eutectic alloys reveal excellent HCF
properties both at ambient and elevated temperatures. However, there
is some deterioration in fatigue resistance at $825^{\circ}C$, especially for
AG-170 where the decrease is approximately 28%. High temperature
fatigue strength is highly sensitive to microstructural parameters
such as microstructural perfection, interfiber spacing, and colony
size. Therefore, various imperfections present in some of the spec-
imens may have attributed to shorter lives. Neglecting microstruc-
tural parameters, most mechanical properties have a tendency to de-
cline with increased temperature. The fatigue strength of in-situ
composited is no exception.

Raising the temperature alters the fatigue deformation

123

mechanism. At 25°C, failures were surface initiated and propagation proceeded along crystallographic planes (StageI cracking) in agreement with previous work on aligned eutectics.[1,4,20,29,30,51] Intense planar slip in the Ni-rich matrices of Nitac 14B and Cotac 744 initiated cracks in the brittle carbide fibers. Continued cycling resulted in the formation of voids at the sites of fiber cracks, and the eventual growth and coalescence of these voids into a broad crack front. Thus, failure in these ductile matrix-brittle fiber composites was attributed to microvoid coalescence and growth.

There was no opportunity for holes to be created by cleavage in AG-170, the ductile-ductile composite. No dimples were present on the fracture surface. Instead, it was faceted and fibers fractured in a ductile, chiselpoint manner. Fiber pullout and interfacial debonding accounted for failure.

At 825°C there was no evidence of Stage I cracking in any of the alloys. Smaller propagation regions and larger overload areas were observed. Ultimate fatigue failure occurred by the non-crystalline, Stage II mode. This difference in failure mode may also account for the difference in fatigue resistance at the two temperatures. Stage I cracking is often regarded as a slower mode of growth than Stage II cracking.

The higher fatigue strength at room temperature should not be ascribed to Stage I cracking alone. Other factors also contribute to the superior fatigue lives at 25°C. The matrix phase experiences a lessened work hardening capacity at elevated temperatures. Lower

stresses are required for matrix slip. Therefore, dislocations can easily move through the matrix. Additional slip systems also are operative at higher temperatures. The intense planar slip which was active at room temperature becomes more diffuse as the temperature is raised to 825°C. This slip dispersal is typical of most Ni-base superalloys at temperatures in the vicinity of 800°C.[75] It resulted in coarser, more widely spaced slip bands and more rounded crack tips which are suggestive of higher local concentratons of plastic deformation. These higher concentrations contribute to the lower fatigue resistance at 825°C.

Even though the fatigue properties of these three eutectics show a small degradacion at 825°C, they still remain superior to those of the matrix material alone. Obviously the fibers play a major role during cyclic stressing. Bibring[8] attributed the elevated temperature strength of composites to load transfer from the matrix to the fibers. This may prove to be the case in the AG-170 alloy where the ductile Mo fibers break in a chiselpoint manner. Forsyth et al.[76] first suggested the primary role of the reinforcing phase in delaying crack propagation. Other authors[48,77] had similar views and proposed that the presence of strong fibers deflected propagating fatigue cracks out of their preferred paths. Direct evidence to support this concept is found in failures of heat treated AG-170 and Cotac 744, where longitudinal cracking was noted along colony boundaries. Further explanation of this mechanism in terms of a crack reinitiation at boundary breaks will be given in Section 5.2. The presence of

fibers may also have a direct influence on crack propagation by the blockage of long-range matrix slip.

The most exceptional feature of the TEM results was the observation of dislocation activity in the fibers of Nitac 14B and AG-170. The Mo fibers in AG-170 (Fig. 35) demonstrated significant dislocation activity. Activity was observed to a smaller extent in the TaC fibers of Nitac 14B (Fig. 34), but not at all in NbC. It is surprising that fiber deformation has occurred even in carbide fibers. Nevertheless, the difference in plasticity of the three fiber types seems to have little effect on fatigue resistance of the three alloys. Clearly AG-170 with its ductile α-Mo fibers should be superior if fiber plasticity were a major factor in composite fatigue strength. This suggests that the properties of the γ/γ' matrix dominate the resistance to cyclic deformation. This is in accord with previous crack propagation data reported for several eutectic alloys in which it was shown that three γ/γ' Ni-base eutectics had similar resistance to crack growth, while a Co-base alloy revealed more rapid crack growth than any of the γ/γ' alloys.[5]

Reliance on the properties of the matrix phase helps to explain the apparent superiority of Nitac 14B as shown in Fig. 14. Numerous alloying elements help to improve the strength of the Nitac 14B matrix, which contains 60 vol % γ'. On the contrary, AG-170 has a large volume fraction of reinforcing phase (20 vol % in comparison with 3-5 vol % for Nitac 14B and Cotac 744) and, therefore, must contain a lesser amount of γ' phase. Fig. 9 gives a view of the rela-

tive amounts of γ, γ' and fibers present in each alloy. Clearly, Nitac 14B shows the largest amount of fine γ'. Both AG-170 and Cotac 744 contain coarse γ', encasing the fibers. The fine γ' particles present in Nitac 14B help to increase the flow stress of the matrix and increase fatigue strength by blocking dislocation motion through the matrix.

5.2 Heat Treatment

Aging of each of the three aligned eutectics produces a considerable increase in high temperature fatigue properties. The greatest effects of heat treatment are demonstrated by AG-170, which undergoes a 29% increase in fatigue limit at 825°C. This finding may prove beneficial in the eventual application of these materials as turbine blade alloys. Solutionizing treatments seem to have little effect on the room temperature fatigue strengths although aging did yield some improvement in fatigue lives, particularly at high stresses. These significant improvements can be explained by the microstructural variations produced by heat treating and the associated changes in failure mode.

"Solutionizing" of Nitac 14B, which causes precipitation of fine γ', has virtually no effect on its room temperature fatigue life. The as D.S. and solution treated S-N curves for 25°C fall within a single scatterband. Little change was seen in the overall fracture appearance of P.S.T. Nitac 14B. The fracture is still surface initiated and Stage I propagated, but is more angled with a flatter fatigue zone and a larger overload region. The mode of failure remains

microvoid growth and coalescence.

Partial solution treatment of the ductile $\gamma/\gamma'-\alpha$ alloy results in a cubic γ' network. However, it has different outcomes for cellular versus aligned AG-170. (Recall that aligned microctructures of AG-170 possess a continuity of stucture across boundaries, while cellular structures exhibit a total breakdown of structure and loss of coherency across cell boundaries. See section 4.3.2.1.) Partial solution treatment has little effect on aligned material where the method of damage accumulation is similar to the as D.S. condition. Nevertheless, solution treatments did cause an 18% increase in the fatigue life of cellular AG-170. This effect may be partly due to the slower crack propagation rate across the incoherent boundaries due to crack branching. Also, the irregular structure and variation in fiber orientations is thought to hinder crack propagation.

Obviously, cell boundary cracking is prevalent in the material which possesses a cellular microstructure. This longitudinal cracking may actually be beneficial when it occurs to a limited extent. Crack branching occurs down cell boundaries, blunts the crack and diverts the crack path, resulting in a slower rate of crack growth.

This mechanism is also operative in aged AG-170, tested at room temperature. Aging of AG-170 alters the microstructure even further and causes the precipitation of a new Mo phase. At high stresses aging has an even greater effect than solutionizing, as seen in Fig. 18. Fracture surfaces of aged AG-170 tested at 25°C appear very different from the as D.S. and P.S.T. profiles. Sharp facets are no

longer seen. Instead, fracture proceeds outward from the surface ini-
tiation site in a series of parallel steps. Closer examination reveals
this ledgelike cracking to be a result of interface debonding, with the
fibers remaining intact. Longitudinal splitting of the interface may
also contribute to the excellent fatigue resistance. It retards crack
growth by deflecting the propagating fatigue crack out of its original
path so that reinitiation must occur before propagation can proceed.
Grossman and Stoloff[4] have previously attributed the high relative
fatigue strength of lamellar γ/γ'-δ alloys to this mechanism.

Aged specimens of Nitac 14B and Cotac 744 do not exhibit in-
terface delamination at 25°C even though they do possess increased fa-
tigue resistance at high stresses. The damage mechanism remains micro-
void coalescence and growth. Therefore, improvements must be related
to improved matrix strength and some crack branching down cell boun-
daries.

Though fractures of aged specimens were usually surface ini-
tiated, one Nitac 14B specimen displayed an impurity-initiated, inter-
nal origin. (Fig. 43) The impurity is two-phase, consisting of ceramic
and crystalline phases. The ceramic phase is probably an aluminide
which entered the melt from the alumina crucible. It contains den-
drites which presumably are parts of the melt that could not be dir-
ectionally solidified. Other such origins related to impurities and
microstructural imperfections also have been identified. (Some AG-170
specimens exhibited dendritic surface initiations at 825°C, while one
aged Cotac specimen also showed an impurity-initiated, internal origin

at 825°C.) These events illustrate that fatigue of D.S. eutectics is not necessarily an initiation controlled process. In fact, it may be propagation controlled. If fatigue were initiation controlled, the Nitac specimen (or any of the others mentioned) containing the impurity particle would have failed in a very short time. The propagation rate would have exponentially increased immediately after initiation. Instead the specimens had long lives (e.g. the life of the aged Nitac sample exceeded 10^6 cycles), demonstrating the plausibility of propagation controlled high cycle fatigue. This is in agreement with the earlier conclusions of Tartaglia[5] and Austin[70].

By far the most beneficial effects of heat treatment on fatigue properties of the three in-situ composites are noted at 825°C. Aging proves especially favorable for AG-170 where the fatigue life is improved more than two orders of magnitude at constant stress levels.

The considerable effect of aging on the fatigue behavior of AG-170 at both 25°C and 825°C can be explained by the variation in hardness. Recall (Table II) that heat treatment causes the most drastic changes in the hardness of AG-170. The hardness of partially solutionized material increased by 26% over the as D.S. value, while aging resulted in a phenomenal 41% increase. An approximate linear relationship exists between the hardness and 0.2% offset yield strength of steels.[78] The tensile strength of steel is also directly proportional to hardness. If these correlations are assumed for nickel-base eutectics, then the tensile strength of the alloys should increase upon heat treatment. AG-170, displaying the most pronounced hardness

variations, should also exhibit a substantial change in the flow stress. This is confirmed in Table III where it can be seen that the tensile strength of aged AG-170 has considerably increased over the as D.S. condition.

The higher flow stresses of heat treated AG-170 imply higher stresses are required for matrix slip. The cuboidal γ/γ' network resulting from heat treatment limits dislocation motion through the matrix. Thus, in this Ni-Al-Mo alloy heat treatment causes microstructural changes which result in a substantial hardness differential and corresponding increases in the yield stress. A higher plastic deformation capacity is achieved and, consequently, fatigue lives are prolonged.

Differences in the fracture surface appearance of aged AG-170, tested at 825°C, suggest a change in failure mode in accord with the higher flow stress. The mechanism is one of slow crack growth. The fracture surface is sharply faceted with an internal origin. No evidence of crystallographic cracking has been observed, although striations have been found on one specimen. The fibers in the overload regions are more severely necked than previously observed. The heat treatment, while increasing the matrix strength, lowers the ductility of the matrix and leaves the fiber ductility unchanged. The advancing crack does not propagate quickly through the fine γ' network of the matrix. However, after the crack has finally proceeded through the matrix, the fibers neck to support the load. The increased necking of the fibers results from their increased contribution in supporting the excess load.

Table III

Comparison of Tensile and Fatigue Properties at 25°C – Vacuum

Alloy	Condition	σ_Y (0.2%) MPa	σ_{UTS} MPa	ε_F %	$\sigma_{max_{10}7}$ MPa	$\dfrac{\sigma_{max_{10}7}}{\sigma_{UTS}}$
Nitac 14B	As D.S.	847	1517	11.2	1000	0.78
	P.S.T.	731	1100	5.3	945	0.85
	Aged	772	1669	14.8	827	0.50
AG-170	As D.S.*	724	1496	18.5	1000	0.67
	P.S.T. (Aligned)	1207	1572	4.3	1034	0.66
	Aged	1213	1310	4.6	1082	0.83
Cotac**	As D.S.	--	1503	13	1000	0.67

* Test results obtained at G.E. Research and Development Center. (22)

** Values obtained by ONERA(14) for Cotac 744 after the following treatment: 20 minutes/1200°C/AC + 16 hours/850°C/AC.

Aged Nitac 14B and Cotac 744 do not show such substantial increases in hardness over the as D.S. condition. Their hardness increases only approach 20%, with Nitac 14B demonstrating the larger improvement. Although the hardness of aged Nitac 14B is not as large as that of aged AG-170, the aged Nitac alloy still exhibits a higher fatigue limit at 825°C. It has the advantage of superior fatigue properties in the as D.S. condition owing to its high matrix strength and large γ' volume fraction. (Section 5.1) However, the relative improvement by aging is much larger in AG-170 as indicated by the hardness variations.

The small improvement aging has on the fatigue life of the carbide-reinforced alloys also is related to microstructure. Improved fatigue behavior results partly from alteration of the γ' size and morphology. Aging of Nitac 14B and Cotac 744 causes a more uniform distribution of hyperfine γ'. A precipitation hardening mechanism acts to increase matrix strength. It follows that fatigue properties, which are hypothesized to be matrix controlled (as discussed in Section 5.1), should also improve. The fine γ' precipitates interfere with crack propagation by inhibiting dislocation pileups and redistributing the stress field associated with dislocation arrays. The rate of crack propagation is retarded as the cracks are forced to bow between the precipitate particles. The presence of fine γ' particles explains the increased hardness and toughness of these two alloys. More energy is required for fracture. This would account for the observation of matrix cracking on the side of aged specimens, tested at 825°C.

Aging also forms a γ' coating of cell boundaries. In moderation, this coating usually coats the boundary and limits slip in this region. Nevertheless, cell boundary cracking was observed to occur in aged Nitac 14B and Cotac 744. It contributes to the superior fatigue lives as previously discussed. The presence of smaller colonies provides more boundaries to deflect and blunt the crack in the fatigue zone.

5.3 Frequency

Frequency-induced changes in fatigue life of eutectic alloys at elevated temperature in vacuum are a strong indication of a creep-fatigue interaction. The earliest evidence that creep damage reduces the high temperature fatigue life of D.S. alloys was reported by Maurer et al.[1] for Al-Al$_3$Ni. Coffin and coworkers[62,63] have attributed such frequency effects in conventional alloys to enhanced environmental attack.

Aged Nitac 14B exhibits a very pronounced frequency effect at 825°C(0.6 T_m). Decreasing the test frequency from 20 Hz to 0.02 Hz drastically reduces the fatigue life. However, little change is noted between 20 Hz and 2 Hz. All tests were conducted in a vacuum of 10^{-6} torr, sufficient to suppress, but not eliminate environmental attack. Nitac 14B demonstrates excellent oxidation and hot corrosion resistance. Observation of the fracture surfaces with a stereomicroscope and the scanning electron microscope confirmed them to be oxide-free. Therefore, environment can be eliminated as a major contributing factor.

Specimens tested at 20 Hz exhibit a surface initiated fracture and Stage II cracking while those tested at low frequencies reveal a very different fracture profile which is essentially featureless. The initiation sites are not easily identified. The fracture regimes are nondistinctive, characteristic of creep fracture. However, final failure is known to occur by shear along active slip planes at an angle of 45° to the stress axis. The presence of shear lips also are indicative of a creep failure.

The dimples present on fracture surfaces imply that failures are ductile. The total fracture energy is related to dimple size -- energy increases as the depth and width of dimples increases. Dimple size is magnified at least two or three times as frequency is lowered to 0.02 Hz. (See Fig. 60.) The larger dimples suggest increased fracture ductility. An analogous upward trend in fatigue ductility with lower test frequency was also found for basic Nitac[2] and Cotac[45]. The increased reduction in areas of those alloys, also tested at 825°C, was thought to arise principally from creep. Indeed, ductility should be independent of frequency in a pure fatigue process. Therefore, the increase in dimple size is straightforward evidence for the presence of a significant creep-fatigue interaction.

Slip activity also changes as frequency is changed. Fig. 61 revealed the transformation from planar to wavy slip with decreasing frequency. Leverant and Gell[77] have interpreted this change in slip character as a transition from a fatigue damage mechanism at high frequency to one of creep damage at lower frequencies. This presents

additional evidence for cyclic creep in Nitac 14B at low frequencies.
Larger cavities and voids have been observed on the side surfaces of
aged specimens tested at 0.2 and 0.02 Hz. These cavities usually exist
at cracked fibers and eventually coalesce along deformation bands.

Plots of specimen life (cycles and hours) versus frequency
are shown in Fig. 62a and b. Fig. 62a shows relatively little change
occurs in the number of cycles to failure at 20 and 2 Hz. However, a
substantial drop in cycles to failure can be observed as the frequency
is lowered to 0.02 Hz. The duration curve, Fig. 62b, illustrates a
different trend. There is an initial increase in specimen life with
decreased frequency. As the frequency is reduced still further, the
curve proceeds concave downward and life is shortened.

If the only deformation mechanism in operation were fatigue,
the number of cycles to failure at a given stress level would remain
constant with decreasing frequency. On the other hand, in a purely
creep-type test the time to failure remains independent of frequency.
The slope of the curves of Fig. 62 show that neither pure creep nor
pure fatigue is occurring in the Nitac 14B system. As the frequency
decreases from a very high value, there is initially no effect on the
number of cycles to failure. (See Fig. 62a.) Very little change in
slope is noted as the frequency changes from 20 Hz to 2 Hz, indicating
pure fatigue is still the controlling mechanism. However, further fre-
quency reductions produce a departure from the "pure fatigue" line.
The downward trend in the data suggests that creep is occurring. At
lower frequencies, the slope of the log N_f versus log v curves show
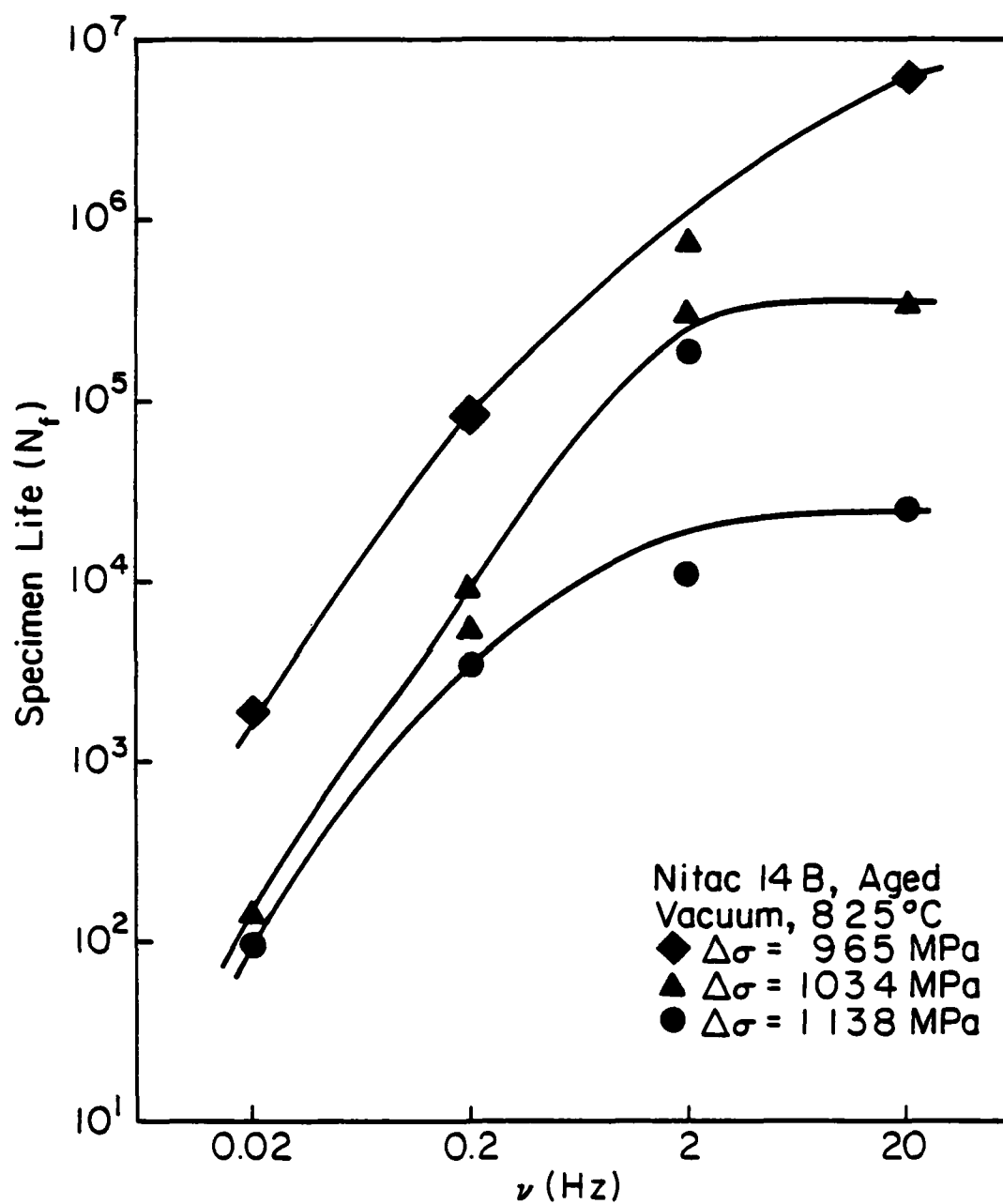
Figure 62   Effect of frequency on the fatigue behavior of aged Nitac 14B
at 825°C in vacuum.   (a) Fatigue life (cycles) vs. test fre-
quency.
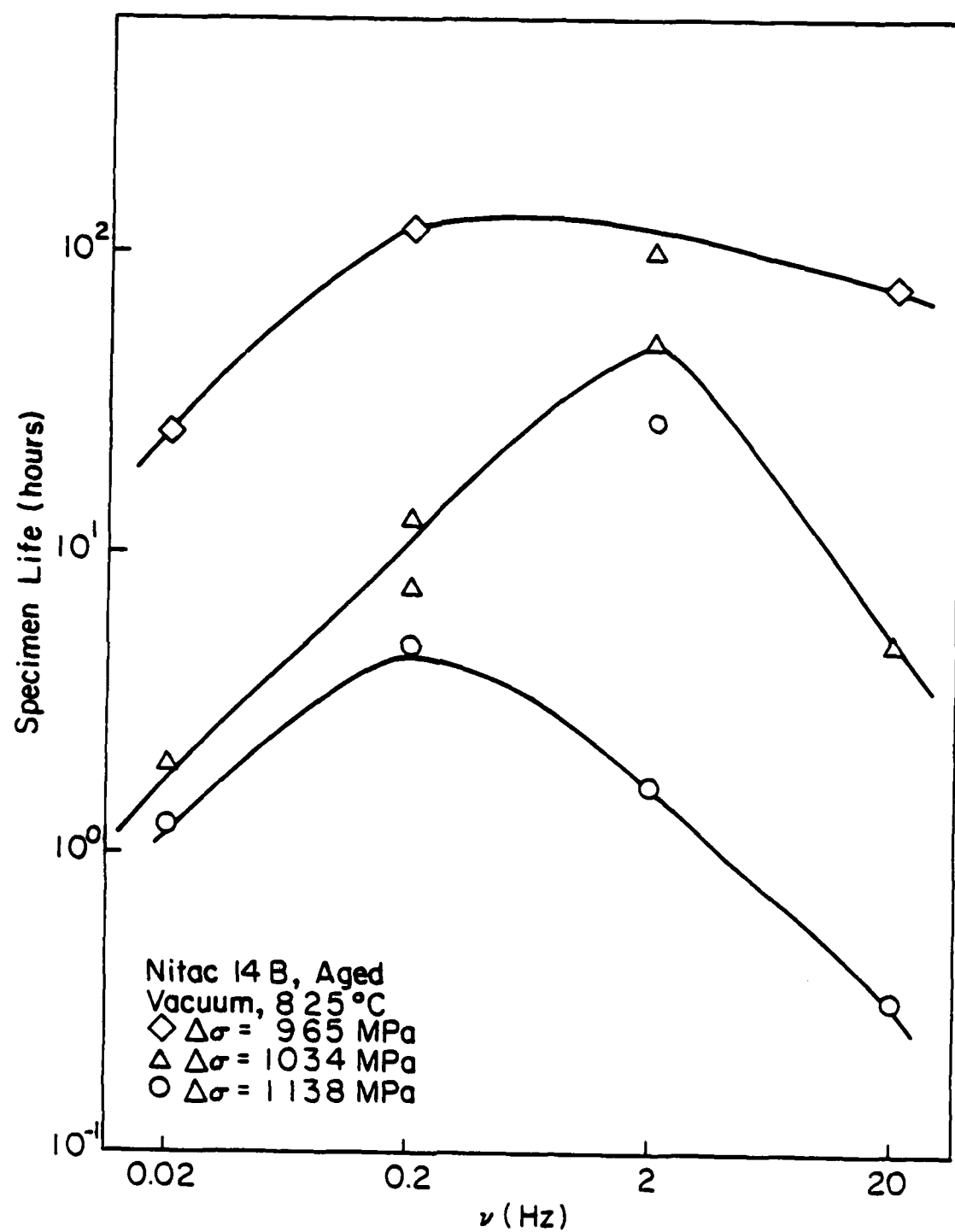
Figure 62 Effect of frequency on the fatigue behavior of aged Nitac 14B
at 825°C in vacuum. (b) Fatigue life (time) vs. test
frequency.

some deviation from the ideal slope of 1.

Fatigue mechanisms produce specimen failure in a constant number of cycles, independent of frequency. Therefore, a specimen failing by pure fatigue should exhibit increasing time to failure with decreasing frequency. The duration versus frequency curves of Fig. 62b initially demonstrate this trend. However, upon decreasing the frequency still further, the times to failure show a marked decrease. This is additional evidence for the operation of a creep mechanism at low frequencies.

Johnson[29] has devised a graphical model which describes these effects quite well. It is illustrated in Fig. 63 where the dotted lines represent the "pure fatigue" and "pure creep" lines. Fig. 63a shows the effects of decreasing frequency on N_f. If fatigue is the controlling mechanism, decreasing the frequency from a very high value initially has no effect on the cycles to failure. Further decreases in frequency result in longer times spent at high stresses. This tends to enhance creep, which also decreases N_f.

As previously discussed it is expected that fatigue life, measured in elapsed time, should increase with decreasing frequency at high frequencies where fatigue processes dominate. Then, as shown in Fig. 63b, further reduction of the test frequency will actually produce a departure in failure time from that of pure fatigue. Creep becomes operative and results in shorter specimen lives than predicted by pure fatigue.

Nitac 14B behaves in accordance with this qualitative model.
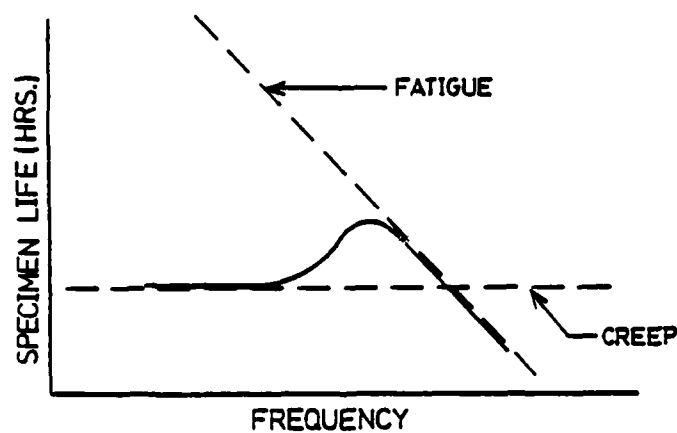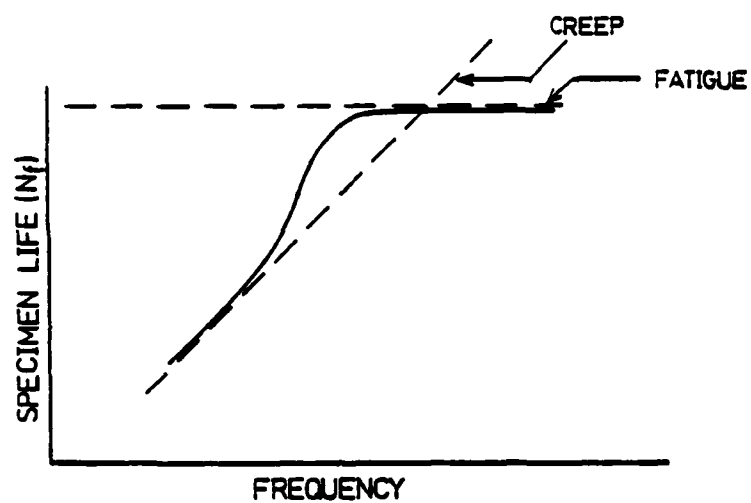
Fig. 63 Predicted shape of the fatigue life vs. test frequency curve
for a "large" range of predicted test frequencies.[29]
(a) N_f vs. frequency. (b) t_f vs. frequency.

The curves of Fig. 62 are similar to the hypothetical, solid curves of Fig. 63. Therefore, Nitac 14B, like the Ni,Cr,Al-TaC system[29], behaves in a manner dictated by creep processes when tested at 825°C in the frequency range 20-0.02 Hz. The decrease in both t_f and N_f with reduced frequency suggests creep has interacted with the overall fatigue process.

It is unlikely that strain rate or stress effects substantially contribute to the observed variations in fatigue behavior with changing frequency. Nitac 14B is a very high strength material with an approximate flow stress of 1000 MPa at 825°C in the aged condition. This extremely high flow stress is attributed to the unusual strengthening of fine, ordered γ' precipitates. The high flow stress outweighs the effects of high mean stresses due to tension-tension cycling and lower imposed stress rates at low frequencies.

5.4 Comparisons with Other Alloys

The advanced eutectic alloys described in this study reveal the same excellent HCF properties as their model system predecessors. Tables III and IV list the fatigue strengths for the various conditions which were investigated. The fatigue properties of Nitac 14B, Cotac 744 and AG-170 are far superior to those of both wrought and conventionally cast superalloys, particularly when compared as a ratio of maximum cyclic stress at 10^7 cycles to UTS.

Unusually high endurance ratios, between 0.5 and 0.89, have been obtained. Nitac 14B demonstrates the highest fatigue strength of

Table IV

Comparison of Tensile and Fatigue Properties at 825°C – Vacuum

Alloy	Condition	σ_Y (0.2%) MPa	σ_{UTS} MPa	ϵ_F %	$\sigma_{max_{10}}7$ MPa	$\dfrac{\sigma_{max_{10}}7}{\sigma_{UTS}}$
Nitac 14B	As D.S.	858	1034	14.1	896	0.87
	Aged	1054	1124	17.6	1000	0.89
AG-170	As D.S.	1190	1337	20	758	0.57
	Aged	1165	1192	12	965	0.81
Cotac 744*	As D.S.**	—	1103	11.5	862	0.78
	Aged					

* Interpolated values from ONERA[14] for Cotac 744 after the following heat treatment: 20 minutes/1200°C/AC + 16 hours/850°C/AC.

** As D.S. and aged Cotac 744 have approximately the same fatigue limit at 825°C.

the three at room temperature. Fig. 64 graphically represents the outcome at 25°C. Except for the $\gamma/\gamma'-\delta$ eutectic, which has a ratio of 0.84[4], Nitac 14B remains superior with $\sigma_{max_{10^7}}/\sigma_{UTS} = 0.78$. Cotac 744 and AG-170 also show improvements, in the vicinity of the fatigue limit, over all of the earlier eutectics studied in our laboratory.

Elevated temperature results are compared in Fig. 65 where the fatigue properties of Nitac 14B can be seen to be unparalleled once again, with a 53% advantage over AG-170. Cotac 744 exhibits a reasonable endurance ratio of 0.78. However some of the first generation eutectics display comparable fatigue ratios. The apparent superiority of Nitac 14B is attributed to its high strength and ductility. More importantly, it contains a very large volume fraction of γ' precipitates which contribute to its strength and retard the rate of crack propagation. Nitac 14B is considered an excellent candidate for high pressure turbine blades on the basis of its elevated temperature fatigue strength.

Heat treatments have been employed as a means of improving high temperature fatigue strength by altering the microstructure. Solutionizing and aging treatments have proved successful as illustrated in Fig. 66. It can be seen that the fatigue strength of Nitac 14B has improved still further, so that it demonstrates an outstanding endurance ratio of 0.89. However, the most substantial improvement is exhibited by AG-170 where aging causes a 42% increase in endurance limit over the 825°C, as D.S. condition. The fatigue limits of Nitac 14B and AG-170 are now comparable. Microstructural modifications of

25°C
20 Hz

AG - 15
AG - 34
AG - 170
γ/γ' - 8 (0% Cr)
Nitac
Nitac 14 B
Cotac
Cotac 744

N_f (cycles to failure)

$\Delta\sigma/\sigma_{UTS}$
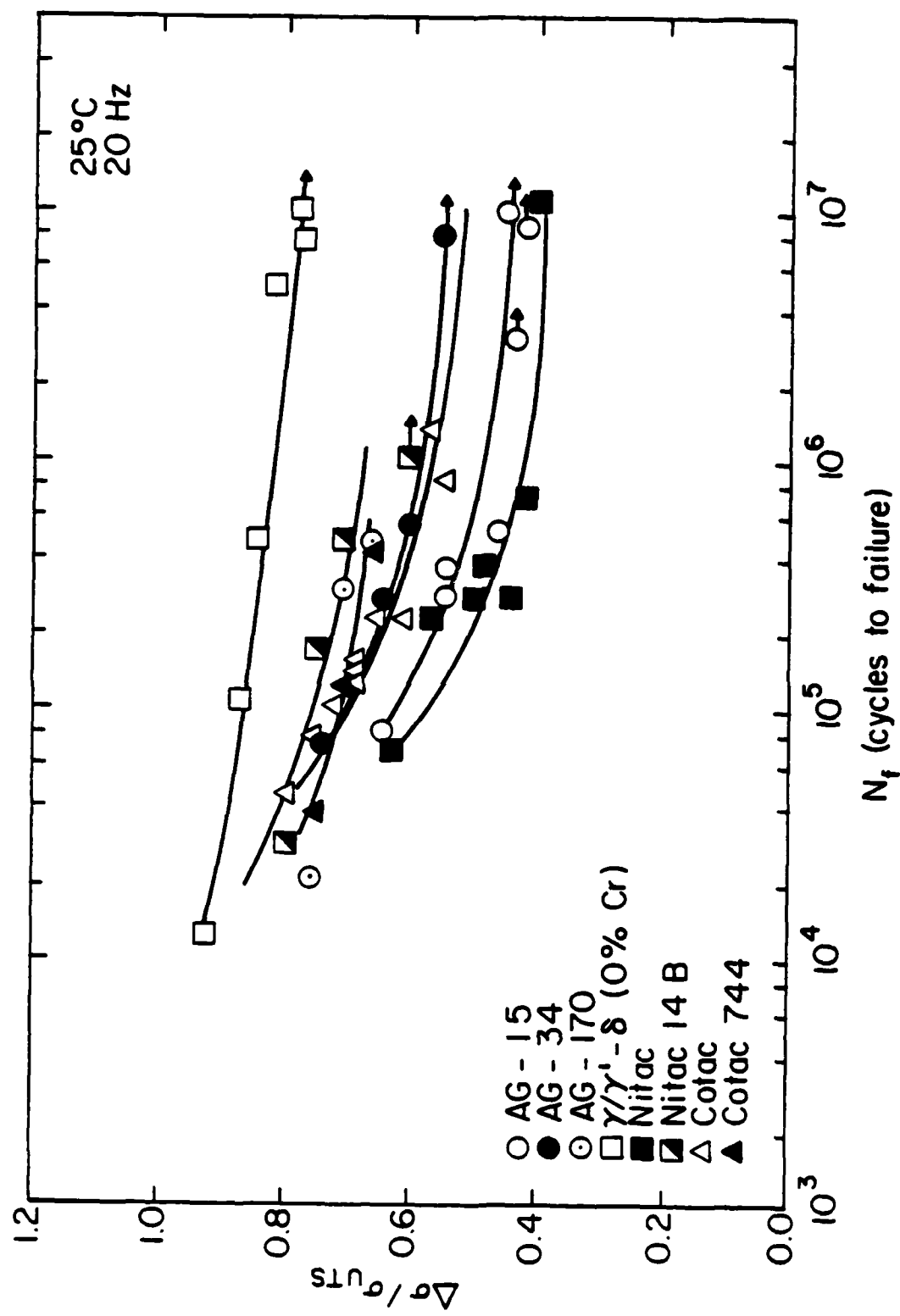
Fig. 64   Room temperature S-N curves for various eutectic alloys normalized with their respective ultimate tensile strengths.
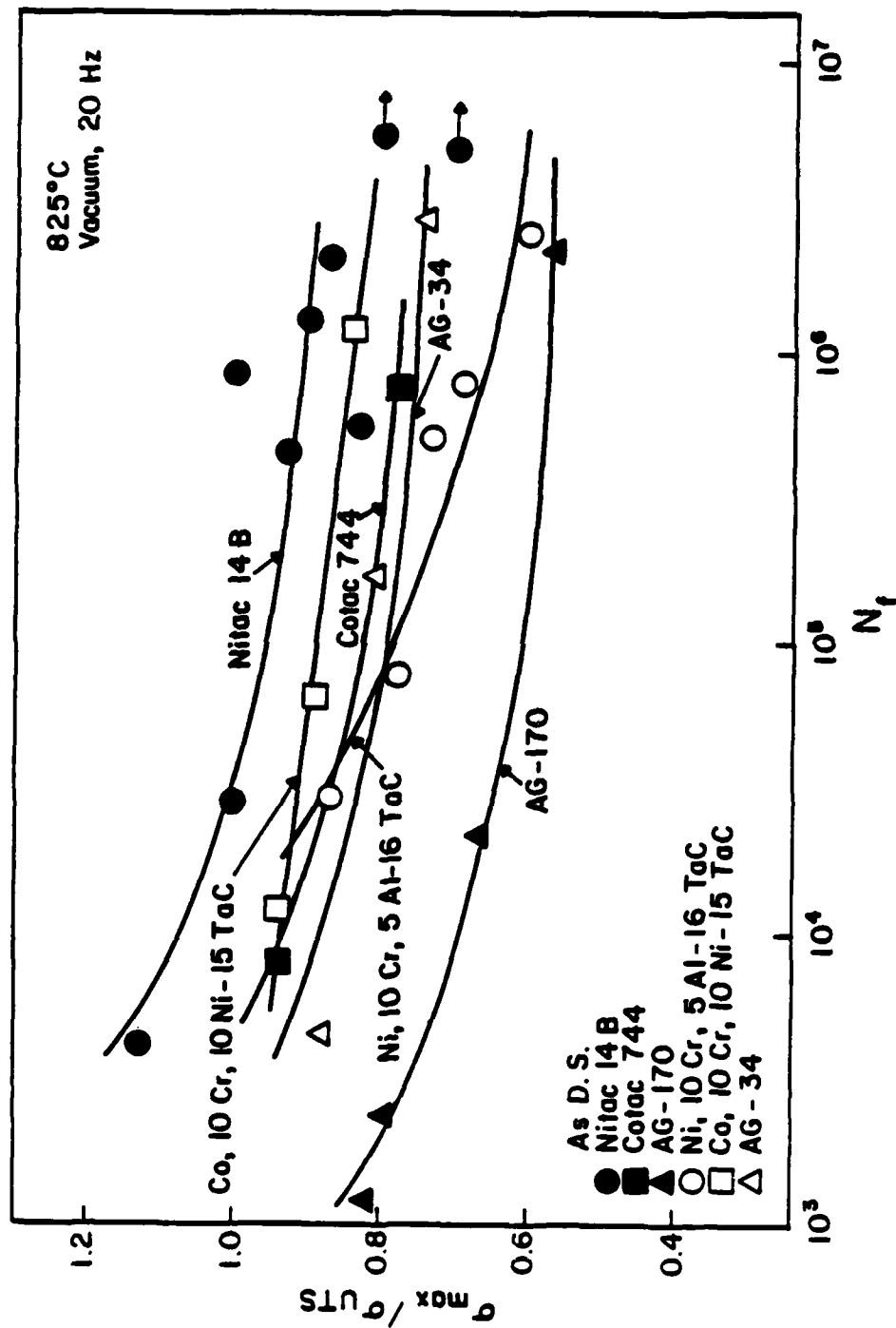
Fig. 65   Normalized high cycle fatigue properties of the three advanced eutectic alloys and their earlier counterparts at 825°C.
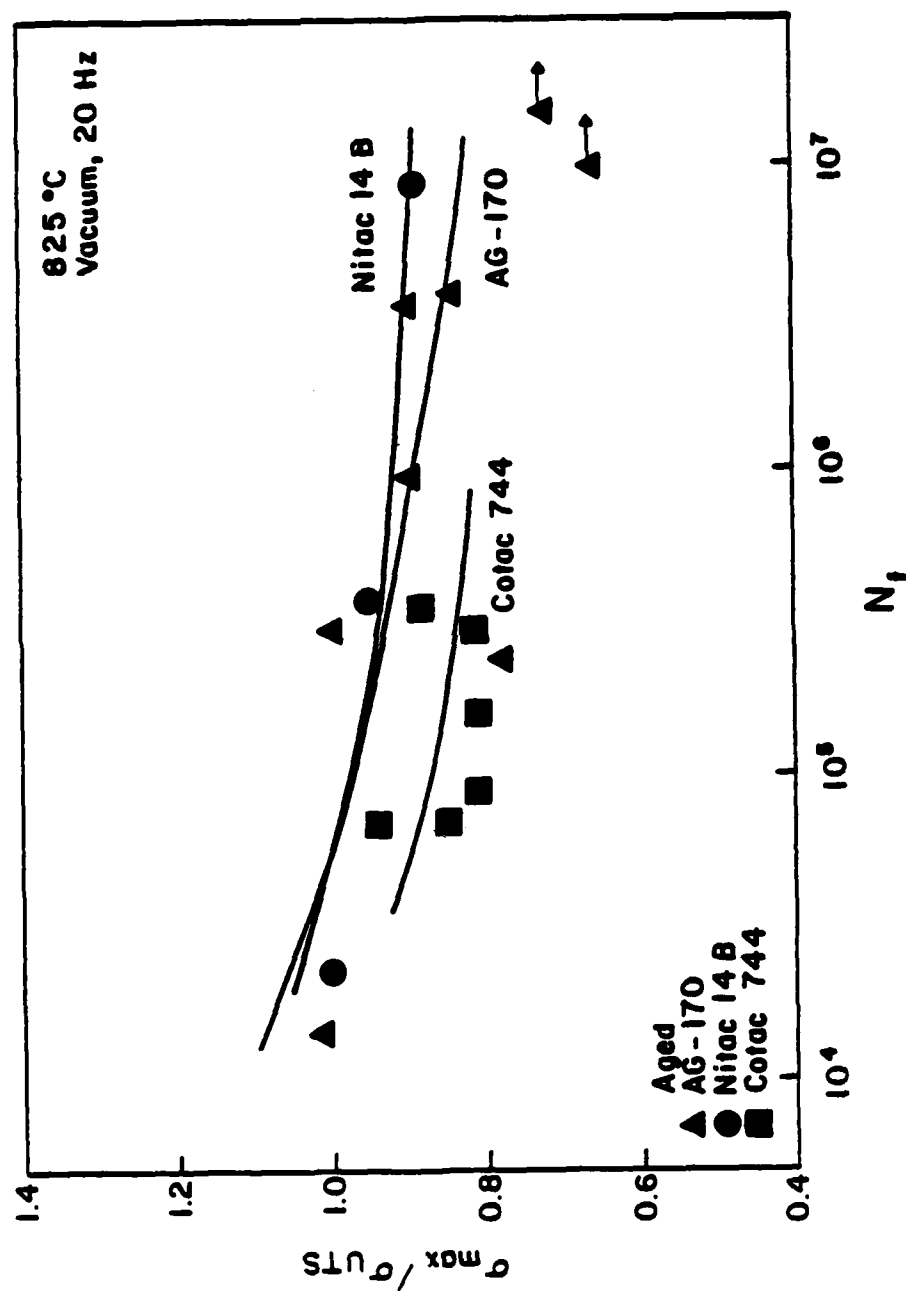
Fig. 66 Comparison of endurance ratios for the three advanced alloys in the aged condition and tested at 825°C.

the γ/γ'-Mo alloy, which cause a considerable hardness increase, account for this substantial improvement.

Overall, all three eutectics have been shown to possess exceptional fatigue properties. Nitac 14B exhibits the best fatigue resistance under most of the conditions tested. Its fatigue ratio of 0.89 at 825°C in the aged condition is by far its most striking feature. With fatigue properties such as these, directionally solidified eutectics will continue to offer strong competition against the more practical, potential turbine blade materials -- single crystal and ODS superalloys. One example is depicted in Fig. 67 where the fatigue resistance of Nitac 14B has been contrasted with both columnar grained and single crystal Mar M-246. Nitac 14B is clearly superior. However the large difference may result partly from environmental differences. The outlook is hopeful.
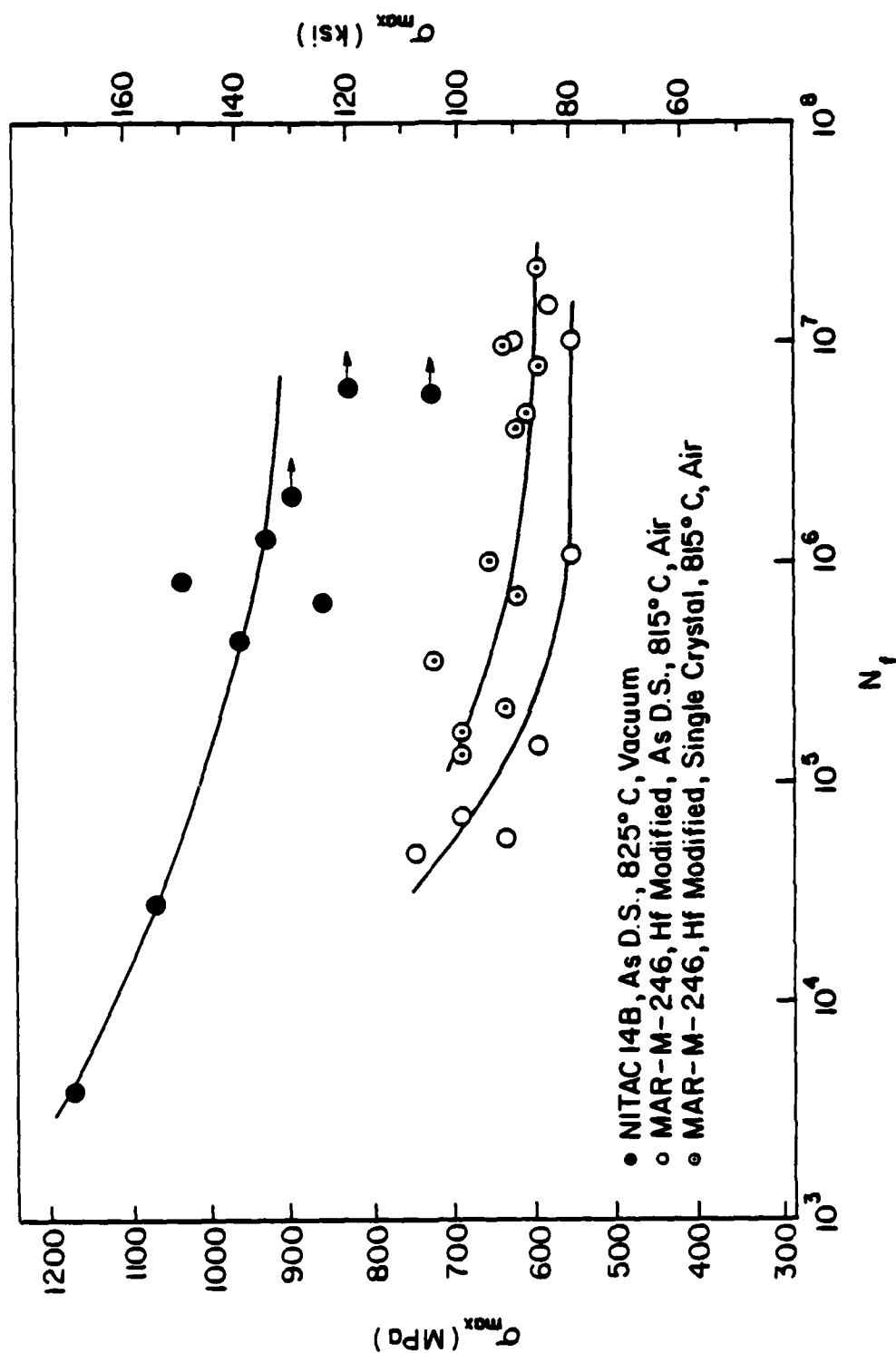
Fig. 67 Comparison of high cycle fatigue fate for Nitac 14B and Mar M-246 at elevated temperature. (Data for Mar M-246 from Ref. (79)).

PART 6

CONCLUSIONS

1. Based on endurance ratio, the three eutectic alloys have good elevated temperature fatigue properties relative to the $25^{\circ}C$ properties. Nitac 14B exhibits superior high cycle fatigue resistance to the other two alloys at both $25^{\circ}C$ and $825^{\circ}C$.

2. Fibers crack readily in Nitac 14B and Cotac 744 , but not as easily in AG-170. Also, TEM has revealed significant dislocation activity in TaC fibers and Mo fibers as a result of high cycle fatigue. These observations indicate that fiber deformation and ductility do not influence fatigue resistance. Rather, high cycle fatigue properties are controlled by the matrix.

3. Post solidification heat treatment considerably alters the micro-structure of the three aligned eutectics and has a beneficial effect on fatigue properties. At ambient temperatures the effect is small and appears to be confined to high stress levels, except for AG-170 where aging considerably increases the room temperature fatigue life. The high cycle fatigue resistance of all three alloys at $825^{\circ}C$ is markedly improved by post solidification aging treatments. AG-170 demonstrates the most substantial improvement.

4. Microstructure has a considerable influence on the high cycle fatigue resistance of these eutectic alloys. The relatively good fatigue resistance of materials possessing cellular microstruc-

149

tures appears to be the result of crack branching down cell boundaries.

5. Fatigue life of aged Nitac 14B is strongly dependent on frequency at 825°C in vacuum. At low frequencies, failures are no longer surface initiated. Distinct overload and fatigue zones are not produced. Decreased specimen life, increased slip dispersal and larger dimple size (i.e. increased ductility) are straightforward evidence for the presence of a significant creep-fatigue interaction.

PART 7

SUGGESTIONS FOR FUTURE WORK

Although this study has proved the superiority of three advanced directionally solidified eutectics in high cycle fatigue, it has created further questions which must be answered before these alloys can be used for turbine blade applications.

First, more extensive tensile work needs to be performed. Tensile results for this investigation were obtained from only 1 specimen/condition, not nearly enough for conclusive strength and ductility values. Tensile fracture surfaces should be compared with fractured fatigue specimens to determine if fibers fracture in a similar manner.

The observed frequency effects have contributed to the understanding of creep-fatigue interactions in D.S. eutectics at elevated temperatures. However, more extensive fatigue testing of Nitac 14B utilizing various hold times and waveforms may better confirm the operation of a creep mechanism. Creep tests also should be performed to establish baseline data to which varying frequency fatigue data can be extrapolated. Comparative examinations of creep and low frequency fatigue fractures using SEM and TEM will substantiate whether there is enhanced cyclic creep at lower strain rates. Similarities or differences observed in the dislocation substructures should be the final verification. More extensive TEM examination of the specimens tested at 20 Hz will aid in explaining the mechanism of damage accumulation.

Crack propagation studies need to be performed for a more

151

complete investigation. At varying frequencies, the results of these studies will distinguish whether initiation or propagation is frequency dependent. Propagation tests on as D.S. specimens will verify if a varying crack growth rate is truly a critical factor in the differences in fatigue properties among the three alloys.

Finally, further heat treatments should be attempted to simulate an actual coating cycle for these alloys, and the subsequent fatigue properties examined. Such data may prove useful for practical application.

PART 8

REFERENCES

1. G.E. Maurer, D.J. Duquette, N.S. Stoloff, <u>Met. Trans. A</u>, Vol. 7A, 1976, p. 703.

2. W.A. Johnson and N.S. Stoloff, <u>Met. Trans. A</u>, Vol. 11A, 1980, p. 307.

3. C. Koburger, N.S. Stoloff, D.J. Duquette, <u>Proc. 2nd Conf. on In-Situ Composites</u>, Xerox, Lexington, MA, 1976, p. 587.

4. J.E. Grossman and N.S. Stoloff, <u>Met. Trans. A</u>, Vol. 9A, 1978, p. 117.

5. J.M. Tartaglia and N.S. Stoloff, <u>Met. Trans. A</u>, Vol. 12A, 1981, p. 1119.

6. M.F. Henry, Ph.D. Thesis, Rensselaer Polytechnic Institute, Troy, NY, 1974.

7. N.S. Stoloff in <u>Strengthening Mechanisms and Alloy Design</u>, Academic Press, NY.

8. H. Bibring, <u>Proc. Conf. on In-Situ Composites</u>, NMAB-II, Lakeville, CT, 1973, p. 1.

9. M.F. Henry, General Electric Co. Research and Development Center, Schenectady, NY, private communication.

10. J.L. Walter and H.E. Cline, <u>Proc. Conf. on In-Situ Composites</u>, NMAB-II, Lakeville, CT, 1973, p. 61.

11. M.F. Henry and E.F. Koch, <u>Pract. Metallography</u>, 1973, Vol. 10, no. 8, p. 439.

12. H. Bibring, T. Khan, M. Rabinovitch, J.F. Stohr, <u>Proc. 3rd Int. Symp. on Superalloys</u>, Seven Springs, PA, 1976.

13. T. Khan, <u>Proc. 3rd Conf. on In-Situ Composites</u>, Boston, MA, 1978, p. 378.

14. T. Khan, J.F. Stohr, H. Bibring, <u>Proc. 4th Int. Symp. on Super-alloys</u>, Champion, PA, 1980, p. 531.

15. E. Maroni, J.F. Stohr, M. Aucouturier, <u>Proc. 3rd Conf. on In-Situ Composites</u>, Boston, MA, 1978, p. 341.

16. M.R. Jackson, J.L. Walter, M.F. Henry, Quarterly Technical Narrative No. 1, NASA Contract NAS 3-19711, General Electric Co. Research and Development Center, Schenectady, NY, August 1975.

17. T. Ishii, D.J. Duquette, N.S. Stoloff, Acta Met., Vol 29, 1981, p. 1467.

18. M.F. Henry, M.R. Jackson, J.L. Walter, Final Report on NASA Contract NAS 3-19711, General Electric Co. Research and Development Center, Schenectady, NY, April 1978.

19. M.F. Henry, Scripta Met., Vol. 10, 1976, p. 955.

20. J. Tartaglia, Ph.D. Thesis, Rensselaer Polytechnic Institute, Troy, NY, 1980.

21. F.D. Lemkey, Final Report on NAVAIR Contract N62269-75-C-0129, United Technologies Research Center, East Hartford, CT, December 1975.

22. M.F. Henry, M.R. Jackson, M.F.X. Gigliotti, P.B. Nelson, Final Report on NASA Contract NAS 3-20383, General Electric Co. Research and Development Center, Schenectady, NY, January 1979.

23. M.F. Henry, Proc. Conf. on In-Situ Composites, NMAB-II, Lakeville, CT, 1973, p. 173.

24. N.S. Stoloff, Proc. 3rd Conf. on In-Situ Composites, Boston, MA, 1978, p. 357.

25. E. Thompson, F. George, E. Breinan, Proc. Conf. on In-Situ Composites, NMAB-II, Lakeville, CT, 1973, pp. 71-82.

26. H.E. Cline and D.F. Stein, Trans. TMS-AIME, Vol. 245, 1969, p. 841.

27. E. Thompson, D. Koss, J. Chesnutt, Met. Trans., Vol. 1, 1970, p. 2807.

28. R. Gangloff and R. Hertzberg, Proc. Conf. on In-Situ Composites, NMAB-II, Lakeville, CT, 1973, p. 89.

29. W. Johnson, Ph.D. Thesis, Rensselaer Polytechnic Institute, Troy, NY, 1978.

30. Y.G. Kim and N.S. Stoloff, Met. Trans., Vol. 5, 1974, p. 809.

31. R. Kossowsky, Met. Trans., Vol. 1, 1970, p. 1909.

32. M. Gell and R.H. Barkalow, Proc. 3rd Int. Conf. on Strength of Metals and Alloys, Cambridge, Vol. 1, 1973, p. 261.

33. M.R. Jackson, J.L. Walter, M.F. Henry, Third Quarterly Report on NASA Contract NAS 3-19711, General Electric Co. Research and Development Center, Schenectady, NY, Feb. 1976.

34. J.P. Trottier, T. Khan, J.F. Stohr, M. Rabinovitch, H. Bibring, Cobalt, 1974, p.3.

35. D.A. Woodford, Met. Trans., Vol. 8A, 1977, p. 639.

36. Semi-Annual Interim Report No. 8 on AF Contract F 33615-77-C-5200, General Electric Aircraft Engine Group, Cincinnati, Ohio, Nov. 1981, p. 71.

37. N.S. Stoloff and D.J. Duquette in CRC Crit. Reviews in Solid State Sciences, Vol. 4, No. 4, 1974, pp. 615-687.

38. N.S. Stoloff in Reviews on High Temperature Materials, Vol III, No. 4, 1978, pp. 231-276.

39. N.S. Stoloff in Advances in Composite Materials, Applied Science Publishers, Barking, Essex, England, 1978, pp. 247-285.

40. C. Koburger, D.J. Duquette, N.S. Stoloff, Acta Met., Vol. 26, 1978, p. 81.

41. Y.G. Kim, G.E. Maurer, N.S. Stoloff in Fatigue of Composite Materials, ASTM STP 569, Philadelphia, PA, 1975, p. 210.

42. M. Patarini and T.Z. Kattamis, Proc. Conf. on In-Situ Composites, NMAB-II, Lakeville, CT, 1973, p. 187.

43. H. Bibring, G. Seibel, M. Rabinovitch, Mem. Sci. Rev. Met., Vol. 69, 1972, p. 341.

44. H. Bibring, J.P. Trottier, M. Rabinovitch, G. Seibel, Mem. Sci. Rev. Met., Vol. 68, 1971, p. 23.

45. C. Koburger, D.J. Duquette, N.S. Stoloff, Met. Trans. A, Vo.. 11A, 1980, p. 1107.

46. A. de Silva, G. Chadwick, Met Sci. J., Vol. 4, 1970, p. 63.

47. G.J. May, Met. Trans., Vol. 6A, 1975, p. 1115.

48. B. Scarlin, Met. Trans., Vol. 8A, 1977, p. 1941.

49. J.M. Tartaglia, N.S. Stoloff, Met. Trans. A, Vol. 12A, Nov. 1981, p. 1891.

50. C. Owen, M.S. Thesis, Rensselaer Polytechnic Institute, Troy, NY, 1978.

51. C. Koburger, Ph.D. Thesis, Rensselaer Polytechnic Institute, Troy, NY, 1978.

52. D.D. Pearson and F.D. Lemkey, First Quarterly Report on NAVAIR Contract N 62269-78-C-0271, United Technologies Research Center, East Hartford, CT, Nov. 1978.

53. Y.G. Nakagawa, A. Ohotomo, Y. Saiga, Proc. 4th Int. Symp. on Super-alloys, Seven Springs, PA, 1980, p. 267.

54. J.E. Northwood, R.S. Smith, N. Stephenson: Memorandum No. M 325, National Gas Turbine Engine Establishment, 1959.

55. D.A. Jablonski, J.V. Carisella, R.M. Pelloux, Met. Trans. A, Vol. 8A, Dec. 1977, p. 1893.

56. A.H. Meleka, Met. Rev., Vol. 7, 1962, p. 43.

57. A.J. Kennedy, Processes of Creep and Fatigue in Metals, John Wiley & Sons, Inc., NY, 1963.

58. E.G. Ellison, J. Mech. Eng. Sci., Vol. 11, 1962, p. 318.

59. D.J. White, Proc. Inst. of Mech. Eng., Applied Mechanics Group, Vol. 184, 1969-70, p. 223.

60. M.R. Achter, Fatigue Crack Propagation, ASTM STP 415, Philadelphia, PA, 1967, p. 181.

61. A.J. Nachtigall, S.J. Klima, J.C. Freche, C.A. Hoffman, NASA TN-D 2898, June 1965.

62. L.F. Coffin, Jr., Met. Trans., Vol. 3, 1972, p. 1777.

63. L.F. Coffin, Jr. in Fatigue at Elevated Temperatures, ASTM STP 520, Philadelphia, Pa, 1973, p. 1.

64. J. Wareing, Met. Trans. A, Vol. 6A, 1975, p. 1367.

65. J. Wareing, Met. Trans. A, Vol. 8A, 1977, p. 711.

66. E. Krempl and C.D. Walker in Fatigue at High Temperature, ASTM STP 459, Philadelphia, PA, 1969, p. 75.

67. J.T. Berling and J.B. Conway, First Int. Conf. on Pressure Vessel Tech., Delft, Holland, 1969.

68. A.D. Coles and D. Skinner, J. Royal Aero. Soc., Vol. 69, 1965, p. 53.

69. K. Sadananda and P. Shahinian, Mat. Sci. and Eng., Vol. 38, 1979, p. 81.

70. C.M. Austin, Ph.D. Thesis, Rensselaer Polytechnic Institute, Troy, NY, 1979.

71. D.C. Lord and L.F. Coffin, Jr., Met. Trans., Vol. 4, 1973, p. 1647.

72. L.F. Coffin, Jr., Symp. on Creep-Fatigue Environment Interactions, Fall Meeting of AIME, Milwaukee, WI, Oct. 1979.

73. D.D. Pearson and F.D. Lemkey, Final Report on NAVAIR Contract N62269-77-C-0055, United Technologies Research Center, East Hartford, CT, 1978.

74. M.F. Gigliotti, General Electric Co. Research and Development Center, Schenectady, NY, private communication, July 1982.

75. M. Gell and G.R. Leverant in Fatigue at Elevated Temperatures, ASTM STP 520, Philadelphia, PA, 1973, pp. 37-66.

76. P.J. Forsyth, R.W. George, D.M. Ryder, Appl. Mat. Res., Vol. 3, 1964, p. 223.

77. G. Leverant and M. Gell, Met. Trans., Vol. 6A, 1975, pp. 367-371.

78. L.H. Van Vlack, Elements of Materials Science and Engineering, Addison Wesley, Reading, MA, 1975, p. 9.

79. Aerospace Structural Metals Handbook, Code 4216, 1981, p. 26.

Personnel:

Principal Investigator:	N. S. Stoloff	10/1/79 - present
Graduate Research Asst:	K. Jones	9/82 - present
Graduate Research Asst:	K. Dannemann	9/80 - 9/82
Graduate Research Asst:	N. Bylina	6/82 - present
Undergraduate Res. Asst:	E. McMahon	5/82 - 8/82
Undergraduate Res. Asst:	S. Krapcho	5/82 - 8/82

Publications Arising from AFOSR Support

J. M. Tartaglia and N. S. Stoloff "Fatigue of Ni-Al-Mo Aligned Eutectics at Elevated Temperatures", Met. Trans. A, V. 12A, 1981, p. 1981 (previously reported in letter dated 28 Jan., 1982.)

K. A. Dannemann, T. Ishii, D. J. Duquette and N. S. Stoloff, "Microstructure and Fatigue Behavior of Nickel-Base Eutectic Composites, Strength of Metals and Alloys" (ISMA 6), Editor: R. C. Gifkins, Pergamon Press, Oxford, pp. 141-146.

K. A. Dannemann, N. S. Stoloff and D. J. Duquette, "High Cycle Fatigue of Three Advanced Nickel-Base Eutectic Composites", submitted to Met. Trans. A.

K. A. Dannemann, "Microstructure and Fatigue Behavior of Three Ni-Base Eutectic Composites", M.S. Thesis, Rensselaer Polytechnic Institute, 9/82.

Presentations Arising from AFOSR Support

"Fatigue of Eutectic Composites", invited seminar to Dept. of Materials Eng., UCLA, Los Angeles, CA, Mar. 4, 1982.

"Fatigue of High Temperature Alloys", invited seminar to Southwest Res. Inst., San Antonio, TX, March 24, 1982.

"Fatigue of Eutectic Composites", invited seminar, University of Bordeaux, Bordeaux, France, June 14, 1982.

"Eutectic Superalloys", invited lecture to Mitsubishi Metal Industries, Toyko, Japan, August 10, 1982.

"Microstructure and Fatigue Behavior of Nickel Base Eutectic Composites", 6th Int. Conf. on Strength of Metals and Alloys, Melbourne, Australia, Aug. 18, 1982.

Advanced Degrees Awarded

K. A. Dannemann, M.S. Thesis, "Microstructure and Fatigue Behavior of Three Ni-Base Eutectic Composites", submitted for degree award in December 1982.

4 -

DT